

Teresa Maria da Silva Sousa

From parametric decoding of simple mental states to neurofeedback: insights into the neuroscience of cognitive control

Tese de Doutoramento em Engenharia Biomédica, orientada pelo Professor Doutor Miguel Castelo-Branco e pelo Professor Doutor Urbano Nunes
e apresentada à Faculdade de Ciências e Tecnologia da Universidade de Coimbra

Setembro de 2016



UNIVERSIDADE DE COIMBRA



UNIVERSITY OF COIMBRA

FACULTY OF SCIENCES AND TECHNOLOGY

**From parametric decoding of simple mental states to neurofeedback:
insights into the neuroscience of cognitive control**

Thesis presented to obtain a Ph.D. degree in Biomedical Engineering at the
Faculty of Sciences and Technology of the University of Coimbra

Teresa Maria da Silva Sousa

September of 2016

Supervised by: Prof. Dr. Miguel Castelo-Branco

Co-Supervised by: Prof. Dr. Urbano Nunes



UNIVERSIDADE DE COIMBRA
FACULDADE DE CIÊNCIAS E TECNOLOGIA

**Da descodificação paramétrica de estados mentais simples ao
neurofeedback:
Contribuições para a neurociência do controlo cognitivo**

Tese de Doutoramento apresentada à Faculdade de Ciências e Tecnologia da Universidade de
Coimbra, para prestação de provas de Doutoramento em Engenharia Biomédica

Teresa Maria da Silva Sousa

Setembro de 2016

Orientada por: Prof. Dr. Miguel Castelo-Branco

Co-orientada por: Prof. Dr. Urbano Nunes

The studies presented in this thesis were carried out at the Institute for Biomedical Imaging and Life Sciences (IBILI), Faculty of Medicine, at the Institute for Nuclear Sciences Applied to Health (ICNAS), at the Institute of Systems and Robotics (ISR), Faculty of Sciences and Technology, University of Coimbra, Portugal, and at Maastricht Brain Imaging Center (M-BIC), Faculty of Psychology and Neuroscience, University of Maastricht, Netherlands.

This research work was funded by a PhD grant with reference SFRH / BD / 80735 / 2011 from the Portuguese Foundation for Science and Technology and by the BIAL project 373/14.

Copyright© 2016 Teresa Sousa



Para ti Mãe

“What is essential is invisible to the eye.”

Antoine de Saint-Exupéry in *The Little Prince*

ACKNOWLEDGMENTS

First of all, I would like to express my sincere gratitude to my supervisors. To Prof. Miguel Castelo-Branco, I want to thank him for the enthusiastic and fruitful discussions, for all his suggestions and support. His supervision, help and advice were invaluable to carry out the research studies presented on this thesis. It is an honor to work with someone with such passion and expertise on neuroscience field. To Prof. Urbano Nunes, I want to thank him for introducing and training me as researcher and for providing me confidence to follow my own directions. I am very grateful for his contributions, continued support and advice. I truly admire the simplicity and expertise of both.

Prof. Rainer Goebel gave me the opportunity to work and learn with him and his group in M-BIC. I want to thank him for the opportunity, shared ideas and help. I also would like to thank Brain Innovation team and Valentin Kemper for all their support.

I am deeply grateful to Prof. Gabriel Pires for the discussions about data processing and analysis, motivation and advice. Thank you for being a continuous help on my research work.

My PhD host institutes, IBILI, ICNAS, ISR and also M-BIC, provided me the conditions and resources to accomplish my PhD work using the most recent methods and equipment in neuro-engineering research. I am very grateful to them.

I feel especially indebted with the participants who volunteered for the studies and gave many hours of their time. You were one of the most important helps in my work.

I would also like to thank the friends that I met at ISR which helped me all the time with their joy and care. I am especially grateful to Jérôme, Ricardo, Omar and Alexandre for the valuable discussions.

To my colleagues from IBILI and ICNAS, I would like to thank for their help, kindness and support. I want particularly thank the ones that actively participated on my project and my office partners for the day-by-day patience and care. João, Otilia, Ana, Gabriel and Ricardo, thank you for the help during the more complicated moments of this PhD work.

I wish to thank the friendship and all the relaxing moments shared with my old friends Hugo, Vera and Nariguetas. They are always important, but mainly during a PhD work! Thank you. You are the best!

My close family has been truly important for their support and help in all my needs. I am especially grateful to Sérgio, my sisters and my parents. Sérgio, thank you for all the times you shared my concerns, that you solved problems for me and made my day easier with *haute cuisine* and magic. Sofia and Margarida, my sisters and my best friends, thank you for the unconditional support and for being always present. I am mainly grateful to my lovely parents, I am very fortunate to have their strong and encouraging example. You are one part of me.

CONTENTS

List of Abbreviations	i
Abstract	iii
Resumo	vii
General introduction	1
1.1. Mechanism underlying brain activity patterns.....	3
1.1.1. How to measure brain activity.....	4
1.1.2. How to decode brain activity.....	9
1.2. From brain-computer interfaces to neurofeedback.....	13
1.2.1. State-of-the-art of neurofeedback systems.....	14
1.2.2. Neurofeedback system setup.....	17
1.2.3. Brain activity control levels based on self-regulation.....	19
1.3. Goals and key contributions.....	22
1.4. Thesis outline.....	23
Visual motion imagery neurofeedback based on the hMT+/V5 complex	33
2.1. Introduction.....	37
2.2. Materials and methods.....	39
2.2.1. Participants.....	39
2.2.2. fMRI data acquisition.....	40
2.2.3. Online data analysis.....	40
2.2.4. Functional definition of the target region-of-interest.....	41
2.2.5. Neurofeedback runs and experimental design.....	41
2.2.6. Offline data analysis.....	43
2.3. Results.....	44
2.3.1. hMT+/V5 localization.....	44
2.3.2. hMT+/V5 modulation.....	45
2.3.3. Whole-brain group analysis.....	47
2.4. Discussion.....	50
2.5. Conclusion.....	53
APPENDIX.....	57
Control of brain activity in hMT+/V5 at three response levels using fMRI-based neurofeedback .	61
3.1. Introduction.....	65

3.2.	Materials and methods	67
3.2.1.	Ethics statement and participants.....	67
3.2.2.	Experimental design	68
3.2.3.	fMRI data acquisition	68
3.2.4.	Real-time fMRI data processing	69
3.2.5.	Functional definition of the target ROI (localizer experiments using visual stimulation)	70
3.2.6.	Neuromodulation runs (NF experiments using visual imagery)	71
3.2.7.	Offline data analysis	71
3.3.	Results.....	73
3.3.1.	hMT+/V5 localization	73
3.3.2.	hMT+/V5 modulation: imagery based control of brain activity at 3 response levels	74
3.4.	Discussion	77
3.5.	Conclusion	78
	APPENDIX.....	81
	Visual motion imagery as a tool for multiclass EEG-based BCI.....	87
4.1.	Introduction.....	91
4.2.	Methods.....	93
4.2.1.	Participants	93
4.2.2.	Experimental design	93
4.2.3.	Data acquisition	94
4.2.4.	Data analysis	95
4.2.5.	Imagery data classification	96
4.2.6.	Statistical Analysis.....	97
4.3.	Results.....	98
4.3.1.	Visual motion stimulation.....	98
4.3.2.	Visual motion imagery.....	99
4.3.3.	Visual motion imagery classification.....	102
4.4.	Discussion	103
4.5.	Conclusion	104
	APPENDIX.....	111
	Perceptual interpretation of visual motion revealed at high-resolution 7T fMRI	117
5.1.	Introduction.....	121
5.2.	Material and Methods	123
5.2.1.	Participants	123
5.2.2.	Experimental design overview.....	123

5.2.3.	Stimuli	123
5.2.4.	Imaging data acquisition.....	127
5.2.5.	Offline data analyses	128
5.3.	Results.....	131
5.3.1.	Behavioral analysis results	131
5.3.2.	hMT+/V5 localization	133
5.3.3.	Stimulus validation for axes of motion preference mapping.....	134
5.3.4.	Ambiguous and unambiguous imaging analysis results	135
5.3.5.	hMT+/V5 shows domains that are selective for the type of percept	135
5.4.	Discussion.....	137
5.5.	Conclusion	138
	APPENDIX	143
	General discussion and Conclusions	147
6.1.	General discussion	149
6.2.	Conclusions.....	157
	Curriculum vitae	161

LIST OF ABBREVIATIONS

ADHD	Attention deficit hyperactivity disorder
ANOVA	Analysis of Variance
AR	Auto-regressive
BCI	Brain-computer interface
BOLD	Blood-oxygenation-level dependent
DMN	Default mode network
ECoG	Electrocorticography
EEG	Electroencephalography
EMG	Electromyography
EOG	Electrooculography
EPI	Echo planar imaging
ERSP	Event-related spectral perturbation
FA	Flip angle
FDR	False discovery rate
FFT	Fast fourier transform
FFX	Fixed effects
fMRI	Functional magnetic resonance imaging
fNIRS	Functional near-infrared spectroscopy
FOV	Field of view
GE	Gradient echo
GE-PD	Gradient echo proton-density
GLM	General linear model
GRAPPA	Generalized partially parallel acquisitions
hMT+/V5	Human (middle temporal) motion complex
HRF	Hemodynamic response function

ICA	Independent component analysis
LFP	Local field potentials
MEG	Magnetoencephalography
MPRAGE	Magnetization-prepared rapid-acquisition gradient echo
MRI	Magnetic resonance imaging
NF	Neurofeedback
PD	Proton density
PET	Positron emission tomography
PPI	Psychophysiological interactions
PSD	Power spectral density
RF	Radiofrequency
RFX	Random effects
ROI	Region of interest
RSP	Relative spectral power
SEM	Standard error of the mean
sLORETA	Standardized low resolution brain electromagnetic tomography
SVM	Support vector machine
TE	Echo time
TR	Repetition time

ABSTRACT

The physiological activity of nervous system is constantly changing in response to contextual changes, which shapes our perception, emotions and cognitive reasoning. Many researchers, clinicians and health professionals have become increasingly interested in translating the understanding of the function of human nervous system and behavior into health technology and human performance.

A brain-computer interface (BCI) system uses neurophysiological signals originating in the brain to activate or deactivate external devices or computers. In addition to the assistive functions as communication and control to injured subjects, BCIs offer the opportunity for enhancing neural functions and developing therapies for neural disabilities when applied as a neurofeedback (NF) approach. NF technology allows the participants to observe what their brain is doing in real time. This enables to learn, in an operant manner, how to control brain activity, which might have potential therapeutic impact in disorders of anxiety, attention and motor performance, for example.

The voluntary control of brain activity is trained by mean of mental tasks typically known to influence a specific brain network, as for example mental calculation, motor imagery and emotional recalling. Methods to better determine the nature of the brain activity dynamics and plasticity through the formation of self-regulation are still under development. Typically, self-regulation of brain activity is based on binary control: the users try to increase or to decrease/abolish a given brain activity modulation. This thesis presents a research effort developed with the main goal of increase the intrinsic levels of control within each class of volitional brain activity control.

Here, we explored the hypothesis of achieve up to three control levels of hMT+/V5 activity using visual motion imagery strategies with different number of motion alternations. We took advantage of the specific recruitment of this brain region to visualized and imagined motion features to go from binary to multilevel/parametric voluntary brain activity control. The performed tests were primarily based on 3 Tesla functional magnetic resonance imaging (fMRI) data and then the proposed brain activity self-regulation approach was also studied using electroencephalography (EEG). Furthermore, the high-resolution 7 Tesla fMRI technique was used to explore with more detail the functional properties of the hMT+/V5 brain region during visual motion perception and to propose a future work to study the possibility of multilevel modulation of functional connectivity.

The strategies to achieve self-regulation of brain activity can be applied not only in NF approaches but also to achieve more direct and flexible assistive BCI systems. Thus, the increase of volitional brain activity control levels might not only allow for more precise NF but also for improved assistive BCI systems. The research work presented in this thesis may contribute to the technical improvements of BCI systems, to increase their application range and to the understanding of neural mechanisms underlying cognitive control.

First, the feasibility of training healthy volunteers to up-regulate and down-regulate the activity of the hMT+/V5 complex using fMRI-based NF and visual motion imagery strategies was tested. We show that hMT+/V5 activity can be volitionally modulated by focused imagery and that a specific brain network is recruited during visual motion imagery leading to successful NF training. The results presented contribute also to the debate on the relative value of sensory versus default-mode brain regions in the NF clinical applications.

Then, the hypothesis whether more than two modulation levels can be achieved in a single brain region was tested. Participants performed three distinct imagery tasks with different numbers of motion alternation during fMRI-based NF training. Three control levels (two up-regulation levels and one down-regulation level) of brain activity in the hMT+/V5 complex were achieved. Based on our results we suggest that it is possible to design a multilevel system of control based on brain activity self-regulation of a specific brain region and using similar strategies across participants. Empirical contributions to the comparison between the binary and multilevel control processes and between the passive imagery and the active imagery processes assisted by feedback are also provided.

The hypothesis whether visual motion imagery can be used as a tool to at least achieve multiclass (>2) EEG-based BCI was tested. The imagery strategies previously studied with fMRI-based NF were applied. We expected that this would be achieved by detection of differential modulations, regardless of their polarity, in the EEG domain. EEG signals were acquired during passive visual motion imagery in order to identify the evoked brain activity patterns by each imagery strategy. Although we did not find levels of brain activity during the different imagery tasks, we suggest visual motion imagery as a simple tool to achieve a multiclass BCI systems. Furthermore, we contribute for the discussion about the role of frontal alpha activity and for the comparison between the univariate and multivariate signal analyses.

Finally, we used high-resolution 7 Tesla fMRI to map functional sub-domains in the hMT+/V5 region and to show that the tuning of these sub-domains is for the interpretation

of the perceptually relevant motion features regardless of the physical stimulation. These results contribute for the discussion about the neural correlates of perceptual switches in hMT+/V5 brain region at columnar-level and can be used as the first step for a NF study aiming to modulate brain connectivity as a function of perceptual decision.

Keywords: neurofeedback, brain-computer interfaces, visual motion perception, visual motion imagery.

RESUMO

A atividade fisiológica do sistema nervoso varia constantemente em resposta a mudanças contextuais, moldando a nossa percepção, emoções e raciocínio. O sistema nervoso e comportamento humano têm sido alvo de intensa investigação por parte de neurocientistas, médicos e outros profissionais de saúde, nomeadamente para a melhoria de tecnologias da saúde e do desempenho humano.

Uma das aplicações que tem despertado mais interesse na área da neuroengenharia baseia-se nos sistemas de interface cérebro-computador (BCI, do inglês *Brain-Computer Interface*), que usam sinais cerebrais para codificar a ativação ou desativação de comandos de um aparelho externo ou computador. Para além de permitirem auxiliar pessoas com capacidades reduzidas em tarefas de comunicação e controlo, as BCIs podem ser aplicadas como métodos de *neurofeedback* (NF), permitindo a melhoria da função dos circuitos neuronais e o desenvolvimento de terapias para tratamento de problemas neurológicos e psiquiátricos. Os sistemas de NF permitem a observação em tempo real da atividade cerebral o que facilita a aprendizagem do controlo voluntário da atividade cerebral, tendo por base o condicionamento operante. Estes métodos apresentam potencial terapêutico, por exemplo, em perturbações de ansiedade ou da atenção e em patologias que afetem o desempenho motor.

Atualmente, estão em desenvolvimento vários estudos que visam uma melhor compreensão da dinâmica da atividade cerebral e da sua plasticidade, recorrendo a métodos focados na capacidade de regulação voluntária da atividade cerebral, também conhecida como capacidade de neuromodulação voluntária. A neuromodulação voluntária pode ser treinada usando tarefas mentais, como por exemplo o cálculo mental, a imaginação motora e recordações emotivas, que influenciam redes neuronais específicas e conhecidas. Tipicamente, esta capacidade permite dois níveis de controlo voluntário: um baseado no aumento e outro na diminuição de um padrão específico de atividade cerebral. Esta tese teve como principal objetivo o estudo da possibilidade de regular voluntariamente mais do que dois níveis de atividade cerebral.

Os trabalhos apresentados nesta tese exploram a hipótese de obter até três níveis de controlo a partir da neuromodulação voluntária da região hMT+/V5, recorrendo para isso a estratégias de imaginação da visualização de movimento não-motor baseadas em diferentes quantidades de alternância de movimento. Tirou-se partido do recrutamento desta região

cerebral especificamente durante a visualização ou imaginação da visualização de movimento, para estudar estratégias de neuromodulação voluntária que permitam ir do controlo binário (dois níveis de atividade por cada classe de controlo) ao multinível (vários níveis de atividade por cada classe de controlo). Inicialmente, as estratégias de neuromodulação voluntária propostas foram testadas usando imagem por ressonância magnética funcional (fMRI, do inglês *functional Magnetic Resonance Imaging*) a 3 Tesla e depois usando a eletroencefalografia (EEG). Além disso, foi usada a técnica de fMRI a 7 Tesla para explorar com mais detalhe as propriedades funcionais da região hMT+/V5 e para propor como trabalho futuro o estudo da possibilidade de controlo multinível baseado na conectividade funcional.

As estratégias de neuromodulação voluntária podem ser usadas em sistemas BCI de assistência ou em sistemas BCI aplicados como métodos de NF. Assim, ao aumentarmos os níveis de controlo através da neuromodulação voluntária contribuimos para o desenvolvimento de métodos de NF mais precisos e também para a melhoria dos sistemas BCI de assistência. Os trabalhos apresentados contribuem não só para melhorias metodológicas dos sistemas BCI, como também aumentam as suas possibilidades de aplicação e permitem a melhor compreensão dos mecanismos neuronais relacionados com o controlo cognitivo.

Primeiro, testou-se a viabilidade de neuromodulação voluntária da atividade na região hMT+/V5, em participantes saudáveis, com recurso a treino NF e fMRI. Os resultados mostraram que a atividade desta região pode ser voluntariamente regulada usando estratégias de imaginação visual de movimento e nos casos de neuromodulação bem-sucedida foi recrutada uma rede neuronal específica. Além disso, este estudo contribui para a discussão do potencial dos métodos de NF focados em regiões sensoriais para aplicações clínicas.

De seguida, foi testada a hipótese de obter três níveis de controlo baseados na neuromodulação da mesma região cerebral recorrendo a treino com NF. Os participantes usaram três tarefas de imaginação visual baseadas em diferentes quantidades de variação de movimento. Foram conseguidos três níveis de controlo: dois através do aumento e um da diminuição da atividade na região hMT+/V5. Assim, sugere-se que é possível obter controlo multinível baseado na neuromodulação voluntária da atividade de uma região específica e de forma similar entre participantes. Os resultados apresentados contribuem também para a

comparação empírica entre processos de controlo binário e multinível e entre imaginação passiva e ativa (assistida por *feedback*).

As estratégias de imaginação propostas foram também estudadas com EEG. Explorámos a hipótese de que os diferentes níveis de neuromodulação seriam também encontrados no sinal elétrico cerebral. Os sinais foram registados durante imaginação passiva. Apesar de não terem sido encontrados três níveis de atividade, usando um algoritmo de classificação foi possível distinguir os padrões evocados por cada tarefa de imaginação. Este fato sugere a viabilidade das estratégias de imaginação visual de movimento para obter múltiplas classes de controlo em sistemas BCI. Para além disso, este estudo contribui também para a discussão do papel da atividade alfa frontal e para a comparação entre análise univariada e multivariada de sinais neurofisiológicos na descodificação de padrões de atividade cerebral.

Por fim, foram mapeados subdomínios funcionais da região hMT+/V5 usando fMRI a 7 Tesla e foi demonstrado que a resposta preferencial destes subdomínios a diferentes orientações de movimento corresponde ao movimento percebido, independentemente do padrão de movimento real. Estes resultados contribuem para o estudo dos mecanismos neuronais relacionados com mudanças de percepção de movimento ao nível dos subdomínios perceptuais da região hMT+/V5. Adicionalmente, de uma forma preliminar, trazem boas perspectivas para o desenvolvimento de uma nova estratégia de neuromodulação multinível baseada na percepção visual de movimento.

Palavras-chave: *neurofeedback*, interfaces cérebro-computador, percepção visual de movimento, imaginação de movimento visualizado.

CHAPTER 1

GENERAL INTRODUCTION

Specific brain functions evoke reproducible patterns and sequences of neural activity letting the opportunity for carrying on studies focused both in mechanistic understanding and in providing brain-computer interactions. Current neuro-engineering technologies allow us to detect these brain activity patterns and determine the corresponding behavioral or perceptual operation. This concept, referred as brain decoding, spans a variety of research areas ranging from interactions between the nervous system and external devices through the brain-computer interface (BCI) technologies to its application in neurofeedback (NF) approaches based on the interpretation and volitional modulation of neural activity.

This thesis presents a work developed with the main goal of increasing the number of control levels, or at least open new possibilities in brain activity self-regulation to apply on BCI technologies. This would help to improve current BCI systems and would allow for NF approaches that go beyond binary control.

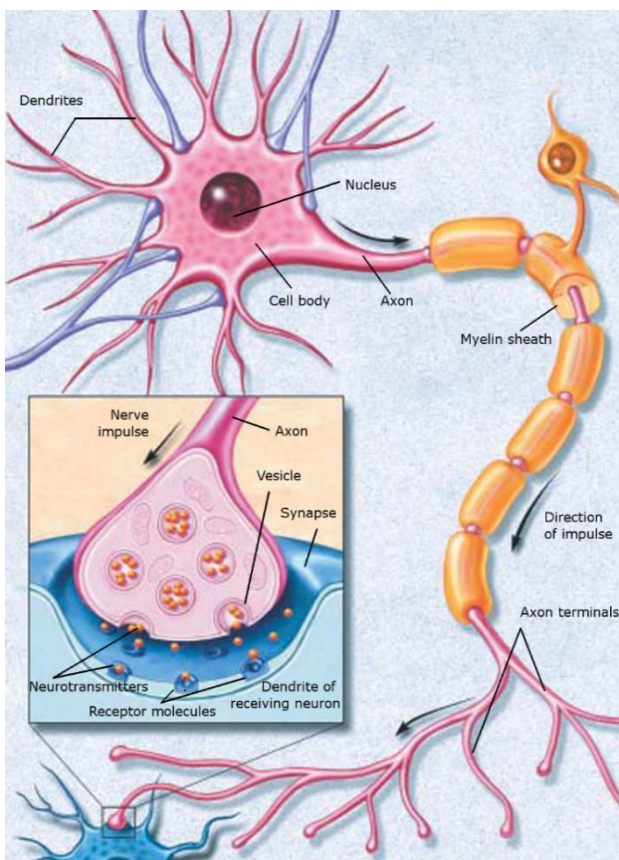
In the current chapter we provide an overview of the main concepts and methods behind these technologies are outlined, the state-of-the-art is presented and, the goals, key contributions and outline of the developed research work are described.

1.1. Mechanism underlying brain activity patterns

The brain is composed by a vast neural network working in harmony to control numerous conscious and subconscious functions. In all species the brain action is mainly based on two classes of cells: neurons and glia cells. Neurons are commonly considered the most important cells in the brain, since these cells are the signaling units of the nervous system. Glia cells perform a number of critical functions, as structural support or insulation of the neurons. The brain outer layer of neural tissue, the cerebral cortex also known as gray matter, contains billions of neurons and glia, and is responsible for many high-order functions such as perception, consciousness or attention (Bear et al. 2016).

By means of axons (a thin protoplasmic fiber that extends from the cell body and project to other areas), neurons have the ability of send signals to specific target cells over long distances. The transmitted signals are electrochemical pulses called action potentials and last less than a thousandth of a second. The axonal membrane ion channels open and close

to let through electrically charged ions. Some channels allow sodium ions (Na^+) to go through, while others allow potassium ions (K^+). When channels open, the Na^+ or K^+ ions flow down opposing chemical and electrical gradients, in and out of the cell, in response to electrical depolarization of the membrane. Through this process, action potentials are transmitted along axons at speeds of 1 - 100 meters per second to specialized regions called synapses, where the axons contact the dendrites of other neurons. When an action potential, traveling along an axon, arrives at a synapse, it causes a chemical called a neurotransmitter to be released. Then, the neurotransmitter binds to receptor molecules in the membrane of the target cell (figure 1.1). Some neurons emit action potentials constantly, at rates of 10 -



100 per second, usually in irregular patterns; other neurons are quiet most of the time, but occasionally emit a burst of action potentials (Kandel et al. 2013).

The brain functions depend on the ability of neurons to communicate (The Society for Neuroscience 2002). Thus, the brain activity is controlled by a variety of biochemical and metabolic processes, mainly due to the interactions that take place at synapses.

Figure 1.1. Neuronal communication. A neuron fires by transmitting electrical signals along its axon. When signals reach the end of the axon, they trigger the release of neurotransmitters that bind to receptor molecules of adjacent neurons. Adapted from (The Society for Neuroscience 2002).

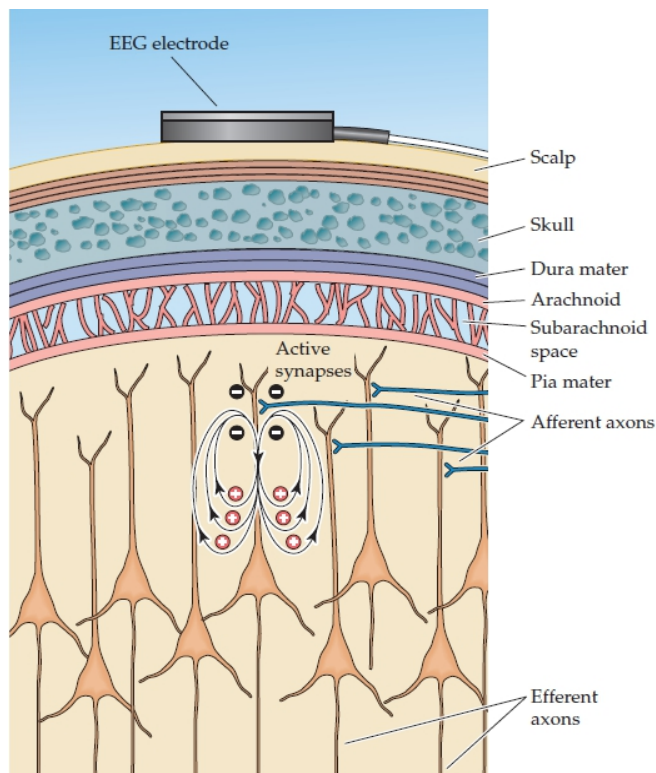
1.1.1. How to measure brain activity

Brain activity is measured based on changes in the membrane potential of activated neurons or, indirectly, based on changes in energy metabolism required to activate neurons using electrophysiological techniques or imaging techniques, respectively (Carter & Shieh 2010; Crosson et al. 2010). Electrical, magnetic or metabolic variations can be invasively or non-invasively recorded. The invasive recordings consist in measuring the brain electrical activity on the surface of the cortex (electrocorticography, ECoG) or within the cortex

(action potentials; local field potentials, LFP). Non-invasive recordings are obtained as electrical activity from the scalp (electroencephalogram, EEG), magnetic field fluctuation (magnetoencephalogram, MEG) or hemodynamic/metabolic changes (functional magnetic resonance imaging, fMRI; functional near infrared spectroscopy, fNIRS; positron emission tomography, PET). As the studies of this thesis were based on EEG and fMRI data, these techniques are briefly described below.

A) Electroencephalography

When a large number of neurons are synchronously active, the electric fields that they generate as result of the electrochemical processes used for signaling can be large enough to reach the scalp surface and can be measured using EEG (Berger 1929; Niedermeyer & Lopes Da Silva 2005). The EEG systems record over time the electric field generated by neural activity through electrodes attached to the scalp (figure 1.2). The electrodes placed at



standard positions according to the 10-20 international system (or extended versions of this standard) record the difference in potential between this electrode and a reference one (Chatrian et al. 1985; Jasper 1958; Oostenveld & Praamstra 2001).

Figure 1.2. The electroencephalogram (EEG) measurement principles. The EEG electrode measures a synchronous signal as result of the activity of a large number of neurons similarly responding at more or less the same time in the underlying regions of the brain, each of which generating a small electrical field that changes over time. The neural activity makes the more superficial extracellular space negative with respect to deeper cortical regions. Reproduced from (Purves et al. 2004).

The recorded brain waves reflect rhythmic fluctuations in the excitability of underlying neuronal populations. These cortical oscillations vary according to the brain state and function and have been linked to many cognitive and behavioral processes (Buzsáki 2006; Niedermeyer & Lopes Da Silva 2005). Several waves oscillating at specific frequency

ranges have been consistently observed: delta (less than 3 Hz), theta (4-8 Hz), alpha (8-12 Hz), beta (12-30 Hz) and gamma (higher than 30 Hz).

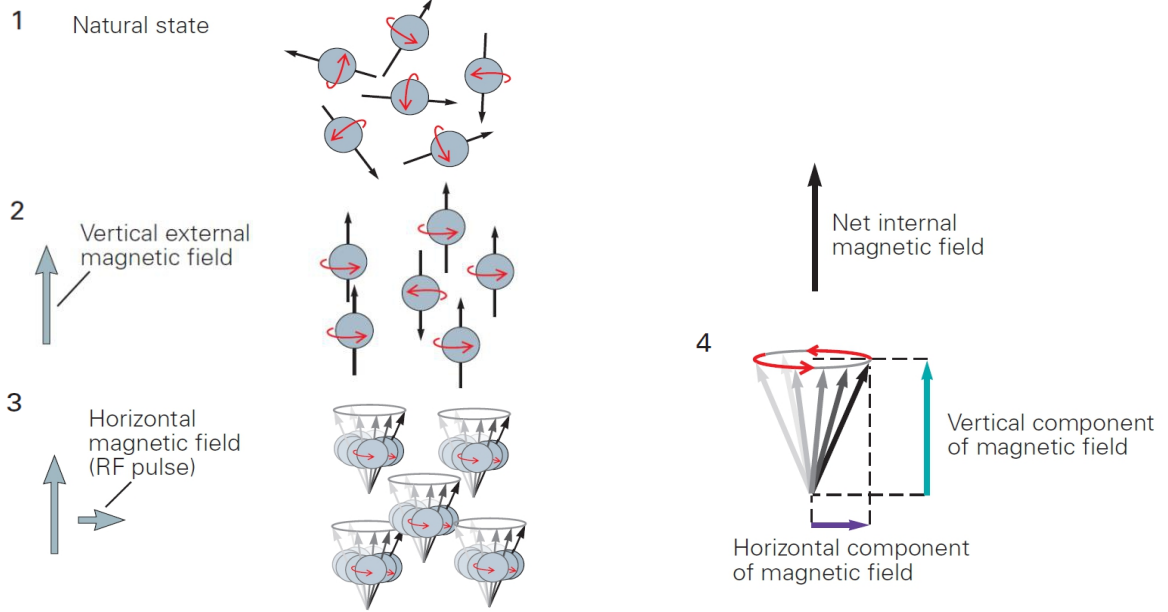
EEG devices are simple, relatively low cost, and safe, with a measurement preparation relatively fast and high temporal resolution. However, EEG presents some limitations, namely, limited frequency range, low spatial resolution, and susceptibility to several types of artifacts. An EEG electrode measures the potentials resulting from the summation of the synapses of a large number of neurons under the area beneath the surface of the electrode and, from surrounding regions up to 10 cm due to volume conduction in the skull and scalp (Srinivasan 1999), resulting on a mixing of brain components coming from different neurophysiologic sources. Furthermore, the combined effect of the skull signal attenuation, the noise sources as neurophysiologic artifacts and external electromagnetic interferences, further degrade the quality of the signals.

B) Functional MRI

The nuclei rotation of some atoms in the body acts as a small spinning magnet, normally with random directions so the tissue essentially has no net magnetization. However, when placed in a strong magnetic field they will line up with the field and spin at a frequency that is dependent on the field strength (Bloch 1946; Purcell et al. 1946). This is the base of the magnetic resonance imaging (MRI) (Brown et al. 2014).

Applying a short radiofrequency (RF) pulse tuned to the spinning frequency of the atoms nuclei causes them to become unaligned with the field. Summed across all of the individual nuclei, this process creates a rotating magnetic field that changes in time (figure 1.3-A). Then, turning off the RF pulse the atoms nuclei gradually realign themselves with the field emitting energy in an oscillatory way. It is this alternating electric current that is measured in MRI (figure 1.3-B). The amplitude of the measured electric current varies over time at a rate that is dependent upon a number of factors, including the type of tissue in which the nuclei are embedded. Thus, differences in tissue type appear as different intensities in the resulting images. Furthermore, using magnetic gradients, i.e. magnetic fields in which the strength of the field changes gradually along an axis, makes possible to obtain three-dimensional MRI images (Lauterbur 1973). Almost all MRI scanners create images based on the distribution of water in different tissues using detectors tuned to the radio frequencies of spinning hydrogen. By changing the scanning parameters, images based on a wide variety of different contrast mechanisms can be generated (Brown et al. 2014). The MRI allows to

A Magnetic resonance



B Relaxation processes emphasized in MRI

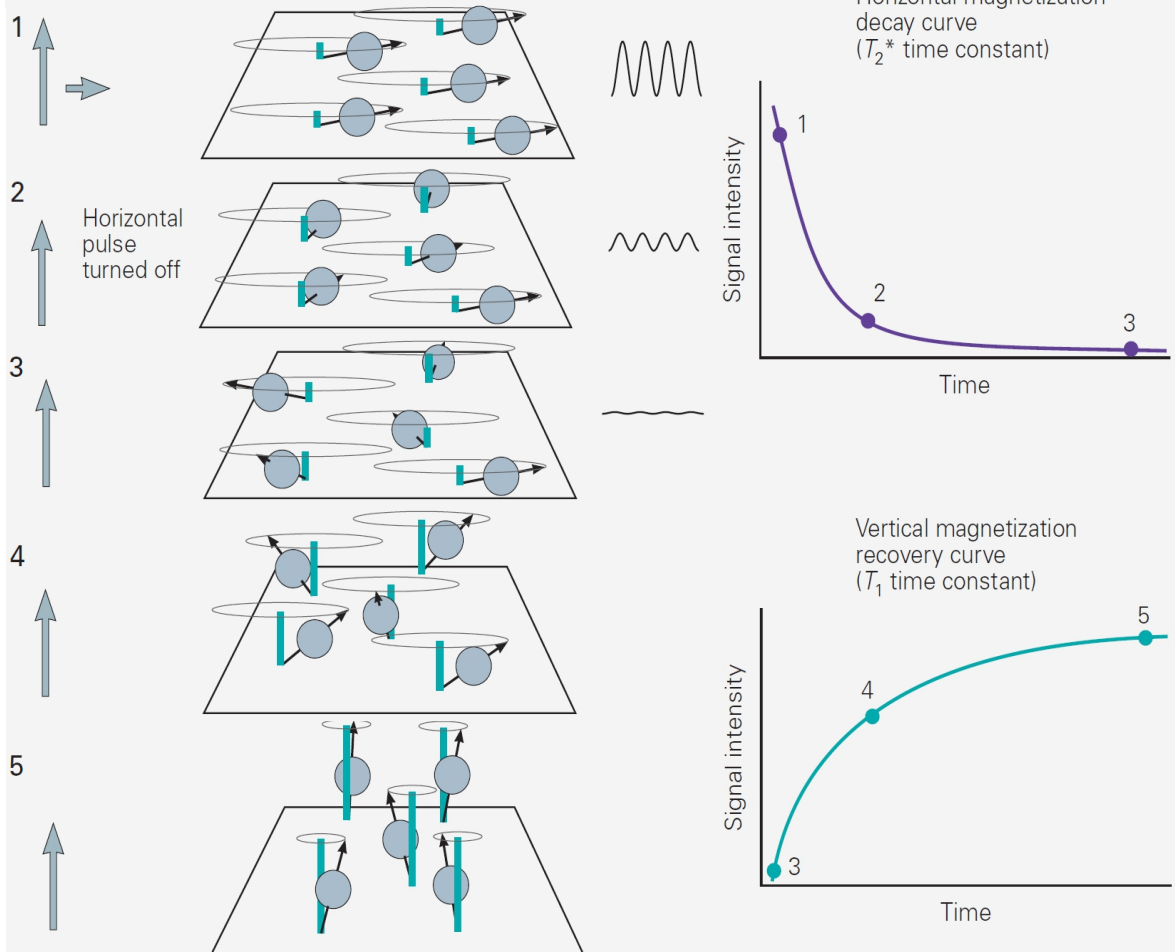


Figure 1.3. Magnetic resonance imaging (MRI). A. Protons act as a small spinning magnet with random direction (1). When placed in a magnetic field the protons align with it (2). A RF pulse applied in a different

direction makes the protons precess around their own axes (3). Summing these individual effects creates a net magnetic field variable in time and the signal measured in MRI is originated (4). **B.** With the protons aligned vertically, a horizontal RF pulse is applied (1). Turning off the RF pulse, protons continue to precess (2). Then occurs a relatively quickly dephasing that leads to a decay in the measured current with a time constant called T2 and the protons realign with the vertical magnetic field. The time constant of this recovery process (slower than the dephasing) is called T1 (3-5). To yield a time series of measurements that reflect changes in rates of decay and recovery, the entire process should be repeated. Adapted from (Kandel et al. 2013).

construct detailed images of the brain with high spatial resolution. Moreover, the strong magnetic field and RF pulses used in MRI scanning are harmless. Thus, the MRI is considered a relative safe and versatile technique.

The energy consumption of the brain does not vary greatly over time, but active neurons with high metabolic demands receive more blood than relatively inactive neurons due to the required energy on the electrochemical processes that underlie synaptic activity and action potentials. When a brain area is activated it begins to use more oxygen and within seconds the flow of oxygen-rich blood to this area increases. The fMRI technique is based on the detection and mapping of these local metabolic changes in cerebral blood flow (Buxton 2009). The changes in the concentration of oxygen and blood flow allow to detect blood oxygenation level-dependent (BOLD) changes in the magnetic resonance signal (Kwong et al. 1992; Ogawa et al. 1990). fMRI takes advantage of the fact that oxyhemoglobin and deoxyhemoglobin have different magnetic properties. When oxygen is extracted from the hemoglobin, the iron (that is also contained in hemoglobin) is exposed and introduces inhomogeneity in the nearby magnetic field. Greater inhomogeneity causes in the atoms nuclei a faster desynchronization and consequently, a shorter decay time. Thus, an increase of oxyhemoglobin in areas with greater neural activity, results in a longer decay time due to the higher homogeneity in the magnetic field (figure 1.4).

Compared to EEG it has better spatial resolution. However, it presents poorer temporal resolution, in the order of seconds, i.e., BOLD signal is observed only a few seconds after the neural activation due to the characteristics of the hemodynamic response function in the brain.

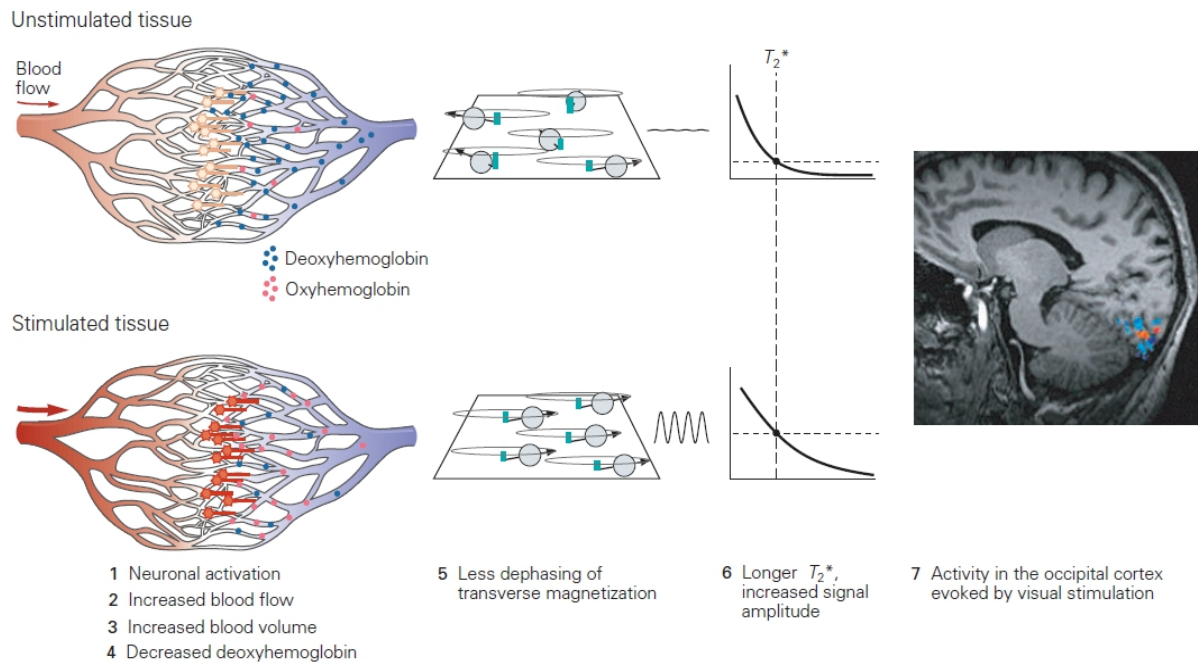


Figure 1.4. Functional magnetic resonance imaging (fMRI). The increase in neural activity results in a decreasing in deoxyhemoglobin concentration (due to the increased blood flow) causing dephasing to occur slower, hence slowing down the decay of the measured electric current. The fMRI image shows the locations of metabolic activity based on the changes in deoxyhemoglobin concentration. Colors in the fMRI image indicate regions that responded to stimuli. Reproduced from (Kandel et al. 2013).

1.1.2. How to decode brain activity

The content of different mental processes can be decoded from functional brain imaging measures of the human brain activity. Different activity patterns can reveal how a particular perceptual or cognitive state is encoded in brain (Haynes & Rees 2006).

A) Univariate analysis

In conventional functional neuroimaging approaches, the brain regions activated in association with specific stimulus or task are identified, i.e. the brain locations where the signal changes are significantly correlated with the experimental paradigm are determined. The statistical analysis of fMRI and EEG data is often carried out through univariate approaches (Haynes & Rees 2006; Tong & Pratte 2012). Brain activity from diverse locations is repeatedly measured and then the data from each location are analyzed separately. This yields a measure of any differences in activity, comparing two or more mental states at each individual sampled location. The analysis of one location has no impact on the analysis of any other.

The fMRI analyses are usually based on the general linear model (GLM) (Friston et al. 1995). In this approach, univariate statistical tests are applied at each location of the brain individually and the statistical parameters are then plotted at each position of the brain. First, one creates a standard design matrix (per voxel) whose columns correspond to each regressor (experimental condition or factor that may confound the results). These are created by convolving onsets of each condition of the experimental task with a fixed model of the hemodynamic response function (HRF; an estimate of the fMRI signal change evoked by a burst of neural activity (Boynton et al. 1996)). Then the GLM is conducted facilitating parameter estimations and a wide range of hypothesis testing (as for example, t test or correlation analysis). Voxels that exceed a predefined level of significance will be labeled as active voxels. The GLM approach is highly suitable when the aim of a study is to assess whether the activity level at a single location in the brain is modulated by a specific mental operation (Woolrich et al. 2009), after correction for the massive multiple comparison problem.

In the single-channel EEG analysis, information on the start time and sampling rate of the data collection can allow one to visualize the univariate time series graphically as function of time over the entire duration of data recording. The information contained in the recorded EEG signal can also be encoded through the amplitude and the phase of the subset harmonic oscillations over arrange of different frequencies. The most commonly used measures for EEG univariate analysis are based on the Fourier transforms and the Wavelet transforms that allow to calculate the power spectrum of one or more channels (Niedermeyer & Lopes Da Silva 2005; Tong & Thakor 2009).

The main advantages of univariate analysis approaches are the computational simplicity and the reasonably effective methods. While this is a natural way to seek functional localization, such approach by definition ignores cooperative interactions among brain regions and ignores subtle responses to particular conditions or covariates that might carry some important information. Therefore, multivariate analysis emerged as a potential complementary approach to the univariate analysis (Cox & Savoy 2003; Haynes & Rees 2006; Lemm et al. 2011).

B) Multivariate analysis

Multivariate analyses take into account multiple variables and distributed patterns, simultaneously. This is used to consider the interactions between the locations (activity in a

single location interpreted as an original feature) and how they relate rather than looking at individual channels/voxels. Given the goal of detecting the presence of a particular mental representation in the brain, the primary advantage of multivariate methods over univariate methods is the increased sensitivity. Multivariate approaches extract the information contained in the patterns of activity among multiple brain locations and across multiple identified features so that the relative differences in activity between different locations/features can provide relevant information. Critically, multivariate methods might be able to tell apart the activity patterns for two different conditions even when the data, as projected along any individual dimension, are statistically indistinguishable (figure 1.5) (Cox & Savoy 2003).

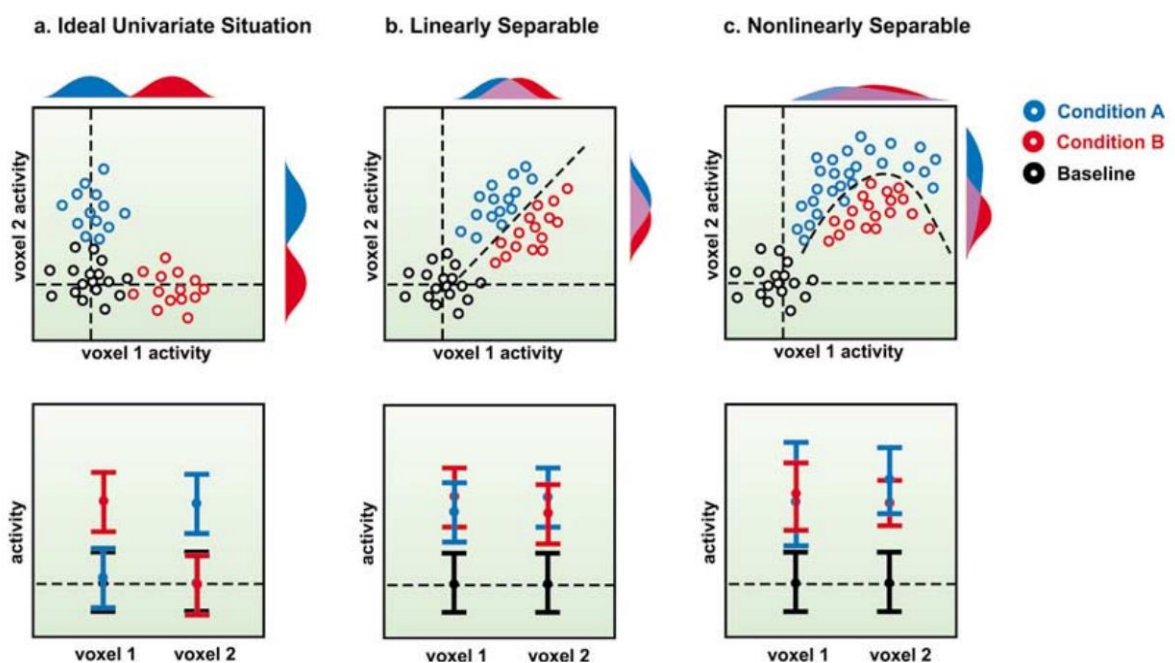


Figure 1.5. Multivariate versus univariate analysis using as example fMRI data. In the graphs the circle corresponds to acquisitions and the colors represent experimental conditions. The colored, filled curves on the right and above the graphs represent the data distribution. (a) In an ideal univariate situation the projected distributions do not overlap, and thus a univariate analysis perfectly discriminates between the two conditions. There is a clear mapping between location and condition. Error bars show that Voxel 1 is significantly more active during Condition A than baseline, but is not active during Condition B. Similarly, Voxel 2 is active during Condition B, but not during Condition A. In (b) both voxels are active relative to baseline during both Condition A and Condition B, but there is no clear mapping between voxel and condition. However, it is obvious that the data from each condition occupy a distinct region of the two-dimensional space and that one need only draw a line between the data clouds to distinguish them. Linear classifiers can perform this basic partitioning of space drawing hyperplanes between different classes of data. (c) Nonlinear classifiers take this basic idea one step further by allowing decision boundaries to take forms other than straight lines or hyperplanes. Reproduced from (Cox & Savoy 2003).

Modern machine learning and pattern recognition algorithms allowed for the development of current multivariate analysis methods (Duda et al. 2001). Based on these

methods the brain states discrimination can be treated as a classification problem (Haxby et al. 2001). Figure 1.6 summarizes the most common pattern recognition algorithms steps. Initially, the raw data are pre-processed in order to reduce the effects of noise and labeled according to the corresponding experimental condition. Then, relevant features are extracted and selected, reducing the complexity of the data set and increasing the capabilities of the prediction scheme. The data are divided into a training set and a testing set: information from the training set is used to train a classifier that maps between brain patterns and experimental conditions. The prediction is performed using the trained model on a new data set (Formisano et al. 2008; LaConte 2011; Lemm et al. 2011; Norman et al. 2006; Pereira et al. 2009).

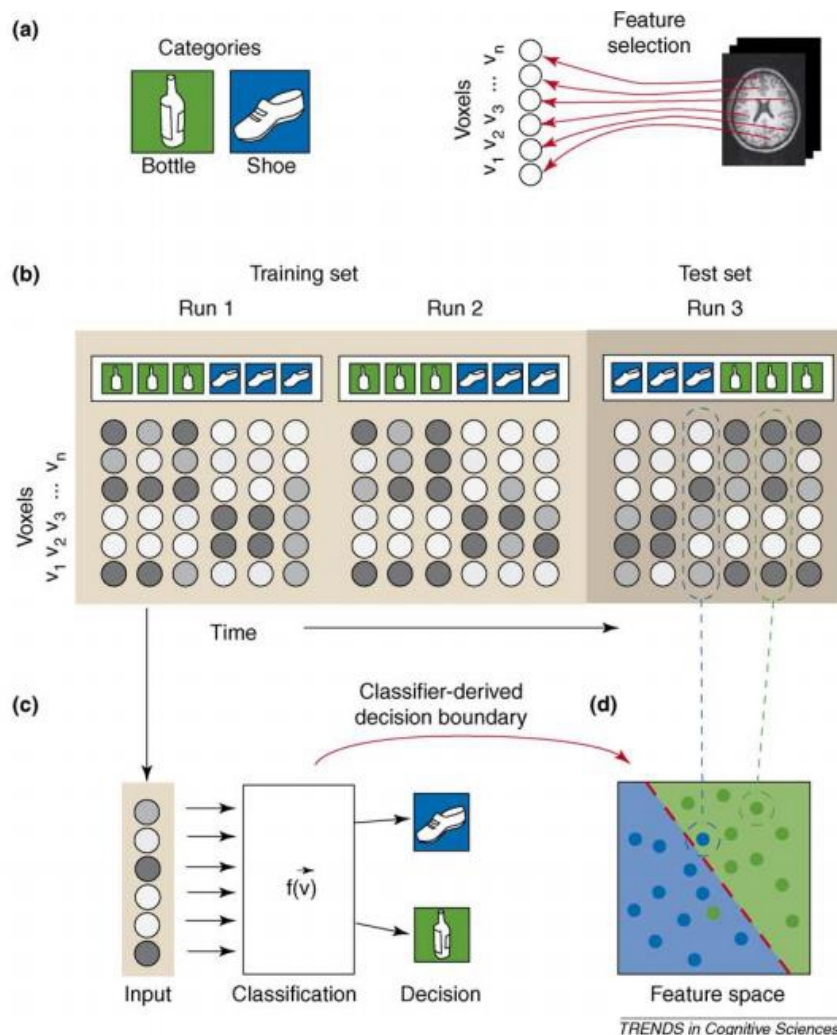


Figure 1.6. General pattern recognition algorithms structure (example). (a) Subjects are presented with different stimuli conditions. After the pre-processing of the raw data, features are extracted and selected to determine which patterns are relevant in the classification analysis. (b) The data are divided into a training set and a testing set. (c) Patterns from the training set are used to train a classifier. (d) The trained classifier function defines a decision boundary (red dashed line, right) in the high-dimensional space of voxel patterns (collapsed here to 2-D for illustrative purposes). Each dot corresponds to a pattern and the color of the dot

indicates its category. The background color of the figure corresponds to the guess the classifier makes for patterns in that region. Reproduced from (Norman et al. 2006).

The BCI development driven technology in this field (Dornhege et al. 2007; Birbaumer 2006). A wide range of methods improvements focused in neuroscience have emerged as dimension reduction and projection methods (De Martino et al. 2008; Hyvarinen et al. 2001; Mørup et al. 2008; Parra et al. 2003; von Bünau et al. 2009), classification methods (Müller et al. 2003; Ray et al. 2015; Tomioka & Müller 2010), spatio-temporal filtering algorithms (Blankertz et al. 2008; Dornhege et al. 2006), synchrony, coherence or causal measures (Marzetti et al. 2008; Meinecke et al. 2005; Nolte et al. 2008; Reid et al. 2016; Wang et al. 2015) and new source localization techniques (Haufe et al. 2008; Noirhomme et al. 2008).

1.2. From brain-computer interfaces to neurofeedback

Although early studies in animals (Fetz 1969; Wyrwicka & Serman 1968) and humans (Kamiya 1969) had shown that neural signals can be translated into feedback, the first BCI study was published by Jacques Vidal in 1973, when he developed a system that could translate EEG signals into computer commands (Vidal 1973). A BCI system measures and convert brain signals into artificial outputs. These systems enable users to act on the world by using their brain signals rather than the brain's normal output pathways of peripheral nerves and muscles. After a training period, the user is able to generate brain signals that encode an intention and the BCI system is able to decode the user brain signals and translate them into device commands that accomplishes the user's intention (Shih et al. 2012).

The BCI systems can be applied as assistive BCIs or as NF approaches (Chaudhary et al. 2016). The assistive BCIs aim to support the daily life of users that lost for example motor or communication functions (McFarland & Wolpaw 2011). These systems are applied to substitute the lost functions enabling for example the control of robotic devices. On the other hand, the NF systems aim to facilitate the restoration of brain function and/or behavior or improve it by self-regulation of brain activity (Thibault et al. 2016). Furthermore, the scope of BCI research can include non-medical applications as user state monitoring and gaming (Lécuyer et al. 2008).

Through NF approaches human subjects can use BCI systems to learn self-regulation of brain activity. Self-regulation of the brain signal offers new ways to study the relation between behavior, brain function, and brain activity. Thus, the NF became an interesting experimental approach in cognitive neuroscience (Weiskopf, Scharnowski, et al. 2004). In

contrast with conventional studies where brain activity is analyzed as a dependent variable on the effect of stimulation or behavior, the NF experiments use the self-regulated brain activity as independent variable allowing to study the effects of volitional neuromodulation on behavior. Modern imaging technologies of the living human brain (e.g., real-time fMRI) and increasingly rigorous NF research protocols and BCI methodologies facilitate more effective applications (Larsen & Sherlin 2013; Sreedharan et al. 2013; Shih et al. 2012; Thibault et al. 2016).

The BCI progress has been driven not only by the development of new analysis techniques but also by an increase in the number of available techniques to record invasively or non-invasively different brain signals. The general BCIs principles are similar for the different systems (Min et al. 2010; Naci et al. 2012; Wolpaw et al. 2002). The BCI cycle (figure 1.7) starts with the user engaging in a task, in the presence or absence of a sensory stimulation. The brain signals are acquired and processed in real-time to extract specific features that reflect the user's intent and then translated into specific commands to an external device. The BCI components are controlled by an operating protocol that defines the operations timing and the details of signal processing, commands and performance.

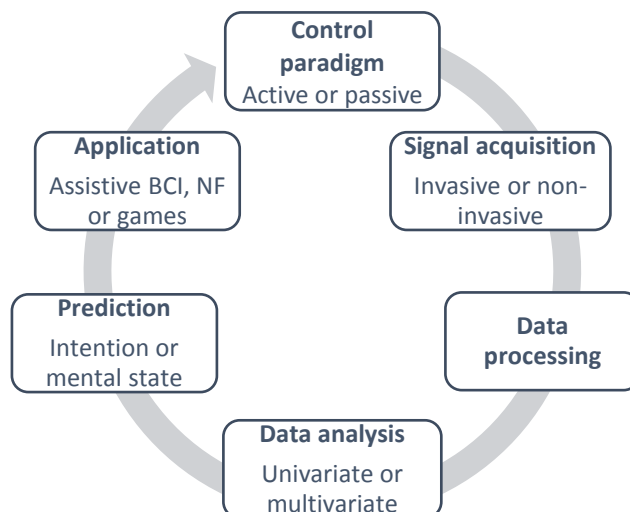


Figure 1.7. Overview of a brain–computer interface (BCI) system. Typically, a BCI system involves online processing and analysis of user's brain responses (invasively or non-invasively acquired), produced either voluntarily (active), or in response to sensory stimulation (passive), to infer a desired command that reflects the user's intention or mental-state to apply in assistive systems, neurofeedback approaches or gaming.

1.2.1. State-of-the-art of neurofeedback systems

NF draws on diverse functional brain imaging methods to help drive brain activity volitional control feeding back to the users information about their own brain activity (Thibault et al.

2016). The first attempt of self-regulation of human brain activity was reported in 1969 (Kamiya 1969). On that study it was shown a quick learning of alpha waves modulation by healthy subjects when receiving a continuous sensory feedback about their brain activity. These findings in combination with similar results from animal studies (Fetz 1969) triggered extensive NF-based research into the link between brain physiology and behavior. These reports also corroborated the notion of brain plasticity creating hope for the treatment of neurological and neuropsychiatric disorders with learned self-regulation of the disordered brain activity (Birbaumer et al. 2013; Thibault et al. 2015).

The NF studies were primarily based on EEG recordings focusing mainly on self-regulation and feedback of frequency bands such as slow cortical potentials (Egner & Gruzelier 2003; Elbert et al. 1980; Kotchoubey et al. 2001; Rockstroh et al. 1984; Rockstroh et al. 1993; Strehl et al. 2006), sensorimotor rhythm (Vernon et al. 2003), theta (Leins et al. 2007), alpha (Lynch et al. 1974; Zoefel et al. 2011) or gamma (Keizer et al. 2010) bands. EEG-based NF has been suggested to treat a range of psychological and neurological disorders as epilepsy (Tan et al. 2009), attention deficit hyperactivity disorder (Arns et al. 2014; Ordikhani-Seyedlar et al. 2016), pain (Hasan et al. 2016), depression and anxiety (Hammond 2005), alcohol addiction (Lackner et al. 2015), autistic spectrum disorder (Coben et al. 2010), Alzheimer (Luijmes 2016) and stroke (Kober et al. 2015; Ramos-Murguialday et al. 2013). It has also been tested to improve the performance (Gruzelier 2014; Vernon 2005) of healthy volunteers in vision (Nan et al. 2013), motor learning (Ros et al. 2014; Rozengurt et al. 2016), memory (Reiner et al. 2014; Wang & Hsieh 2013) and cognitive processing speed (Angelakis et al. 2007). However, EEG-based NF is limited by its low spatial resolution and by the inability to access deeper brain structures. In this sense, the advent of new technologies for non-invasive functional imaging of the living human brain, as fMRI, MEG and fNIRS, has vastly expanded the scope of NF studies (Buch et al. 2008; Sitaram et al. 2007; Weiskopf, Scharnowski, et al. 2004).

Current NF approaches can be based on electromagnetic or hemodynamic signal based training. The imaging method to use should be selected according to the particular research question of each study. Whereas EEG and MEG have poor spatial resolution but millisecond temporal resolution, fMRI has millimetric spatial resolution yet poor temporal resolution, and fNIRS has both poor spatial and temporal resolution (Birbaumer et al. 2009; Thibault et al. 2016). EEG represents a low-cost and potentially mobile option. Although less affected by the resistive properties of the skull than EEG, MEG is very sensitive to

noise of environmental magnetic fields, with non-portable hardware and expensive acquisition and maintenance. fNIRS represents a comparably mobile and cost effective measurement modality. As is the case with fMRI BOLD measurements, the recorded events lag neural activity by several seconds, but the temporal resolution of NIRS is higher (usually is in the order of 100 ms).

In contrast to all other non-invasive BCI measures, when using real-time fMRI the regulation of circumscribed cortical and subcortical structures is possible (Caria et al. 2012; Scharnowski & Weiskopf 2015; Weiskopf, Scharnowski, et al. 2004; Weiskopf 2012). The opportunity to train localized and functionally specific brain activity can improve the understanding on the function of targeted brain areas. Figure 1.8 illustrates some of the mostly targeted brain regions in fMRI-based NF studies (Scharnowski & Weiskopf 2015). The majority of studies described in the literature have used fMRI-based NF for training healthy individuals to self-regulate the brain activity in areas related with motor performance (Berman et al. 2012; Blefari et al. 2015; Bray et al. 2007; Chiew et al. 2012; DeCharms et al. 2004; Hui et al. 2014; Johnson et al. 2012; Scharnowski et al. 2015; Yoo et al. 2008; Zhao et al. 2013), emotional processing (Caria et al. 2007; Caria et al. 2010; Grone et al. 2015; Hamilton et al. 2011; Lawrence et al. 2014; Mathiak et al. 2015; Posse et al. 2003; Sarkheil et al. 2015; Veit et al. 2012; Weiskopf et al. 2003; Zotev et al. 2011), memory (Scharnowski et al. 2015; Weiskopf, Mathiak, et al. 2004; Zhang et al. 2013), visual sensitivity (Scharnowski et al. 2012), linguistic processing (Rota et al. 2009) and auditory performance (Yoo et al. 2006).

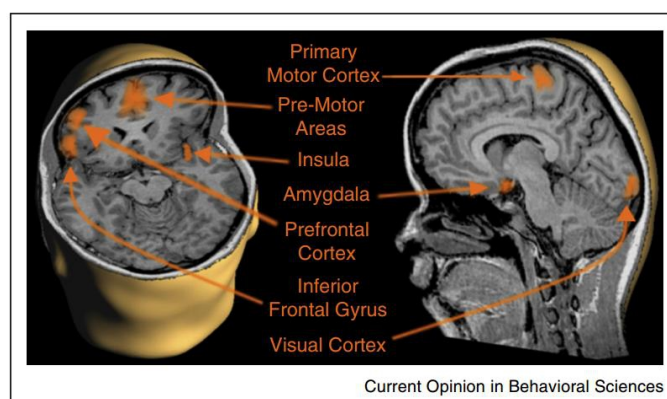


Figure 1.8. Illustration of some of the brain regions most used in neurofeedback studies based on functional MRI. Reproduced from (Scharnowski & Weiskopf 2015).

The behavioral modifications induced by NF training in healthy subjects led to efforts for testing this methodology in clinical populations. The fMRI-based NF effect has been studied

in several clinical domains, including pain regulation (DeCharms et al. 2005; Guan et al. 2015), tinnitus (Haller et al. 2010), Parkinson's disease (Subramanian et al. 2011; Subramanian et al. 2016), depression (Linden et al. 2012; Young et al. 2014; Zotev et al. 2016), stroke (Liew et al. 2016; Sitaram et al. 2012), schizophrenia (Cordes et al. 2015; Dyck et al. 2016; Ruiz et al. 2013), addiction (Canterberry et al. 2013; Karch et al. 2015; Kim et al. 2015; Li et al. 2013), psychopathy (Sitaram et al. 2014), post-traumatic stress disorder (Gerin et al. 2016) and phobia (Zilverstand et al. 2015). The NF approaches based on fMRI measurements represent a powerful tool to explore the mechanisms underlying BCI training effects and the relation between brain functions and behavior, but due to its expensive use and complex hardware may not be feasible to apply in large groups (Birbaumer et al. 2009; Thibault et al. 2016).

A new trend of fMRI-based NF studies is to assess the effects of self-regulation and learning of self-regulation on brain functional connectivity. The results have been indicating that NF training leads to specific changes in connectivity of the target region. Furthermore, the feasibility of NF training based on the functional connectivity between different brain areas and the distributed brain networks has been tested, as it may allow a better representation of brain physiology (Ruiz et al. 2014). The availability of higher magnetic fields (e.g., MRI scanners operating at seven tesla) and the detailed functional information that can be provided is also raising interest amongst researchers (Grone et al. 2015).

1.2.2. Neurofeedback system setup

Researchers have developed distinct NF experimental protocols according to each imaging modality for appropriate brain signals and physiological processes assessment. However, the basic methodological steps (figure 1.9) do not strongly change according to the functional imaging methods used in each NF approach.

NF systems are based in three main elements: the brain signal acquisition, the real-time data processing and analysis, and the feedback. Following previous instructions about the NF study, participants should be engaged in a mental strategy to self-regulate their brain activity. During hemodynamic training, the real-time data analysis quantifies the strength of brain activity from a specific brain region or network, or the connectivity between different regions (Ruiz et al. 2014; Sulzer et al. 2013). On the other hand, the vast majority of studies, during electromagnetic training the real-time data analysis extracts the power of a specific

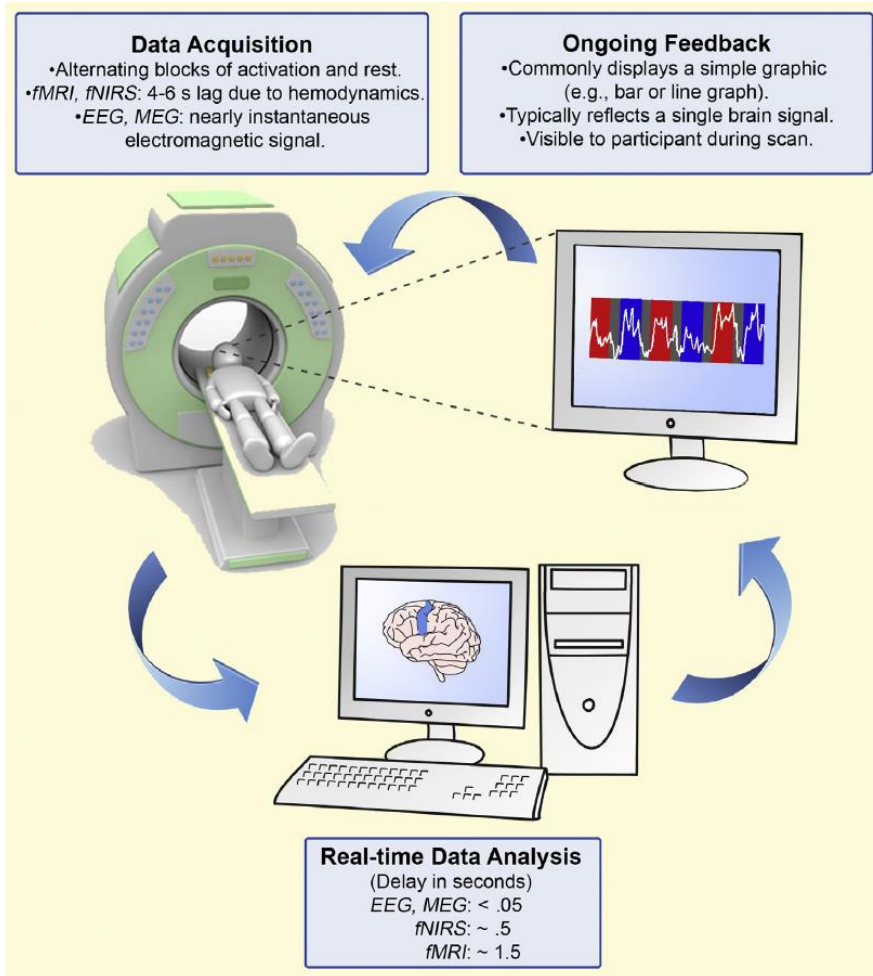


Figure 1.9. Basic setup of a brain-computer interface (BCI) when used as a neurofeedback (NF) approach. Ongoing brain signals from the participant, engaged on a specific mental process, are acquired, processed, and presented as feedback (visual, auditory or haptic). The feedback can reflect signals changes in a specific brain region or EEG channel, or more complex measures considering simultaneously information from different brain regions, channels or frequency-bands. Reproduced from (Thibault et al. 2016).

frequency-band from one or more channels, but more complex features as the power ratio between frequency-bands can also be used (Huster et al. 2014). When a BCI is applied as NF, the feedback variations represent the external device response to the command that translate the users' intention. Thus, the NF training is considered an operant or instrumental conditioning procedure (Birbaumer et al. 2013). The feedback informs the participants about relevant changes in their own brain states and can be provided as a simple increase/decrease in levels of displayed thermometer, by mean of a sound, or in the form of a complex and immersive virtual reality environment. There is a delay between the feedback presented and the participant mental state that depends on the nature of the used brain signals (Thibault et al. 2016).

Each NF study needs to be designed according to its experimental goals. The research questions may range from test the NF induced learning of brain activity self-regulation to demonstrate behavioral effects or test the possibility of NF as treatment in clinical groups (Sulzer et al. 2013). In general, the NF experimental framework starts with the definition of the physiological target and response to be trained. Then, the feedback training runs are performed, which may span several minutes with repetitions in the same session, or repeated sessions over days. When the participants have achieved successful brain activity self-regulation, they are tested to demonstrate whether they are able to maintain the skill of controlling their own activation in the absence of feedback. All NF studies need to employ different control groups or within subject control conditions to control for confounds in learning, behavioral and placebo effects. Furthermore, if the research goals include to study behavioral or clinical improvements specific tests to the participants need to be done before and after learning (Thibault et al. 2016; Weiskopf 2012).

There is no optimal study design for the NF experiments. Although the common basic elements, questions related with the run and blocks length, the given instructions for the neuromodulation strategies (if implicit or explicit), the way to calculate and present the feedback and the type of feedback (continuous or intermittent) are still remaining and a matter for debate. New tests are required to fine-tune various parameters, and to maximize learning and robustness (Sulzer et al. 2013; Thibault et al. 2015).

1.2.3. Brain activity control levels based on self-regulation

Typically, the self-regulation strategies are based in mental tasks to up-regulate and down-regulate the brain activity (Thibault et al. 2016). In most cases, participants receive (before the experiment) examples of possible strategies to influence their brain signal, and then the online feedback allows them to adapt the strategy to voluntarily control brain activity. With the help of the feedback and by trial and error, participants learn to increase and decrease the activity in the targeted brain region (figure 1.10).

Studies in the literature have shown positive results for the volitional control of targeted activity if the feedback is presented in an understandable way and if they are given at least a suggestion of a possible strategy on how to control the brain activity (Ruiz et al. 2014). The process of learning to control a specific brain activity is difficult and demanding. Thus, offering a strategy or a couple of strategies might help participants acquiring brain activity control quicker and more successfully (Sulzer et al. 2013). Furthermore, the cognitive

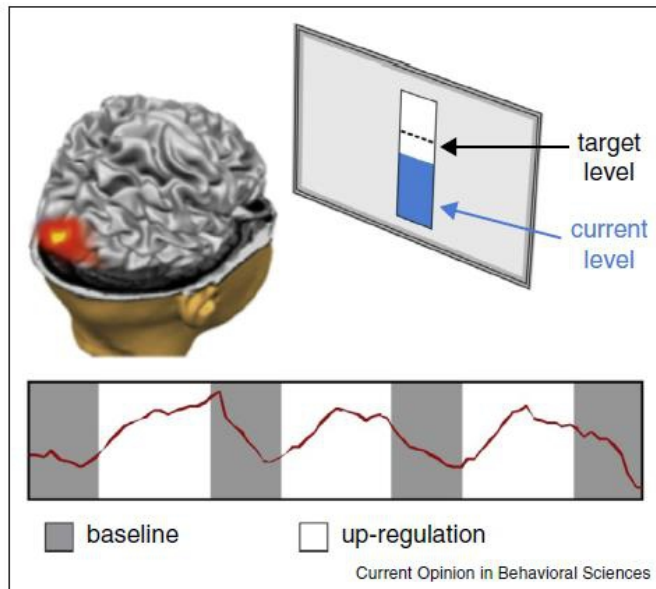


Figure 1.10. Typical brain activity self-regulation training during a neurofeedback experiment. The training runs are composed of baseline blocks and up-regulation blocks. During the up-regulation blocks the participants should increase activity in the targeted brain region and during the baseline blocks the participants should down-regulate the targeted activity, i.e. they should decrease their brain activity in relation to the levels of activation achieved in the previous block. The feedback is presented to the participants via a thermometer icon, for example. Reproduced from (Scharnowski & Weiskopf 2015).

capacity and the attention span also influence the self-regulation training success. Thus, until now the BCI studies using the brain activity self-regulation to encode the user's intention are only based on binary control over a specific brain activity: the users are able to encode two commands based on the increasing and decreasing of a specific brain activity, the activity from a brain region or the power of a specific frequency-band, for example. The most explored self-regulation strategies are based on motor imagery and in recalling emotionally relevant experiences (Huster et al. 2014; Ruiz et al. 2014).

When more than two commands are desired, the users can train the self-regulation of different brain activity patterns. Multiclass control systems are possible, but often only with two levels of control within each class. Users can train the ability of volitional binary control of different brain regions, different frequency-bands or the same frequency-brand but from different brain locations. For example, Lee et al. (2009) presented a real-time fMRI-based BCI to control a 2-dimensional movement of a robotic arm. The subjects were engaged in the right- and/or left-hand motor imagery tasks and the signal originating from the corresponding distinct left and right hand motor areas was translated into horizontal or vertical robotic arm movement. Already in 2004 Yoo and colleagues shown that a multiclass control approach based on self-regulation is possible by exploring different types

of mental tasks, such as mental imagery (right and left hand motor imagery) and covert cognitive tasks (mental speech generation and mental calculation). Both different spatial distribution of activation and its self-regulation allowed spatial navigation in four directions by thoughts (Yoo et al. 2004). More recently, a spelling device based on self-regulation of BOLD activity was presented (Sorger et al. 2012). 27 distinguishable hemodynamic activation patterns were achieved by exploiting spatiotemporal characteristics of hemodynamic responses, evoked by performing differently timed mental imagery task. Participants voluntarily influenced the location of the signal source by performing three different mental tasks (motor imagery, inner speech and mental calculation), influencing the signal onset delay by delaying the start of the mental task as well as the signal duration by varying the mental task duration.

Regarding the EEG based BCIs, Wolpaw & McFarland (2004) demonstrated that a noninvasive BCI using sensorimotor rhythms recorded from the scalp can provide multidimensional control. The participants were trained to self-regulate the amplitude of *mu* and beta frequency-bands over the right and left sensorimotor cortices using motor imagery to control a cursor movement in two dimensions. More recently this study was extended to self-regulation of a cursor movement in 3 dimensions: simultaneous control over vertical, horizontal and depth dimensions (McFarland et al. 2010). A similar approach was used in (LaFleur et al. 2013) to achieve control in three-dimensional space using motor imagery, but now with the support of offline training software and signal processing toolbox to select the most discriminant channels and frequency-bands. An example of a simple multiclass approach based on self-regulation is to use separately different motor-imagery tasks to encode different classes of one dimension control (Schlögl et al. 2005). The multiclass control based on brain activity self-regulation can also be based in other mental strategies, as for example visual imagery. In (Salari & Rose 2013) participants learned to selectively switch between modulating alpha-band or gamma-band oscillations with help of source-based BCI for NF training. Participants reported using a visual imagery strategy (visualizing a concrete figure, object or number at fixation) during the gamma periods and reported being relaxed during the alpha periods.

Only a few studies have attempted to achieve beyond binary control using brain activity self-regulation, i.e. achieve different levels of activity of the same pattern. The implementation of BrainPong, a variant of the classic computer game Pong using the local BOLD signal for control, suggested that with extensive practice subjects can learn to reach

and maintain intermediate levels of brain activity (Goebel et al. 2004). After a training period to modulate regional brain activity to reach specific target levels and to adapt to the hemodynamic response delay, subjects succeeded in controlling the up and down movement of the racket by regulating voluntarily the activity in the selected brain region. However, it is not completely clear the strategies applied by the users to encode the different game commands and which activity levels were achieved. There are few more studies (some of which preliminary reports) supporting the idea that humans are able to voluntarily reach different target levels by modulating their thoughts based on receiving neurofeedback (Dahmen et al. 2008; Sorger et al. 2004; Sorger 2010).

1.3. Goals and key contributions

The main goal of this thesis was to study the feasibility of increasing the number of levels of brain activity volitional control. We aim to test whether we can use volitional neuromodulation to increase the intrinsic number of levels of each class of BCI control. We looked for a strategy that allows to train participants to voluntary migrate between more than two levels of a specific brain activity, which could potentially be used as BCI input. This would allow to go beyond the binary control available until now, i.e. it would be possible not only up-regulate and down-regulate a specific brain activity but also achieve different levels of up-regulation. The volitional multilevel neuromodulation can contribute for more precise and efficient NF approaches or simply to improve the assistive BCI systems.

We decided to focus this work on visual motion imagery as a strategy for brain activity self-regulation due to its naturalistic and dynamic character. It can be used on a direct BCI, allowing the users to express their intentions in a much more natural way. For example, the visual imagery of a moving cursor could make the cursor of an external device move. Furthermore, the visual imagery can present therapeutic potential, for example in attentional disorders, when applied in NF training (Abraham et al. 2006). Also, we can take advantage of previous studies that have shown the reliable recruitment of the human motion complex, known as hMT+/V5 and specifically sensitive to moving objects' features, during visual stimulation or during visual motion imagery (Goebel et al. 1998; Kaas et al. 2010).

To achieve our final goal several intermediary steps needed to be done. The first step was to verify whether it is possible to achieve voluntary modulation of the chosen brain region by mean of NF training. To explore this question a study with fMRI-based NF was

performed, training the participants to up-regulate and down-regulate their own brain activity. We aimed to explore not only the proof-of-concept but also the neural circuit involved on the volitional neuromodulation process. The aim of the second step was to test whether it is possible to design a multilevel system of control based on volitional activity modulation of a specific brain region with at least 3 different levels. An extended version of the first fMRI-based NF study is driven aiming to train multilevel neuromodulation using three visual motion imagery strategies. The third step aimed the real-life transfer of the proposed multilevel neuromodulation approach, testing the three visual motion imagery strategies using EEG. We intended to verify whether the patterns of brain activity evoked according to each imagery task reflect a multilevel linear trend or at least present high potential of multiclass discrimination when tested using a classifier. The combination of all these exploratory studies also contributes for a better understanding of the neural correlates of cognitive control.

The fourth and last step of this work aimed to evaluate the possibility of a new multilevel NF approach using visual motion imagery strategies. We hypothesize that our perception of motion is reflected on the functional connectivity between different hMT+/V5 sub-domains. Thus the multilevel modulation of functional connectivity as function of perceptual decision training would be, at least theoretically, possible. The first work step on this direction is presented taking advantage of high-resolution 7 Tesla (7T) fMRI to explore the perceptual interpretation of visual motion. We wanted to know how bistable perceptual integration and segmentation of interhemispheric 1D directional cues is mapped in hMT+/V5 functional sub-domains. Moving from the macroscopic level neuroimaging (3 Tesla – 3T) to the mesoscopic level (7T) would lead to a deeper understanding of motion features representations and their interaction in the brain.

1.4. Thesis outline

The thesis is organized in six chapters, as illustrated in figure 1.11. The current chapter (chapter 1) introduces the topic of this thesis, by presenting the main concepts and methods behind the BCI systems and its application as NF approach, then the BCI-NF state-of-the-art and applications are briefly described, and finally the goals and main contributions of the research work are highlighted.

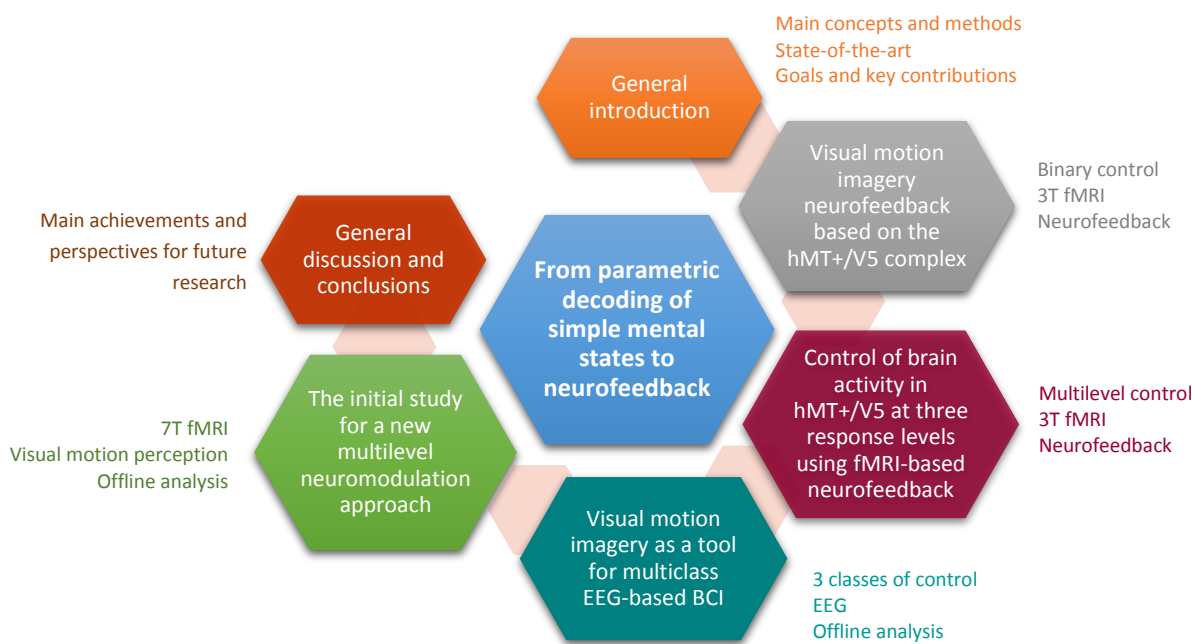


Figure 1.11. Thesis outline.

Chapter 2 presents a study that tested the feasibility of training healthy volunteers to up-regulate and down-regulate the activity in a specific brain region, the hMT+/V5 complex, using real-time fMRI-based NF and visual motion imagery strategies. The results indicated that hMT+/V5 is a region that can be volitionally modulated by focused imagery.

Chapter 3 describes a study where the hypothesis whether more than two modulation levels can be achieved in a single brain region was tested. Three control levels (two up-regulation levels and one down-regulation level) of brain activity in the hMT+/V5 complex were achieved using three distinct visual imagery tasks with different numbers of motion alternation combined with fMRI-based NF.

Chapter 4 presents a study that tested whether visual motion imagery can be used as a tool to achieve multilevel EEG-based BCI. The higher the alternating number of sensory/perceptual signals the stronger would be the expected neural response as demonstrated using fMRI. The hypothesis was that differential modulations, regardless of their polarity, should also be observed at the EEG domain. The results did not show the expected three levels of activity, but suggested the feasibility of visual motion imagery tasks as a simple tool to achieve BCI systems with three different classes of control within a small group of EEG channels.

Chapter 5 sets up a study for a future work: a new multilevel neuromodulation approach based on the connectivity between perceptual sub-domains of hMT+/V5. The final goal

would be to answer the question: can we volitionally control different levels of functional connectivity? The study here described is the first step needed to explore this question. It took advantage of high-resolution 7T fMRI to find evidence for the existence of perception related sub-domains in the hMT+/V5 region. These domains responded preferentially either to coherent or incoherent motion and have shown preferred axes of motion that matched the perceptual reports.

Finally, Chapter 6 provides a general discussion and conclusion on the achievements of the thesis and the perspectives for future research.

References

- Abraham, A. et al., 2006. Creative thinking in adolescents with attention deficit hyperactivity disorder (ADHD). *Child neuropsychology: a journal on normal and abnormal development in childhood and adolescence*, 12(2), pp.111–123.
- Angelakis, E. et al., 2007. EEG neurofeedback: a brief overview and an example of peak alpha frequency training for cognitive enhancement in the elderly. *The Clinical neuropsychologist*, 21(1), pp.110–29.
- Arns, M., Heinrich, H. & Strehl, U., 2014. Evaluation of neurofeedback in ADHD: The long and winding road. *Biological Psychology*, 95(1), pp.108–115.
- Bear, M.F., Connors, B.W. & Paradiso, M.A., 2016. *Neuroscience: Exploring the Brain* 4th Ed., Wolters Kluwer.
- Berger, H., 1929. Über des Elekrenkephalogramm des Menschen. *Arch Psychiat Nervenkr*, 87, pp.527–70.
- Berman, B.D. et al., 2012. Self-modulation of primary motor cortex activity with motor and motor imagery tasks using real-time fMRI-based neurofeedback. *NeuroImage*, 59(2), pp.917–925.
- Birbaumer, N., 2006. Brain-computer-interface research: Coming of age. *Clinical Neurophysiology*, 117(3), pp.479–483.
- Birbaumer, N. et al., 2009. Neurofeedback and brain-computer interface clinical applications. *International Review of Neurobiology*, 86, pp.107–117.
- Birbaumer, N., Ruiz, S. & Sitaram, R., 2013. Learned regulation of brain metabolism. *Trends in Cognitive Sciences*, 17(6), pp.295–302.
- Blankertz, B. et al., 2008. Optimizing spatial filters for robust EEG single-trial analysis. *IEEE Signal Processing Magazine*, 25(1), pp.41–56.
- Blefari, M.L. et al., 2015. Improvement in precision grip force control with self-modulation of primary motor cortex during motor imagery. *Frontiers in Behavioral Neuroscience*, 9(FEB).
- Bloch, F., 1946. Nuclear induction. *Physical Review*, 70(7–8), pp.460–474.
- Boynton, G.M. et al., 1996. Linear systems analysis of functional magnetic resonance imaging in human V1. *Journal of Neuroscience*, 16(13), pp.4207–4221.
- Bray, S., Shimojo, S. & O’Doherty, J.P., 2007. Direct instrumental conditioning of neural activity using functional magnetic resonance imaging-derived reward feedback. *J Neurosci*, 27(28), pp.7498–7507.
- Brown, R.W. et al., 2014. *Magnetic Resonance Imaging: Physical Principles and Sequence Design* 2nd Ed., Wiley-Blackwell.
- Buch, E. et al., 2008. Think to move: A neuromagnetic brain-computer interface (BCI) system for chronic stroke. *Stroke*, 39(3), pp.910–917.
- von Büna, P. et al., 2009. Finding Stationary Subspaces in Multivariate Time Series. *Physical Review Letters*, 103(21).
- Buxton, R.B., 2009. *Introduction to Functional Magnetic Resonance Imaging: Principles and Techniques* 2nd Ed., Cambridge University Press.
- Buzsáki, G., 2006. *Rhythms of the Brain*, Oxford University Press, Inc.
- Canterberry, M. et al., 2013. Sustained reduction of nicotine craving with real-time neurofeedback: Exploring the role of severity of dependence. *Nicotine and Tobacco Research*, 15(12), pp.2120–2124.
- Caria, A. et al., 2007. Regulation of anterior insular cortex activity using real-time fMRI. *NeuroImage*, 35(3), pp.1238–1246.
- Caria, A. et al., 2010. Volitional control of anterior insula activity modulates the response to aversive stimuli. A real-time functional magnetic resonance imaging study. *Biological Psychiatry*, 68(5), pp.425–432.
- Caria, a., Sitaram, R. & Birbaumer, N., 2012. Real-Time fMRI: A Tool for Local Brain Regulation. *The Neuroscientist*, 18(5), pp.487–501.
- Carter, M. & Shieh, J.C., 2010. *Guide to Research Techniques in Neuroscience*, Academic Press.
- Chatrian, G.E., Lettich, E. & Nelson, P.L., 1985. Ten percent electrode system for topographic studies of spontaneous and evoked EEG activity. *American Journal Of Eeg Technology*, 25, pp.83–92.
- Chaudhary, U., Birbaumer, N. & Ramos-Murguialday, A., 2016. Brain-computer interfaces for communication and rehabilitation. *Nature Reviews Neurology*.
- Chiew, M., LaConte, S.M. & Graham, S.J., 2012. Investigation of fMRI neurofeedback of differential primary motor cortex activity using kinesthetic motor imagery. *NeuroImage*, 61(1), pp.21–31.
- Coben, R., Linden, M. & Myers, T.E., 2010. Neurofeedback for autistic spectrum disorder: A review of the literature. *Applied Psychophysiology Biofeedback*, 35(1), pp.83–105.
- Cordes, J.S. et al., 2015. Cognitive and neural strategies during control of the anterior cingulate cortex by fMRI neurofeedback in patients with schizophrenia. *Frontiers in behavioral neuroscience*, 9(June), p.169.
- Cox, D.D. & Savoy, R.L., 2003. Functional magnetic resonance imaging (fMRI) “brain reading”: Detecting

- and classifying distributed patterns of fMRI activity in human visual cortex. *NeuroImage*, 19(2), pp.261–270.
- Crosson, B. et al., 2010. Functional imaging and related techniques: an introduction for rehabilitation researchers. *Journal of rehabilitation research and development*, 47(2), pp.vii–xxxiv.
- Dahmen, B. et al., 2008. When the brain takes BOLD 'steps': Controlling differential brain activation levels via real-time fMRI-based neurofeedback training. In *Human Brain Mapping, 14th edition, Melbourne, Australia*.
- DeCharms, R.C. et al., 2005. Control over brain activation and pain learned by using real-time functional MRI. *Proceedings of the National Academy of Sciences of the United States of America*, 102(51), pp.18626–31.
- DeCharms, R.C. et al., 2004. Learned regulation of spatially localized brain activation using real-time fMRI. *NeuroImage*, 21(1), pp.436–443.
- Dornhege, G. et al., 2006. Combined optimization of spatial and temporal filters for improving brain-computer interfacing. *IEEE Transactions on Biomedical Engineering*, 53(11), pp.2274–2281.
- Dornhege, G. et al., 2007. *Toward Brain-Computer Interfacing*, MIT Press.
- Duda, R.O., Hart, P.E. & Stork, D.G., 2001. *Pattern Classification* 2nd Ed., John Wiley & Sons.
- Dyck, M.S. et al., 2016. Targeting treatment-resistant auditory verbal hallucinations in schizophrenia with fMRI-based neurofeedback - exploring different cases of schizophrenia. *Frontiers in Psychiatry*, 7(MAR).
- Egner, T. & Gruzelier, J., 2003. Ecological validity of neurofeedback: modulation of slow wave EEG enhances musical performance. *Neuroreport*, 14(9), pp.1221–1224.
- Elbert, T. et al., 1980. Biofeedback of slow cortical potentials. I. *Electroencephalography and Clinical Neurophysiology*, 48(3), pp.293–301.
- Fetz, E.E., 1969. Operant conditioning of cortical unit activity. *Science*, 163(3870), pp.955–8.
- Formisano, E., De Martino, F. & Valente, G., 2008. Multivariate analysis of fMRI time series: classification and regression of brain responses using machine learning. *Magnetic Resonance Imaging*, 26(7), pp.921–934.
- Friston, K.J. et al., 1995. Characterizing evoked hemodynamics with fMRI. *Neuroimage*, 2, pp.157–165.
- Gerin, M.I. et al., 2016. Real-time fMRI neurofeedback with war veterans with chronic PTSD: a feasibility study. *Frontiers in psychiatry*, 7(June), pp.1–11.
- Goebel, R. et al., 2004. BOLD brain pong: self-regulation of local brain activity during synchronously scanned, interacting subjects. In *Society for Neuroscience, Washington, DC*.
- Goebel, R. et al., 1998. The constructive nature of vision: Direct evidence from functional magnetic resonance imaging studies of apparent motion and motion imagery. *European Journal of Neuroscience*, 10(5), pp.1563–1573.
- Grone, M. et al., 2015. Upregulation of the Rostral Anterior Cingulate Cortex can Alter the Perception of Emotions: fMRI-Based Neurofeedback at 3 and 7T. *Brain Topography*, 28(2), pp.197–207.
- Gruzelier, J.H., 2014. EEG-neurofeedback for optimising performance. I: A review of cognitive and affective outcome in healthy participants. *Neuroscience and Biobehavioral Reviews*, 44, pp.124–141.
- Guan, M. et al., 2015. Self-regulation of brain activity in patients with postherpetic neuralgia: A double-blind randomized study using real-time fMRI neurofeedback. *PLoS ONE*, 10(4).
- Haller, S., Birbaumer, N. & Veit, R., 2010. Real-time fMRI feedback training may improve chronic tinnitus. *European Radiology*, 20(3), pp.696–703.
- Hamilton, J.P. et al., 2011. Modulation of subgenual anterior cingulate cortex activity with real-time neurofeedback. *Human Brain Mapping*, 32(1), pp.22–31.
- Hammond, D.C., 2005. Neurofeedback treatment of depression and anxiety. *Journal of Adult Development*, 12(2–3), pp.131–137.
- Hasan, M.A. et al., 2016. Reversed cortical over-activity during movement imagination following neurofeedback treatment for central neuropathic pain. *Clinical Neurophysiology*, 127(9), pp.3118–3127.
- Haufe, S. et al., 2008. Combining sparsity and rotational invariance in EEG/MEG source reconstruction. *NeuroImage*, 42(2), pp.726–738.
- Haxby, J. V et al., 2001. Distributed and overlapping representations of faces and objects in ventral temporal cortex. *Science*, 293, pp.2425–2430.
- Haynes, J.-D. & Rees, G., 2006. Decoding mental states from brain activity in humans. *Nature reviews. Neuroscience*, 7(7), pp.523–534.
- Hsueh, J.J. et al., 2016. Neurofeedback training of EEG alpha rhythm enhances episodic and working memory. *Human Brain Mapping*.
- Hui, M. et al., 2014. Modulation of functional network with real-time fMRI feedback training of right premotor cortex activity. *Neuropsychologia*, 62(1), pp.111–123.

- Huster, R. et al., 2014. Brain-computer interfaces for EEG neurofeedback: Peculiarities and solutions. *International Journal of Psychophysiology*, 91(1), pp.36–45.
- Hyvarinen, A., Karhunen, J. & Oja, E., 2001. *Independent Component Analysis*, John Wiley & Sons, Inc.
- Jasper, H.H., 1958. The ten-twenty electrode system of the International Federation. *Electroencephalography and Clinical Neurophysiology*, 10(2), pp.371–375.
- Johnson, K.A. et al., 2012. Intermittent “Real-time” fMRI Feedback Is Superior to Continuous Presentation for a Motor Imagery Task: A Pilot Study. *Journal of Neuroimaging*, 22(1), pp.58–66.
- Kaas, A. et al., 2010. Imagery of a moving object: The role of occipital cortex and human MT/V5+. *NeuroImage*, 49(1), pp.794–804.
- Kamiya, J., 1969. Operant control of the EEG alpha rhythm and some of its reported effects on consciousness. In *Altered states of consciousness*. John Wiley & Sons, Inc., pp. 489–501.
- Kandel, E.R. et al., 2013. *Principles of Neural Science*, McGraw-Hill Medical.
- Karch, S. et al., 2015. Modulation of craving related brain responses using real-time fMRI in patients with alcohol use disorder. *PLoS ONE*, 10(7).
- Keizer, A.W., Verment, R.S. & Hommel, B., 2010. Enhancing cognitive control through neurofeedback: A role of gamma-band activity in managing episodic retrieval. *NeuroImage*, 49(4), pp.3404–3413.
- Kim, D.-Y. et al., 2015. The Inclusion of Functional Connectivity Information into fMRI-based Neurofeedback Improves Its Efficacy in the Reduction of Cigarette Cravings. *Journal of Cognitive Neuroscience*, 27(8), pp.1552–1572.
- Kober, S.E. et al., 2015. Specific effects of EEG based neurofeedback training on memory functions in post-stroke victims. *Journal of NeuroEngineering and Rehabilitation*, 12(1), p.107.
- Kotchoubey, B. et al., 2001. Modification of slow cortical potentials in patients with refractory epilepsy: A controlled outcome study. *Epilepsia*, 42(3), pp.406–416.
- Kwong, K.K. et al., 1992. Dynamic magnetic resonance imaging of human brain activity during primary sensory stimulation. *Proceedings of the National Academy of Sciences of the United States of America*, 89(12), pp.5675–9.
- Lackner, N. et al., 2015. The Effectiveness of Visual Short-Time Neurofeedback on Brain Activity and Clinical Characteristics in Alcohol Use Disorders: Practical Issues and Results. *Clinical EEG and neuroscience*.
- LaConte, S.M., 2011. Decoding fMRI brain states in real-time. *NeuroImage*, 56(2), pp.440–454.
- LaFleur, K. et al., 2013. Quadcopter control in three-dimensional space using a noninvasive motor imagery-based brain-computer interface. *Journal of Neural Engineering*, 10(4), p.46003.
- Larsen, S. & Sherlin, L., 2013. Neurofeedback. An Emerging Technology for Treating Central Nervous System Dysregulation. *Psychiatric Clinics of North America*, 36(1), pp.163–168.
- Lauterbur, P.C., 1973. Image Formation by Induced Local Interactions: Examples Employing Nuclear Magnetic Resonance. *Nature*, 242(5394), pp.190–191.
- Lawrence, E.J. et al., 2014. Self-regulation of the anterior insula: Reinforcement learning using real-time fMRI neurofeedback. *NeuroImage*, 88, pp.113–124.
- Lécuyer, A. et al., 2008. Brain-computer interfaces, virtual reality, and videogames. *IEEE Computer*, 41(10), pp.66–72.
- Lee, J.H. et al., 2009. Brain-machine interface via real-time fMRI: Preliminary study on thought-controlled robotic arm. *Neuroscience Letters*, 450(1), pp.1–6.
- Leins, U. et al., 2007. Neurofeedback for children with ADHD: A comparison of SCP and Theta/Beta protocols. *Applied Psychophysiology Biofeedback*, 32(2), pp.73–88.
- Lemm, S. et al., 2011. Introduction to machine learning for brain imaging. *NeuroImage*, 56(2), pp.387–399.
- Li, X. et al., 2013. Volitional reduction of anterior cingulate cortex activity produces decreased cue craving in smoking cessation: A preliminary real-time fMRI study. *Addiction Biology*, 18(4), pp.739–748.
- Liew, S.-L. et al., 2016. Improving Motor Corticothalamic Communication After Stroke Using Real-Time fMRI Connectivity-Based Neurofeedback. *Neurorehabilitation and neural repair*, 30(7), pp.671–675.
- Linden, D.E.J. et al., 2012. Real-time self-regulation of emotion networks in patients with depression. *PLoS ONE*, 7(6).
- Luijmes, R.E., 2016. The effectiveness of Neurofeedback on cognitive functioning in patients with Alzheimer’s disease. *Neurophysiologie Clinique / Clinical Neurophysiology*, 46(3), pp.179–187.
- Lynch, J.J., Paskewitz, D.A. & Orne, M.T., 1974. Some factors in the feedback control of human alpha rhythm. *Psychosom. Med.*, 36(5), pp.399–410.
- De Martino, F. et al., 2008. Combining multivariate voxel selection and support vector machines for mapping and classification of fMRI spatial patterns. *NeuroImage*, 43(1), pp.44–58.
- Marzetti, L., Del Gratta, C. & Nolte, G., 2008. Understanding brain connectivity from EEG data by identifying systems composed of interacting sources. *NeuroImage*, 42(1), pp.87–98.

- Mathiak, K.A. et al., 2015. Social reward improves the voluntary control over localized brain activity in fMRI-based neurofeedback training. *Frontiers in behavioral neuroscience*, 9(June), p.136.
- McFarland, D.J., Sarnacki, W. a & Wolpaw, J.R., 2010. Electroencephalographic (EEG) control of three-dimensional movement. *Journal of neural engineering*, 7(3), p.36007.
- McFarland, D.J. & Wolpaw, J.R., 2011. Brain-Computer Interfaces for Communication and Control. *Communications of the ACM*, 54(5), pp.60–66.
- Meinecke, F.C. et al., 2005. Measuring phase synchronization of superimposed signals. *Physical Review Letters*, 94(8).
- Min, B.K., Marzelli, M.J. & Yoo, S.S., 2010. Neuroimaging-based approaches in the brain-computer interface. *Trends in Biotechnology*, 28(11), pp.552–560.
- Mørup, M. et al., 2008. Shift-invariant multilinear decomposition of neuroimaging data. *NeuroImage*, 42(4), pp.1439–1450.
- Müller, K.-R., Anderson, C.W. & Birch, G.E., 2003. Linear and nonlinear methods for brain-computer interfaces. *IEEE transactions on neural systems and rehabilitation engineering*, 11(2), pp.165–169.
- Naci, L. et al., 2012. Brain-computer interfaces for communication with nonresponsive patients. *Annals of Neurology*, 72(3), pp.312–323.
- Nan, W. et al., 2013. Peripheral Visual Performance Enhancement by Neurofeedback Training. *Applied Psychophysiology and Biofeedback*, 38(4), pp.285–291.
- Niedermeyer, E. & Lopes Da Silva, F., 2005. *Electroencephalography: Basic Principles, Clinical Applications, and Related Fields* 5th Ed., Lippincott Williams and Wilkins.
- Noirhomme, Q., Kitney, R.I. & Macq, B., 2008. Single-trial EEG source reconstruction for brain-computer interface. *IEEE Transactions on Biomedical Engineering*, 55(5), pp.1592–1601.
- Nolte, G. et al., 2008. Robustly estimating the flow direction of information in complex physical systems. *Physical Review Letters*, 100(23).
- Norman, K.A. et al., 2006. Beyond mind-reading: multi-voxel pattern analysis of fMRI data. *Trends in Cognitive Sciences*, 10(9), pp.424–430.
- Ogawa, S. et al., 1990. Oxygenation-sensitive contrast in magnetic resonance image of rodent brain at high magnetic fields. *Magnetic Resonance in Medicine*, 14(1), pp.68–78.
- Oostenveld, R. & Praamstra, P., 2001. The five percent electrode system for high-resolution EEG and ERP measurements. *Clinical Neurophysiology*, 112(4), pp.713–719.
- Ordikhani-Seyedlar, M. et al., 2016. Neurofeedback Therapy for Enhancing Visual Attention: State-of-the-Art and Challenges. *Frontiers in Neuroscience*, 10(August), p.352.
- Parra, L. et al., 2003. Single-trial detection in EEG and MEG: Keeping it linear. *Neurocomputing*, 5254, pp.177–183.
- Pereira, F., Mitchell, T. & Botvinick, M., 2009. Machine learning classifiers and fMRI: a tutorial overview. *NeuroImage*, 45(1 Suppl).
- Posse, S. et al., 2003. Real-time fMRI of temporolimbic regions detects amygdala activation during single-trial self-induced sadness. *NeuroImage*, 18(3), pp.760–768.
- Purcell, E., Torrey, H. & Pound, R., 1946. Resonance Absorption by Nuclear Magnetic Moments in a Solid. *Physical Review*, 69(1–2), pp.37–38.
- Purves, D. et al., 2004. *Neuroscience* 3rd Ed., Sinauer Associates, Inc.
- Ramos-Murguialday, A. et al., 2013. Brain-machine interface in chronic stroke rehabilitation: A controlled study. *Annals of Neurology*, 74(1), pp.100–108.
- Ray, A.M. et al., 2015. A subject-independent pattern-based Brain-Computer Interface. *Frontiers in behavioral neuroscience*, 9(October), p.269.
- Reid, A.T. et al., 2016. A seed-based cross-modal comparison of brain connectivity measures. *Brain Structure and Function*.
- Reiner, M., Rozengurt, R. & Barnea, A., 2014. Better than sleep: Theta neurofeedback training accelerates memory consolidation. *Biological Psychology*, 95(1), pp.45–53.
- Rockstroh, B. et al., 1993. Cortical self-regulation in patients with epilepsies. *Epilepsy Research*, 14(1), pp.63–72.
- Rockstroh, B. et al., 1984. Operant control of EEG and event-related and slow brain potentials. *Biofeedback and self-regulation*, 9(2), pp.139–60.
- Ros, T. et al., 2014. Neurofeedback facilitation of implicit motor learning. *Biological Psychology*, 95(1), pp.54–58.
- Rota, G. et al., 2009. Self-regulation of regional cortical activity using real-time fmri: the right inferior frontal gyrus and linguistic processing. *Human Brain Mapping*, 30(5), pp.1605–1614.
- Rozengurt, R. et al., 2016. Theta EEG neurofeedback benefits early consolidation of motor sequence learning. *Psychophysiology*.

- Ruiz, S. et al., 2013. Acquired self-control of insula cortex modulates emotion recognition and brain network connectivity in schizophrenia. *Human Brain Mapping*, 34(1), pp.200–212.
- Ruiz, S. et al., 2014. Real-time fMRI brain computer interfaces: Self-regulation of single brain regions to networks. *Biological Psychology*, 95(1), pp.4–20.
- Salari, N. & Rose, M., 2013. A Brain-Computer-Interface for the Detection and Modulation of Gamma Band Activity. *Brain Sciences*, 3(4), pp.1569–1587.
- Sarkheil, P. et al., 2015. fMRI feedback enhances emotion regulation as evidenced by a reduced amygdala response. *Behavioural Brain Research*, 281, pp.326–332.
- Scharnowski, F. et al., 2012. Improving Visual Perception through Neurofeedback. *Journal of Neuroscience*, 32(49), pp.17830–17841.
- Scharnowski, F. et al., 2015. Manipulating motor performance and memory through real-time fMRI neurofeedback. *Biological Psychology*, 108, pp.85–97.
- Scharnowski, F. & Weiskopf, N., 2015. Cognitive enhancement through real-time fMRI neurofeedback. *Current Opinion in Behavioral Sciences*, 4, pp.122–127.
- Schlögl, A. et al., 2005. Characterization of Four-Class Motor Imagery EEG Data for the BCI-Competition 2005. *Journal of Neural Engineering*, 2(4), pp.L14–L22.
- Shih, J.J., Krusienski, D.J. & Wolpaw, J.R., 2012. Brain-computer interfaces in medicine. *Mayo Clinic Proceedings*, 87(3), pp.268–279.
- Sitaram, R. et al., 2012. Acquired Control of Ventral Premotor Cortex Activity by Feedback Training: An Exploratory Real-Time fMRI and TMS Study. *Neurorehabilitation and Neural Repair*, 26(3), pp.256–265.
- Sitaram, R. et al., 2007. Temporal classification of multichannel near-infrared spectroscopy signals of motor imagery for developing a brain-computer interface. *NeuroImage*, 34(4), pp.1416–1427.
- Sitaram, R. et al., 2014. Volitional control of the anterior insula in criminal psychopaths using real-time fMRI neurofeedback: a pilot study. *Frontiers in Behavioral Neuroscience*, 8(October), p.344.
- Sorger, B. et al., 2012. A real-time fMRI-based spelling device immediately enabling robust motor-independent communication. *Current Biology*, 22(14), pp.1333–1338.
- Sorger, B. et al., 2004. Voluntary modulation of regional brain activity to different target levels based on real-time fMRI neurofeedback. In *Society for Neuroscience Society for Neuroscience, 34th edition San Diego, USA*.
- Sorger, B., 2010. *When the brain speaks for itself: Exploiting hemodynamic brain signals for motor-independent communication*. Universitaire Pers Maastricht: Maastricht.
- Sreedharan, S. et al., 2013. Brain-computer interfaces for neurorehabilitation. *Critical reviews in biomedical engineering*, 41(3), pp.269–79.
- Srinivasan, R., 1999. Methods to Improve the Spatial Resolution of EEG. *International Journal of Bioelectromagnetism*, 1(1), pp.102–111.
- Strehl, U. et al., 2006. Deactivation of brain areas during self-regulation of slow cortical potentials in seizure patients. *Applied Psychophysiology Biofeedback*, 31(1), pp.85–94.
- Subramanian, L. et al., 2016. Functional Magnetic Resonance Imaging Neurofeedback-guided Motor Imagery Training and Motor Training for Parkinson's Disease: Randomized Trial. *Frontiers in Behavioral Neuroscience*, 10(June), p.111.
- Subramanian, L. et al., 2011. Real-Time Functional Magnetic Resonance Imaging Neurofeedback for Treatment of Parkinson's Disease. *The Journal of Neuroscience*, 31(45), pp.16309–16317.
- Sulzer, J. et al., 2013. Real-time fMRI neurofeedback: Progress and challenges. *NeuroImage*, 76, pp.386–399.
- Tan, G. et al., 2009. Meta-Analysis of EEG Biofeedback in Treating Epilepsy. *Clinical EEG and Neuroscience*, 40(3), pp.173–179.
- The Society for Neuroscience, 2002. *Brain facts: A primer on the brain and nervous system* 4th Ed., The Society for Neuroscience.
- Thibault, R.T. et al., 2015. Neurofeedback, self-regulation, and brain imaging: Clinical science and fad in the service of mental disorders. *Psychotherapy and Psychosomatics*, 84(4), pp.193–207.
- Thibault, R.T., Lifshitz, M. & Raz, A., 2016. The self-regulating brain and neurofeedback: Experimental science and clinical promise. *Cortex*, 74, pp.247–261.
- Tomioka, R. & Müller, K.-R., 2010. A regularized discriminative framework for EEG analysis with application to brain-computer interface. *NeuroImage*, 49(1), pp.415–432.
- Tong, F. & Pratte, M.S., 2012. Decoding Patterns of Human Brain Activity. *Annual Review of Psychology*, 63(1), pp.483–509.
- Tong, S. & Thakor, N.V., 2009. *Quantitative EEG Analysis Methods and Clinical Applications*, Artech House.
- Veit, R. et al., 2012. Using real-time fmri to learn voluntary regulation of the anterior insula in the presence of threat-related stimuli. *Social Cognitive and Affective Neuroscience*, 7(6), pp.623–634.

- Vernon, D. et al., 2003. The effect of training distinct neurofeedback protocols on aspects of cognitive performance. *International Journal of Psychophysiology*, 47(1), pp.75–85.
- Vernon, D.J., 2005. Can neurofeedback training enhance performance? An evaluation of the evidence with implications for future research. *Applied psychophysiology and biofeedback*, 30(4), pp.347–364.
- Vidal, J., 1973. Toward direct brain-computer communication. *Annu Rev Biophys Bioeng.*, 2, pp.157–180.
- Wang, J.R. & Hsieh, S., 2013. Neurofeedback training improves attention and working memory performance. *Clinical Neurophysiology*, 124(12), pp.2406–2420.
- Wang, Z. et al., 2015. Causality Analysis of fMRI Data Based on the Directed Information Theory Framework. *IEEE Transactions on Biomedical Engineering*, 9294(c), pp.1–1.
- Weiskopf, N. et al., 2003. Physiological self-regulation of regional brain activity using real-time functional magnetic resonance imaging (fMRI): methodology and exemplary data. *Neuroimage*, 19(3), pp.577–86.
- Weiskopf, N., Mathiak, K., et al., 2004. Principles of a brain-computer interface (BCI) based on real-time functional magnetic resonance imaging (fMRI). *IEEE Transactions on Biomedical Engineering*, 51(6), pp.966–970.
- Weiskopf, N., 2012. Real-time fMRI and its application to neurofeedback. *NeuroImage*, 62(2), pp.682–692.
- Weiskopf, N., Scharnowski, F., et al., 2004. Self-regulation of local brain activity using real-time functional magnetic resonance imaging (fMRI). *Journal of Physiology Paris*, 98(4–6 SPEC. ISS.), pp.357–373.
- Wolpaw, J.R. et al., 2002. Brain-computer interfaces for communication and control. *Clinical neurophysiology: official journal of the International Federation of Clinical Neurophysiology*, 113(6), pp.767–91.
- Wolpaw, J.R. & McFarland, D.J., 2004. Control of a two-dimensional movement signal by a noninvasive brain-computer interface in humans. *Proceedings of the National Academy of Sciences of the United States of America*, 101(51), pp.17849–54.
- Woolrich, M.W. et al., 2009. Statistical Analysis of fMRI Data. In *fMRI Techniques and Protocols*. Humana Press, pp. 769–782.
- Wyrwicka, W. & Serman, M.B., 1968. Instrumental conditioning of sensorimotor cortex EEG spindles in the waking cat. *Physiology & Behavior*, 3(5), pp.703–707.
- Yoo, S.S. et al., 2008. Neurofeedback fMRI-mediated learning and consolidation of regional brain activation during motor imagery. *International Journal of Imaging Systems and Technology*, 18(1), pp.69–78.
- Yoo, S.-S. et al., 2004. Brain-computer interface using fMRI: spatial navigation by thoughts. *Neuroreport*, 15(10), pp.1591–1595.
- Yoo, S.-S. et al., 2006. Increasing cortical activity in auditory areas through neurofeedback functional magnetic resonance imaging. *Neuroreport*, 17(12), pp.1273–1278.
- Young, K.D. et al., 2014. Real-time fMRI neurofeedback training of amygdala activity in patients with major depressive disorder. *PLoS ONE*, 9(2).
- Zhang, G. et al., 2013. Improved Working Memory Performance through Self-Regulation of Dorsal Lateral Prefrontal Cortex Activation Using Real-Time fMRI. *PLoS ONE*, 8(8).
- Zhao, X. et al., 2013. Causal interaction following the alteration of target region activation during motor imagery training using real-time fMRI. *Frontiers in human neuroscience*, 7, p.866.
- Zilverstand, A. et al., 2015. fMRI neurofeedback facilitates anxiety regulation in females with spider phobia. *Frontiers in behavioral neuroscience*, 9(June), p.148.
- Zoefel, B., Huster, R.J. & Herrmann, C.S., 2011. Neurofeedback training of the upper alpha frequency band in EEG improves cognitive performance. *NeuroImage*, 54(2), pp.1427–1431.
- Zotев, V. et al., 2016. Correlation between amygdala BOLD activity and frontal EEG asymmetry during real-time fMRI neurofeedback training in patients with depression. *NeuroImage: Clinical*, 11, pp.224–238.
- Zotев, V. et al., 2011. Self-regulation of amygdala activation using real-time FMRI neurofeedback. *PLoS ONE*, 6(9).

CHAPTER 2

VISUAL MOTION IMAGERY NEUROFEEDBACK BASED ON THE HMT+/V5 COMPLEX

EVIDENCE FOR A FEEDBACK-SPECIFIC NEURAL
CIRCUIT INVOLVING NEOCORTICAL AND
CEREBELLAR REGIONS

Based on: Banca, P.*, Sousa, T.*, Duarte, I.C., Castelo-Branco, M., 2015. Visual motion imagery neurofeedback based on the hMT+/V5 complex: evidence for a feedback-specific neural circuit involving neocortical and cerebellar regions. *J. Neural Eng.* 12 (6).

** both authors contributed equally*

We would like to thank the participants for their involvement with this study. We are also very grateful to Carlos Ferreira, João Pedro Marques and Gil Cunha for the help with real-time fMRI set up and scanning.

Abstract

Current approaches in neurofeedback research often focus on identifying, on a subject-by-subject basis, the neural regions that are best suited for self-driven modulation. It is known that the hMT+/V5 complex, an early visual cortical region, is recruited during explicit and implicit motion imagery, in addition to real motion perception.

This study tests the feasibility of training healthy volunteers to regulate the level of activation in their hMT+/V5 complex using neurofeedback based on real-time functional resonance magnetic imaging and visual motion imagery strategies. We functionally localized the hMT+/V5 complex to further use as a target region for neurofeedback. A uniform strategy based on motion imagery was used to guide participants to neuromodulate hMT+/V5.

We found that 15/20 participants achieved successful neurofeedback. This modulation led to the recruitment of a specific network as further assessed by psychophysiological interaction analysis. This specific circuit, including hMT+/V5, putative V6 and medial cerebellum was activated for successful neurofeedback runs. The putamen and anterior insula were recruited for both successful and non-successful runs.

Our results indicate that hMT+/V5 is a region that can be modulated by focused imagery and that a specific cortico-cerebellar circuit is recruited during visual motion imagery leading to successful neurofeedback. These findings contribute to the debate on the relative potential of extrinsic (sensory) versus intrinsic (default-mode) brain regions in the clinical application of neurofeedback paradigms. This novel circuit might be a good target for future neurofeedback approaches that aim, for example, the training of focused attention in disorders such as ADHD.

2.1. Introduction

Neurofeedback (NF) and brain computer interface (BCI) paradigms have been successfully used to train subjects to get volitional control over a given brain region (Sulzer et al. 2013). Real-time functional magnetic resonance imaging (fMRI) allows achieving this goal by flexibly defining targets for neuromodulation. Online analysis of fMRI patterns enables to provide an updated feedback to individuals that can use this information to regulate their own brain activity (DeCharms 2007).

This concept has been applied in general cognitive domains including visual (Scharnowski et al. 2012; Shibata et al. 2011), motor (Subramanian et al. 2011; Weiskopf et al. 2004), language (Rota et al. 2009), emotional (Caria et al. 2007; Caria et al. 2010; Hamilton et al. 2011; Johnston et al. 2010; Linden et al. 2012; Ruiz et al. 2013) and pain processing (DeCharms et al. 2005). Here we focus on the modulation of the mediotemporal area of the visual cortex (hMT+/V5 complex), a visual region that has been associated with visual motion perception and visual motion imagery. Previous studies of implicit motion (Kourtzi & Kanwisher 2000) and motion imagery (Slotnick et al. 2005) have shown robust hMT+/V5 effects when participants are consciously experiencing motion that is physically absent, and in the absence of neurofeedback. We aimed to understand whether the neural correlates of such processes are applicable to the NF context. In particular we were interested in the functional connectivity of successful NF.

The localization criterion for the region serving as region-of-interest (ROI) for NF has been widely variable. Some studies focused on specific anatomically defined regions such as the somatomotor cortex (DeCharms et al. 2004), anterior cingulate cortex (Weiskopf et al. 2003), amygdala (Posse et al. 2003) and the insula (Caria et al. 2007). Others preferred to use functionally defined ROIs as target for neuromodulation (DeCharms et al. 2005; Greer et al. 2014; Hamilton et al. 2011; Ruiz et al. 2013; Subramanian et al. 2011). To avoid the potential problem of obtaining variable anatomical landmarks in relation to particular brain regions with a known function, here we applied an explicit functional localizer using a validated task (Goebel et al. 1998; Graewe et al. 2013; Kaas et al. 2010) that is accepted as functional localizer independently of the anatomical location.

fMRI-based NF without stimulus presentation in the early visual cortex can be quite powerful (Shibata et al. 2011), even enabling perceptual learning. This illustrates the potential of NF approaches in sensory regions. However, this notion is controversial and it has been suggested that focusing on higher level regions related to the default mode network (DMN) might be a more powerful NF approach (Harmelech et al. 2015). The choice of implicit or explicit mental imagery strategies for learning of self-regulation is also a current topic of debate in the field (Sulzer et al. 2013). There are pros and cons associated to the use of implicit and explicit feedback strategies and findings from studies comparing both are inconsistent. On one hand, choosing explicit strategies based on current knowledge of target's brain function are theoretically more efficient for self-regulation and quicker to achieve because subjects are guided. This choice has the advantage of avoiding long and expensive MRI experiments. On the other hand, implicit strategies do not have to directly deal with subjects' compliance to an explicit cognitive instruction. Besides, they may be more advantageous when dealing with subjects with difficulties to understand or report an instruction and with some regions that may have no associated explicit strategies. In our study, we choose to provide an explicit motion imagery instruction with room for individual free exploration of the most appropriate strategy (subjects could 'animate' their imagined motion with their preferable visual object features).

Mental imagery, defined as a perceptual experience that occurs in the absence of external stimulation, has been intensively studied (Borst & Kosslyn 2008) (for a review see Ishai 2010), particularly in the visual motion domain (Goebel et al. 1998). It is well established that visual imagery shares some of the same neural machinery as the actual perception (Farah 1989; Kosslyn & Thompson 2003). O'Craven *et al* found that fusiform face area activates for imagined faces and parahippocampal place area for imagined places (O'Craven & Kanwisher 2000) and it was demonstrated that hMT+/V5 is recruited during explicit (Goebel et al. 1998) and implicit (Kourtzi & Kanwisher 2000) motion imagery in the absence of NF. One can therefore infer that the same area that is localized with appropriate stimulus contrasts can be used as a target for NF based on imagery. Studies suggest that mental imagery recruits higher level cognitive modules, depending on the nature of the imagery task (Harmelech et al. 2015; Kaas et al. 2010; Mellet et al. 1998).

In summary, this study takes advantage of the power of visual motion imagery, of the hMT+/V5 complex's well established motion selectivity (Castelo-Branco et al. 2002; Castelo-Branco et al. 2009; Culham et al. 2001; Goebel et al. 1998; Graewe et al. 2013;

Kaas et al. 2010; Tootell et al. 1995; Watson et al. 1993; Zeki et al. 1991), and of the fact that this region is one of the visual brain regions that can be most reliably localized, to design a NF strategy to train humans to modulate activity in their own hMT+/V5 complex. The underlying idea is that a reliable recruitment of this region by motion imagery (Goebel et al. 1998; Kaas et al. 2010) would make NF approaches based on hMT+/V5 localization and subject driven control of activity in this region theoretically viable. If this goal is achieved, we seek to investigate the neural correlates of potential different patterns of learning. We hypothesize that the feasibility of training healthy volunteers to regulate the level of activation in their hMT+/V5 complex using NF based on visual motion imagery strategies might require the recruitment of a specific high level network which might potentially also be exploited for NF approaches. Moreover, we expect to observe different neural circuits associated with different learning effects.

While the focus on early visual areas is controversial we opted for training a region clearly outside the DMN, which has been suggested to yield powerful NF approaches (Harmelech et al. 2015). The reason is that potential clinical applications of NF involve attentional disorders in which a ‘failure to deactivate the DMN’ has been postulated (Violante et al. 2012). Thereby, NF approaches focused on boosting activity in the DMN might be a very good approach for some mental disorders, but not the ones where the mechanism to regulate activity in DMN is dysfunctional, with strong hyperactivity. Therefore, training of focused imagery or attention to visual features might be a viable alternative as well as BCI approaches aiming to reduce ‘lapses of attention’ (DeBettencourt et al. 2015), given the known links between mental imagery and attention deficit hyperactivity disorder (Abraham et al. 2006).

2.2. Materials and methods

2.2.1. Participants

Twenty healthy participants (11 males; mean age = 28.3, $SD \pm 6.7$) gave informed consent and participated in this study. All volunteers had normal or corrected-to-normal vision, and none of them had a history of neurological, major medical, or psychiatric disorders. The experimental procedures were approved by the ethics committee of the Faculty of Medicine of the University of Coimbra.

Before the experiment, participants were instructed that they would learn to regulate a brain region known to be involved, among other functions, in motion processing (their hMT+/V5 complex). Participants were therefore instructed to use a focused visual motion imagery strategy to regulate their brain activity. The instructions also included an explanation about the time delay between the image collection and the feedback (which corresponds to the hemodynamic delay plus the real-time analysis processing time) and an explanation about the self-paced (prior signaling of NF attempts to ensure validity) procedure of the experiment (see neurofeedback runs and experimental design section).

2.2.2. fMRI data acquisition

Functional and anatomical scans were performed in a 3 Tesla (3T) Siemens Magnetom TimTrio scanner, at the Portuguese Brain Imaging Network, using a 12-channel head coil. To minimize the motion of the participant's head during the acquisition, foam padding was employed. A T1-weighted anatomical scan (160 slices) was acquired prior to functional runs using a turbo field echo gradient echo pulse sequence, TR (repetition time) = 2.3 s, TE (echo time) = 2.98 ms, voxel size = $1 \times 1 \times 1 \text{ mm}^3$, FA (flip angle) = 9° , FOV (field of view) = 256×256 .

Functional data, including a localizer scan and ~ 4 neurofeedback runs (a minimum of 2 was required per participant, which occurred only in three participants), were obtained using blood oxygenation level-dependent (BOLD) contrast echo planar imaging (EPI) covering the entire brain (TR = 3 s; TE = 30 ms; 36 slices; 3 mm thick; flip angle = 90° ; in-plane resolution = $4 \times 4 \text{ mm}^2$). The first two volumes were discarded to allow for T1 equilibration effects. For each participant, 125 volumes were acquired for the localizer run and 150 volumes for each of the NF runs.

2.2.3. Online data analysis

Data from the localizer and NF runs were analyzed online. The fMRI setup used for real-time data processing was based on Turbo-BrainVoyager 2.6 (Brain Innovation, Maastricht, The Netherlands). After acquisition and reconstruction, data from the scanner were sent to the real-time analysis computer. The data were imported, analyzed volume by volume and drift removal and 3D motion detection and correction were performed aligning each volume to a reference volume, which was the first volume scanned.

The statistical analysis was based on an incremental general linear model (GLM) calculation by the real-time fMRI Turbo-BrainVoyager software package. On the NF runs, the mean resultant signal estimated for each incoming functional imaging volume within the selected ROI, in relation to the baseline, was feedback to the participant using an auditory feedback (see neurofeedback runs and experimental design section). Importantly, this modality was used for feedback to prevent that additional visual signals were added.

2.2.4. Functional definition of the target region-of-interest

We used a moving-dot task, as functional localizer, that has been shown to reliably activate movement-related visual networks, including hMT+/V5, which we aimed to target (Goebel et al. 1998; Mikami et al. 1986; Newsome & Pare 1988).

Participants viewed a motion stimulus that was generated from a white single dot oscillating along a vertical trajectory, up and down, against a black background (figure 2.1-A). This single dot was shown across three different conditions where the speed was the manipulated variable: two 30 s blocks of a moving dot, at two distinct speeds (10 deg/s and 5 deg/s), interleaved with a 15 s block of a static dot (figure 2.1-B). Stimulus delivery was controlled by MATLAB (MathWorks) using the Psychophysics toolbox.

2.2.5. Neurofeedback runs and experimental design

To test our hypothesis, volunteers were trained to modulate the level of activation in their hMT+/V5 complex using fMRI-based NF and strategies of visual motion imagery. After defining the target ROI hMT+/V5 for each participant, using the functional localizer, they took part in NF training sessions.

The NF runs were composed of several static imagery blocks (down-regulation blocks used as baseline) interleaved by motion imagery blocks (up-regulation blocks) (figure 2.1-C). At the beginning of each NF run, participants were instructed to press either of two buttons to indicate their intention to either up-regulate (right button) or down-regulate (left button) the target area. Furthermore, they were instructed to always begin each run with a baseline block, to interleave both blocks and to attempt each block with duration of approximately 20 s. The exact duration of each block was decided by the participant. The timings of the response collection were controlled by MATLAB (MathWorks) using the Psychophysics toolbox. This self-pacing criterion allowed the participants to freely decide when to interleave their up-regulation blocks with static imagery blocks (baseline). During

the NF training runs, the fMRI BOLD signals from the ROI were processed in real-time and the level of activity in the ROI was fed-back to the participant. Participants could learn by trial and error, using visual motion imagery, how to regulate the level of activity measured in the target ROI. Each NF run lasted 7.5 minutes.

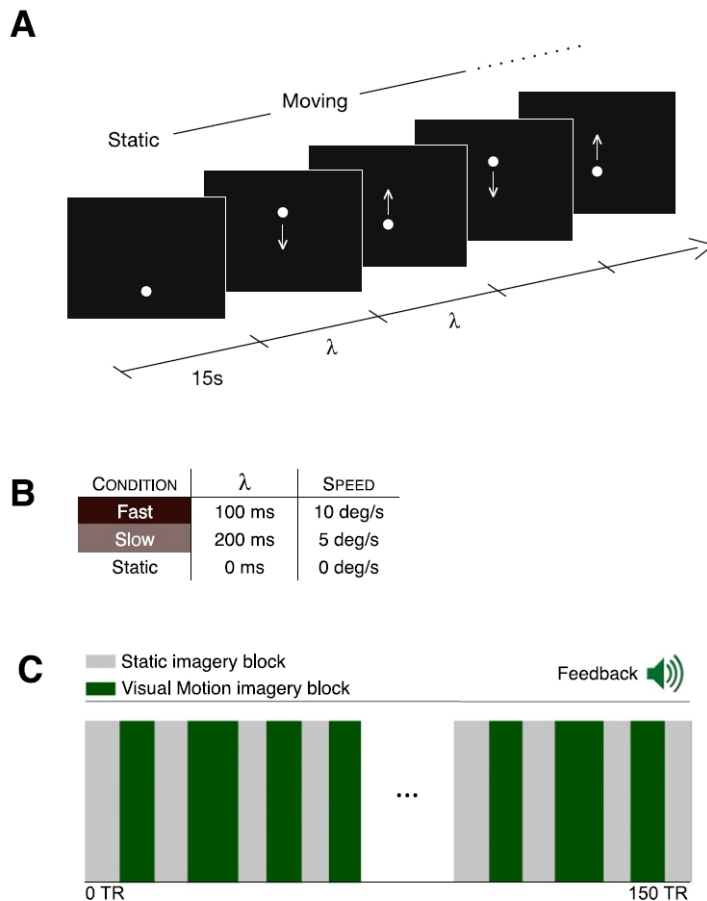


Figure 2.1. Experimental design for the functional localizer and neuromodulation tasks. (A) The functional localizer for the target region-of-interest (ROI) representing the static and motion conditions. The moving stimulus is a white dot oscillating up and down along a vertical trajectory. (B) Three different conditions were used to localize the hMT+/V5 complex: static, slow and fast visual moving stimulus. Thirty seconds blocks of a moving dot, fast (10 deg/s) or slow (5 deg/s), were randomly interleaved with 15 s blocks of a static dot (0 deg/s). The distance covered by the dot (each cycle) was 2 degrees of arc, so the half period (λ) of one oscillation was 200 ms for the slow condition and 100 ms for the fast condition. (C) Example of the design of the neurofeedback session. Static imagery blocks (down-regulation used as baseline: gray blocks) were interleaved by motion imagery blocks (up-regulation blocks: green blocks). Motion imagery was self-paced (indicated a priori to ensure validity) and the participants received an auditory feedback for neuromodulation.

Auditory feedback was chosen to avoid the potential interference that a visual ‘thermometer’ display, as a primary tool for feedback, might eventually cause in hMT+/V5 modulation. Thus, changes in the ‘thermometer’ display were indirectly fed-back by the experimenter to participants via the auditory modality using the intercommunication system of the MRI system. At the beginning of each session, the most comfortable dB level was

verified for each participant. Each participant confirmed that they could clearly hear the experimenter's voice. The 'thermometer' displayed to the experimenter (outside the scanner) the percentage signal change as compared with the previous baseline block. Then the experimenter quantitatively forwarded these changes, in real-time, to the participant thus translating the levels of the standard visual 'thermometer' scale of the Turbo Brain Voyager software (from level 0 - no activation to level 5 - maximum activation). During the baseline blocks, the goal given to the participants was to achieve the level 0, as opposition to the up-regulation blocks goal (to achieve the maximum level). Accordingly, the auditory feedback was given during both imagery tasks. To avoid strong fluctuations of the thermometer display and baseline drifts, temporal filtering was applied by averaging up to three previous time points. After the experiment participants were asked to describe how they tried to manipulate the feedback signal and how effective their strategies were.

For a complete overview of the experimental design please see the supplementary figure 2.A1 in appendix. A scheme of the implemented neurofeedback system set-up is also presented (figure 2.A2).

2.2.6. Offline data analysis

Offline image data analyses were carried out using BrainVoyager QX 2.4 (Brain Innovation, Maastricht, The Netherlands). Pre-processing included 3D motion correction with intra-session alignment, slice-scan-time correction with cubic spline interpolation, temporal high-pass filtering to remove low frequency drifts (GLM Fourier with 2 cycles per run). Functional data were co-registered to anatomical data per participant and subsequently normalized into Talairach space.

Statistical analyses were performed per participant and at group level. The block predictors were time-locked to the onset of the specific conditions (experimental condition = 1, baseline condition = 0). In order to account for the hemodynamic delay and dispersion, each of the predictors was convolved with a double gamma hemodynamic response function (Friston et al. 1998). Furthermore, motion parameters were used as predictors in order to control for the potential influence of motion artefacts in our data. Significant differences between experimental conditions were assessed by using contrast (t) maps. The obtained statistical maps from the localizer runs were corrected for multiple comparisons using Bonferroni correction. Effects were considered significant if $P < 0.05$. The group data analyses were performed using random effects GLM.

To take into account potential between participants variability, specific offline analyses of the NF data were performed per participant to identify the lag with maximal correlation with hMT+/V5 time courses. This lag is a result of the cross correlation analysis (performed for multiple lags and identifying the one with strongest correlation, just like in retinotopic mapping). It provides us information about the mental pacing of the participant and the latency of the neuromodulation signal. Furthermore, to search for possible learning effects in successful NF runs, we analyzed the improvements within (percentage of signal change per run) and between runs (simple comparisons per participant and using the *beta* values). A NF run was labelled as successful if the participant showed an overall positive and statistically significant predictor coefficient (*beta* weight) derived from the correlation of ROI GLM BOLD response and its time course. Successful versus non-successful NF runs were analyzed using the data from all participants to identify the brain regions involved in each case.

Functional connectivity was assessed at group level for successful and non-successful NF runs using psychophysiological interactions (PPI) analyses based on Friston et al. (1997), as described in (O'Reilly et al. 2012). The PPI analysis was based on whole-brain data and was performed using the defined hMT+/V5 ROI as seed. A PPI analysis identifies which voxels increase their connectivity with a seed ROI in a given cognitive context, such as imagery. To perform the PPI analysis, the mean activity of the seed ROI for each TR was extracted. This time course was previously z-transformed to be multiplied TR by TR with the task time course. The result forms a PPI predictor. The task time course was based on the protocol associated with the data. Before being multiplied by the ROI time course, the task time course was convolved with the hemodynamic response function. GLM analysis included the PPI predictor, the hMT+/V5 time course and the task time course. The GLM results show which area significantly increase their relationship with the seed ROI in the imagery context.

2.3. Results

2.3.1. hMT+/V5 localization

The independent localizer scan identified hMT+/V5 complex in all participants, in a region consistent with prior reports of its localization (figure 2.2) (Castelo-Branco et al. 2002; Castelo-Branco et al. 2009; Graewe et al. 2013). As our moving visual stimulus was

displayed in central locations, GLM analysis of BOLD responses in bilateral ROIs showed greater activation levels to motion contrast conditions ($P < 0.001$, for all comparisons, Bonferroni corrected). hMT+/V5 multi-subject cluster peak voxel coordinates at $P < 0.005$ were the following (x, y, z): left $(-45, -66, 2)$ and right $(42, -66, -2)$. Based on this finding, we used a bilateral ROI for subsequent neurofeedback runs, from which the response was extracted for each of the experimental conditions. Participants' responses for each condition were quantified as the percentage of BOLD signal change.

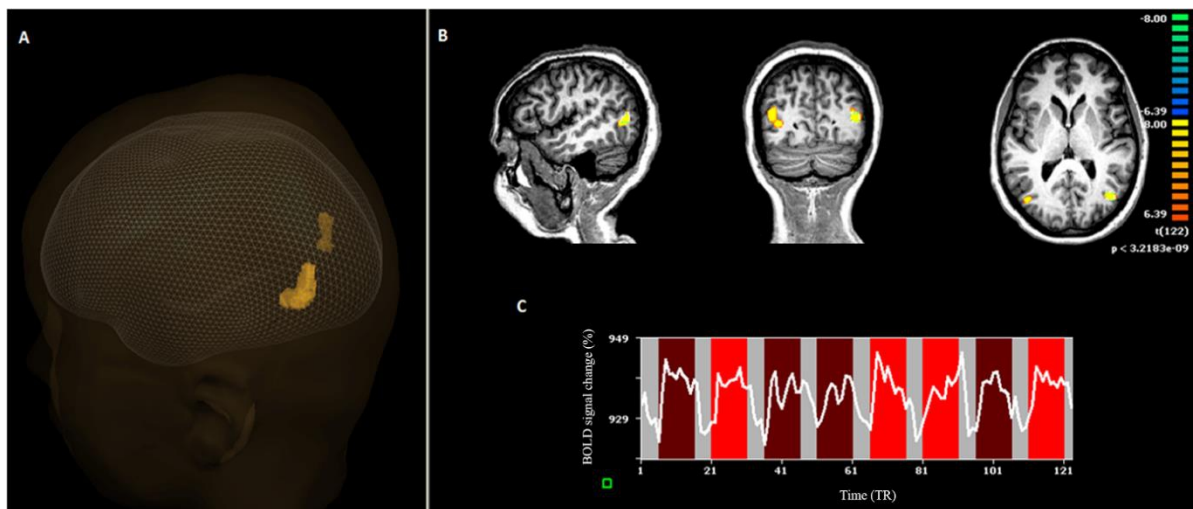


Figure 2.2. Example of hMT+/V5 identification using the defined localizer in one participant. (A) 3D view of the resulting region-of-interest (ROI). (B) General linear model (GLM) conjunction analysis (stringent criterion being that all particular motion versus static contrasts have to be significant for a voxel to be considered positive; for details see text) of blood-oxygenation-level-dependent (BOLD) shows a quite specific degree of localization to bilateral hMT+/V5. Regions are shown at the same statistical threshold level ($P < 0.0001$, corrected). (C) Time courses of hMT+/V5 activity during the localizer run. The blocks represent the different visual stimulus conditions presented to the participant: gray blocks - static dot; dark red blocks - moving dot with low velocity; bright red blocks - moving dot with high velocity.

2.3.2. hMT+/V5 modulation

The target area used for NF was centered on the peak voxel of activation in the hMT+/V5, and the signals from all voxels inside the defined ROI were averaged. Fifteen of the twenty participants were able to successfully regulate BOLD magnitude in the hMT+/V5 complex (see figure 2.3 for example from one participant) in at least one NF run according to the defined criteria (the individually selected ROI showed a significant ($P < 0.05$) increase of activity during visual motion imagery when compared to no-motion imagery). Different patterns of ROI activity self-regulation were observed within and between runs. We have found increased BOLD modulation in ROI across runs or even improvements within the same run (see examples in figure 2.4). Participants reported the use of both positive and

negative mental imagery (on/off). Although the same focused strategy of visual motion imagery was requested, participants were free to ‘animate’ their imagined motion with visual object features other than simple dot motion (positive strategies). Negative strategies were focused mostly on bringing back fixing a static point or static figures.

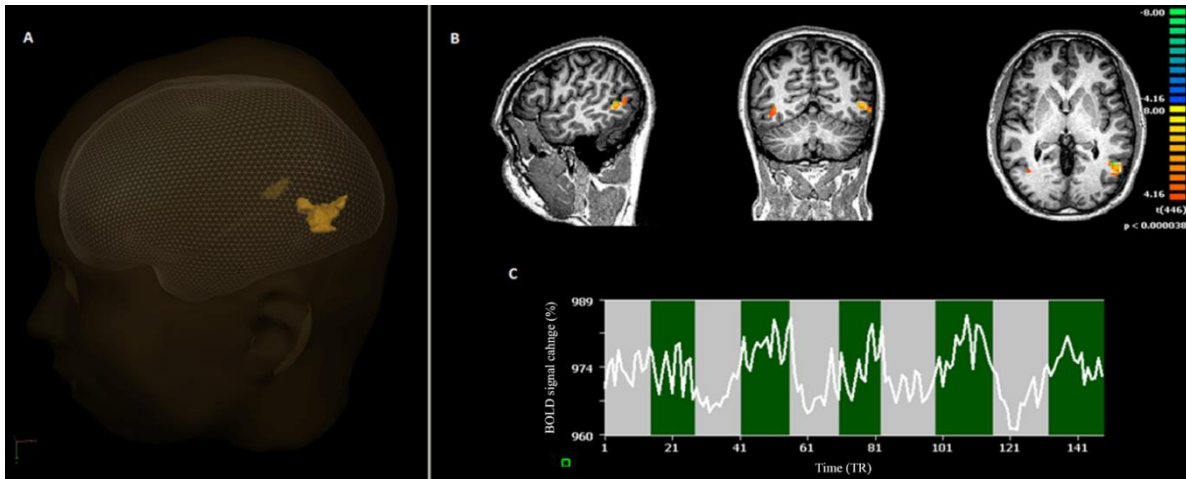


Figure 2.3. Example of a successful neurofeedback (NF) training run. (A) 3D view of the hMT+/V5 region-of-interest (ROI) activation during NF training. (B) Statistical map showing the hMT+/V5 recruitment during a NF run ($P < 0.0001$, corrected). A ROI mask as defined by the localizer was applied. (C) Time course from a NF run. The gray blocks represent the down-regulation (baseline) and the green blocks represent the up-regulation moments. The tests were self-driven.

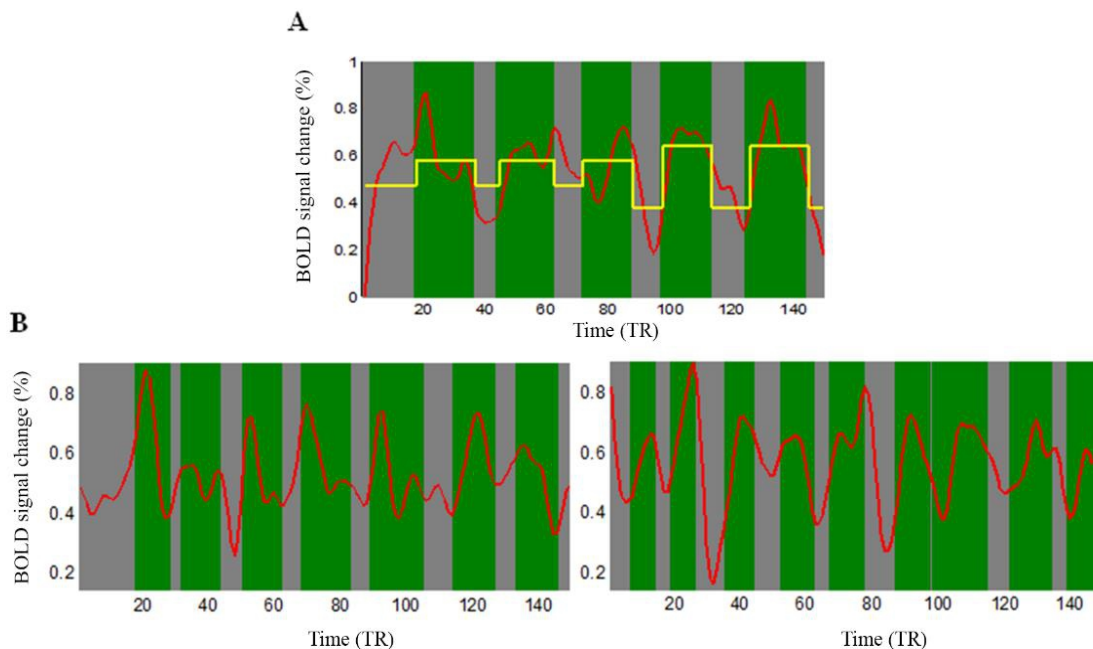


Figure 2.4. Variability of improvements of self-regulation within and across neurofeedback (NF) runs. The red curves depict the smoothed time course during a NF run. The yellow boxcar represents the mean values of time course per blocks. The gray blocks represent the down-regulation and the green represent the up-regulation periods. (A) A case of progressive mean improvement within a run, as highlighted by the yellow

moving average. **(B)** A participant that showed stable performance in a run (left) and improved self-regulation ability in a subsequent run (right, note the larger width of regulation curves).

For the participants with more than one successful NF run, the highest prediction coefficients were found mainly for the second NF run. More specifically, six participants presented the highest modulation performance in the second run, five in the first run, three in the third run and one in the last run. The analyses of the percentage of signal change per trial showed that, within each run, the main differences in activity, as compared to the baseline, were found in the middle trials (suggesting an interaction of learning and fatigue effects).

2.3.3. Whole-brain group analysis

Group analysis (figure 2.5) showed significant hMT+/V5 activations during successful NF runs (RFX, $P < 0.05$, corrected for multiple comparisons). Furthermore, additional imagery related brain activations during successful NF runs were also identified: anterior and posterior insula, putamen, caudate nucleus, cerebellum and putative V6. Their time courses showed up-regulation during positive mental imagery and down-regulation during negative mental imagery in these areas.



Figure 2.5. hMT+/V5 group activity during successful neurofeedback (NF) runs. Statistical map showing hMT+/V5 mask as identified by the localizer corresponds to the region recruited for group analysis of successful NF runs (RFX, $q(FDR) = 0.05$).

Comparing successful (table 2.1) and non-successful runs (table 2.2) some common regional activations were found (insula and putamen). However, successful NF recruited a region corresponding to the coordinates of V6, the cerebellum during visual motion imagery (figure 2.6-A) and the caudate nucleus whereas non-successful NF primarily recruited a frontal (premotor) region, which was not activated in successful NF (figure 2.6-B).

Table 2.1. Summary of regions activated during successful neurofeedback (NF) runs. The brain regions activated during successful NF are known to be involved either in motion perception or decision making. Peak voxels according Talairach coordinates and the number of used voxels recruited in each region using the contrast up-regulation versus down-regulation are presented (RFX, $q(FDR) = 0.05$).

Brain area		Talairach coordinates (x,y,z)	Voxels
MT	Left	(-45.63,-56.96,-3.30)	449
	Right	(41.63,-58.29,-2.86)	35
Cerebellum	Left	(-7.57,-66.10,-22.60)	461
	Medial	(-0.54,-66.11,-19.30)	780
	Right	(9.31,-65.31,-26.69)	514
V6	Left	(-14.26,-75.62,39.15)	484
	Right	(14.12,-73.23,38.60)	158
Insula	Posterior	(-33.14,21.93,8.35)	450
	Anterior	(34.22,23.44,5.93)	27
Putamen	Left	(-24.89,-5.32,12.07)	453
	Right	(24.80,-5.35,10.41)	187
Caudate nucleus	Left	(-13.07,17.74,11.68)	131
	Right	(13.29,17.14,12.21)	66

Table 2.2. Summary of regions activated during non-successful neurofeedback (NF) runs. Peak voxels according Talairach coordinates and the number of used voxels are presented based on the contrast up-regulation versus down-regulation (RFX, $q(FDR) = 0.05$).

Brain area		Talairach coordinates (x,y,z)	Voxels
Insula	Left	(-31.53,20.15,11.19)	159
Putamen	Left	(20.62,1.32,9.42)	355
	Right	(-24.85,1.30,8.01)	267
Frontal Cortex	Left	(-28.69,-10.04,53.05)	468

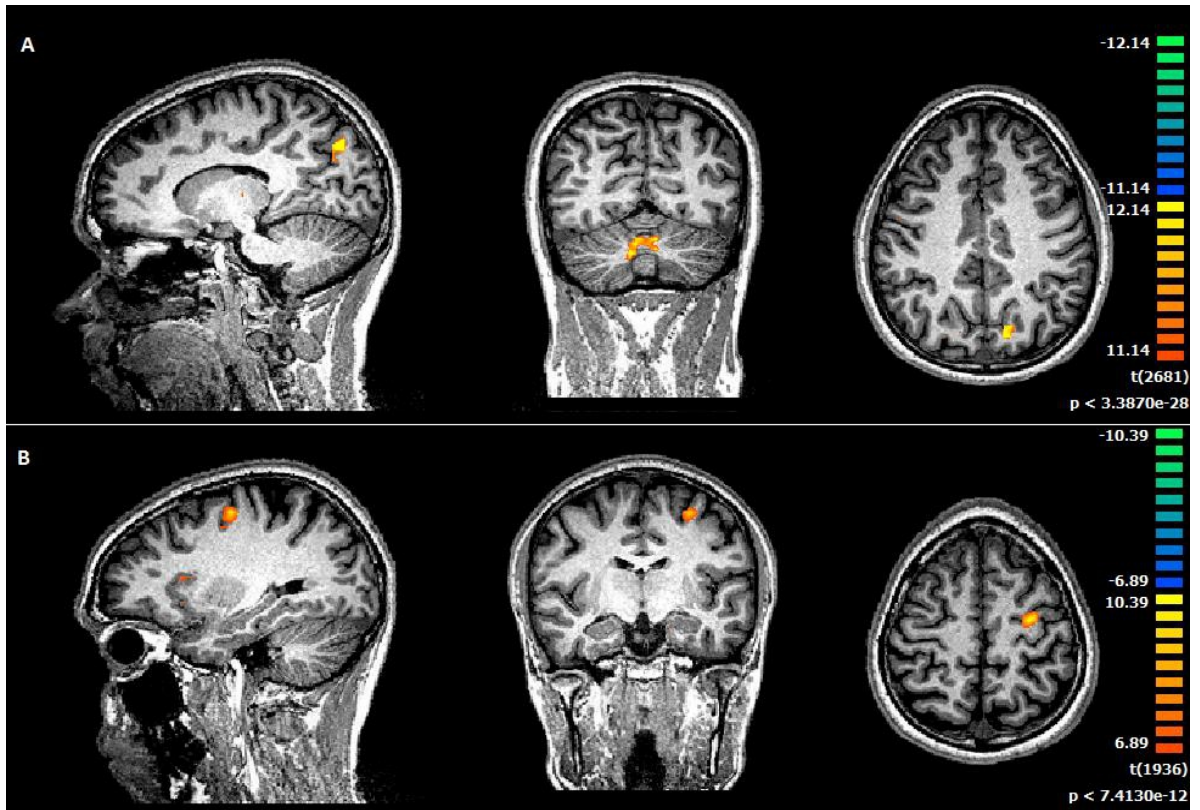


Figure 2.6. Successful versus non-successful neurofeedback (NF) run analysis ($P < 0.0001$, corrected). (A) Significantly activated areas in the former are in a region corresponding to V6 and the middle cerebellum. (B) The strongest activation in the latter is in premotor frontal cortex. The contrasts used were successful up-regulation vs. down-regulation (A) and non-successful up-regulation vs. down-regulation (B).

To further explore the neural correlates of the observed learning effects, we performed a PPI analysis using the defined hMT+/V5 ROI as seed. PPI analysis (figure 2.7) showed significant ($P = 0.001$) connectivity between hMT+/V5 and putamen, middle cerebellum and putative V6 for the successful NF runs. For the non-successful runs the strongest interaction was between hMT+/V5 and the frontal premotor cortex. The main PPI differences comparing successful and non-successful runs, using the contrast successful runs PPI versus non-successful runs PPI, were found between hMT+/V5 and the putative V6 (stronger interactions in the successful runs) and between hMT+/V5 and the frontal premotor cortex (stronger interactions in the non-successful runs). Furthermore, the middle cerebellum presented significant ($P < 0.05$) stronger interactions with the hMT+/V5 ROI in the successful runs.

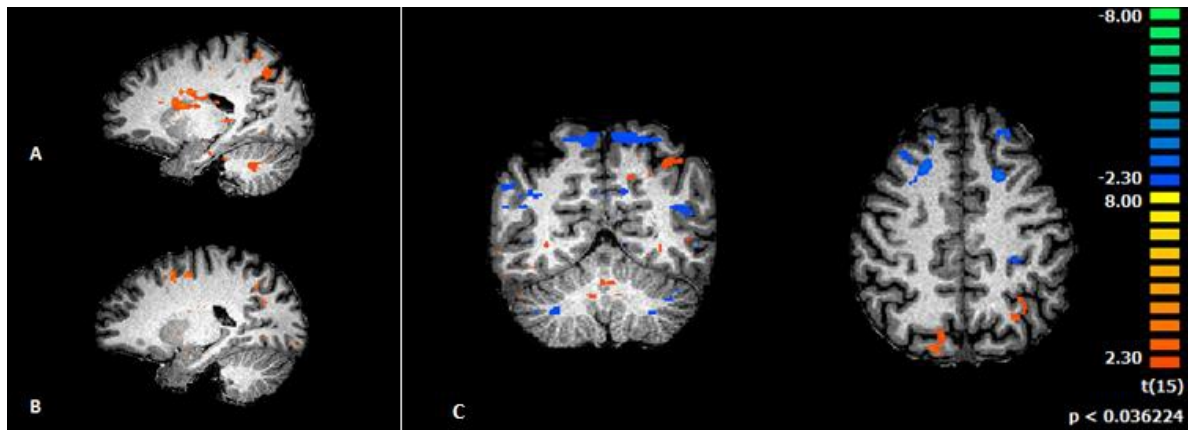


Figure 2.8. Psychophysiological interactions (PPI) of the hMT+/V5 complex during successful and non-successful neurofeedback (NF) runs. The hMT+/V5 complex showed interactions with the middle cerebellum, the putamen and the putative V6 during successful runs (A). During non-successful runs (B) the strongest interaction was with the premotor frontal cortex. PPI maps are presented at threshold of $P = 0.001$, using RFX group analysis. (C) Significant differences ($P = 0.04$) using the PPI contrast for successful vs non-successful NF runs were mainly found in putative V6 (higher interaction with the hMT+/V5 in the successful runs) and in premotor frontal cortex (higher interaction with the hMT+/V5 in the non-successful runs). Different psychophysiological interactions are also confirmed at the middle cerebellum for successful (higher interaction with the hMT+/V5) and non-successful runs.

2.4. Discussion

In this study we trained healthy participants to regulate the level of activation of their hMT+/V5 complex, a region involved in motion perception and imagery, using fMRI-based NF. The hMT+/V5 complex is well activated by visual motion imagery (Goebel et al. 1998) thereby allowing for a self-driven and self-monitored (using feedback) brain modulation.

Seventy five percent of our participants were able to effectively use this strategy to achieve their proposed goal. We found different patterns of learning effects and characterized their neural basis and functional connectivity. Most of our participants successfully regulate the target region in the first two NF runs (albeit only in about half of the runs, on average). This demonstrates an ability to quickly learn how to modulate their brain but also a growing influence of fatigue as the session progresses. A specific neural circuitry was found to be involved in successful learning, as corroborated by PPI analysis. This circuitry involves not only visual areas such as V6 and hMT+/V5 but also the striatum and cerebellum.

Only a few previous NF approaches have focused on the visual cortex (Scharnowski et al. 2012; Shibata et al. 2011). These studies focused on ROIs that encompassed several early visual areas (including areas V1, V2 and V3). Here, we proposed a ROI definition based on a functional criterion that was subsequently used as a NF strategy, taking advantage of

hMT+/V5 motion selectivity and imagery responses. Our approach of focusing on a single ROI forces a similar strategy in all participants, which may actually be an advantage because focused visual motion imagery is relatively simple to learn and to instruct in a generalized way. Moreover the single ROI choice potentially renders group effects more homogeneous. To prevent mixing of imagined and perceived feedback we opted for auditory feedback (Posse et al. 2003), which allowed to isolate motion responses just in terms of the imagery component. Furthermore, as we controlled for motion artefacts by including these parameters as predictors, we could assure that our results are not explained by higher participants' motion in the scanner during the NF runs.

Although we focused on hMT+/V5 as a region for NF modulation, our results suggest that other regions would potentially be equally effective, in particular those more closely involved in decision-making, attention and imagery. The whole-brain analysis showed additional brain activations during the hMT+/V5 visual motion imagery modulation training: insula, putamen (in successful and non-successful runs), cerebellum, caudate nucleus, and putative V6 (particularly in successful runs, as also shown by PPI analysis). These additional regions found during NF training based on imagery, which were reliably activated across participants, are known to contribute to motion perception and/or imagery (including the putamen and cerebellum), attention (striatum) (DeBettencourt et al. 2015) and to decision making, such as the anterior insula (Rebola et al. 2012). Furthermore, there are previous studies using NF to modulate the BOLD signal in the latter (Caria et al. 2010) in particular using emotional imagery.

The basal ganglia and the cerebellum are also known to have non-motor functions and to be recruited during imagery (Bauer et al. 2013). Both the caudate and putamen respond to simple visual motion stimuli and their recruitment is therefore unsurprising (Kovács et al. 2008; Nagy et al. 2008; Romero et al. 2008). Moreover, it is worth pointing out that basal ganglia regions have also recently been successfully trained in NF experiments aiming to improve sustained attention abilities (DeBettencourt et al. 2015) and to exert control over nucleus accumbens, an important brain area implicated in motivation and learning and known to be impaired in psychiatric disorders (Greer et al. 2014). Moreover, it has been suggested that hMT+/V5 motion imagery specific activation results from a top-down influence from frontoparietal regions (Goebel et al. 1998; Kaas et al. 2010; Mechelli et al. 2004). This particular neural network seems to be central in visual motion imagery (Kaas et al. 2010). In our study we found both frontal and occipitoparietal (putative V6) activations

(the latter only found for successful NF). We previously found that this network activates in difficult and effortful task conditions (Graewe et al. 2013). Here we only found frontal activation in non-successful runs. Importantly, our results also show many similarities with the motion imagery study of Kaas et al. where significant activation of right anterior insula, right basal ganglia, and left middle occipital gyrus was found (Kaas et al. 2010).

Previous evidence suggests that the cerebellum may have a critical role in motion perception (Händel et al. 2009). This study demonstrated that visual motion processing in the cerebral cortex critically depends on an intact cerebellum and established a correlation between cortical function and impaired visual perception resulting from cerebellar damage. Our results showed that this is also the case for visual motion imagery. We found midline cerebellar activations, particularly in successful NF runs. These results are consistent with evidence in patients with midline lesions that showed perceptual deficits very similar to the ones reported following cortical area hMT+/V5 lesions in primates (Ignashchenkova et al. 2009; Nawrot & Rizzo 1995). To our knowledge this is the first study establishing a direct functional link between the hMT+/V5 and the cerebellum particularly in active motion imagery. We propose that our findings are consistent with the suggestion raised from these reports of a cerebellar mechanism involved in perceptual stabilization. Such mechanism may be very important in motion imagery, where stabilization of the imagined visual representation is required. Our study supports an additional important role for these particular structures in visual motion imagery tasks.

Our findings demonstrated that given appropriate fMRI-based NF information, individuals could significantly enhance the regional BOLD activity in the hMT+/V5 complex by visual motion imagery strategies. Reliable up-regulation of the target area already during the first two sessions in most participants converges with the previous report of effective hMT+/V5 activation with visual motion imagery (Goebel et al. 1998). Previous studies (Caria et al. 2007; DeCharms et al. 2005; Weiskopf et al. 2004) also showed that one single-day training with fMRI-based NF training is enough to achieve learning. Our study therefore suggests that hMT+/V5 is at least as effective as other brain regions used as targets of NF approaches: the right anterior insula (Caria et al. 2007), somatomotor cortex and ACC (DeCharms et al. 2004) and amygdala (Zotев et al. 2011).

One of the main neuroscientific contributions of this study was the identification of a specific brain circuitry recruited only during successful NF training. This core circuit involved in visual motion imagery includes regions previously known to be involved in

motion perception (putative V6, putamen, cerebellum and hMT+/V5). Our findings raise the interesting question that this whole circuit might also be used as a target for NF. We suggest that the use of functional connectivity based NF instead of the more classical region based approach may be advantageous and should be considered in future NF studies. A recent study has actually confirmed this (Kim et al. 2015).

Finally, an important point of our study is that it may help highlight the debate on the relative potential of extrinsic (sensory) versus intrinsic (default-mode) brain regions in the clinical application of NF paradigms. While a focus on the DMN may yield powerful NF approaches (Harmelech et al. 2015) here we opted for an early visual area because of our interest in clinical applications of NF involving attentional disorders such as ADHD and Neurofibromatosis type 1, in which a ‘failure to deactivate the DMN’ has been postulated (Violante et al. 2012). It is known that in ADHD mental imagery is impaired (Abraham et al. 2006; Williams et al. 2013). We believe that training of focused imagery or attention to visual features might be a reasonable approach, as well as other approaches attempting to reduce ‘lapses of attention’ in such disorders (DeBettencourt et al. 2015). ‘BCI-eligibility’ might therefore not only depend on ‘learning’ abilities but also on the particular clinical condition to be treated.

2.5. Conclusion

We found that volitional control of hMT+/V5 visual area by using fMRI-based NF training is possible and quick to learn. This neuromodulation did not depend on recruitment of frontoparietal regions, typically found in many imagery tasks. Successful NF training on hMT+/V5 modulation allowed for the identification of a specific neural circuit involved in visual motion imagery and perceptual stabilization, which included putative V6 and the medial cerebellum. This circuit activated during NF related motion imagery, but not in non-successful runs and may be a viable approach as a target for attentional disorders where a boost of activity of the already hyperactive DMN is undesirable.

References

- Abraham, A. et al., 2006. Creative thinking in adolescents with attention deficit hyperactivity disorder (ADHD). *Child neuropsychology: a journal on normal and abnormal development in childhood and adolescence*, 12(2), pp.111–123.
- Bauer, C.C. et al., 2013. *Basal Ganglia—An Integrative View*, ed F A B A C Bauer (Rijeka: InTech).
- Borst, G. & Kosslyn, S.M., 2008. Visual mental imagery and visual perception: structural equivalence revealed by scanning processes. *Memory & cognition*, 36(4), pp.849–862.
- Caria, A. et al., 2007. Regulation of anterior insular cortex activity using real-time fMRI. *NeuroImage*, 35(3), pp.1238–1246.
- Caria, A. et al., 2010. Volitional control of anterior insula activity modulates the response to aversive stimuli. A real-time functional magnetic resonance imaging study. *Biological Psychiatry*, 68(5), pp.425–432.
- Castelo-Branco, M. et al., 2002. Activity patterns in human motion-sensitive areas depend on the interpretation of global motion. *Proceedings of the National Academy of Sciences of the United States of America*, 99(21), pp.13914–13919.
- Castelo-Branco, M. et al., 2009. Type of featural attention differentially modulates hMT+ responses to illusory motion aftereffects. *Journal of neurophysiology*, 102(5), pp.3016–3025.
- Culham, J. et al., 2001. Visual motion and the human brain: what has neuroimaging told us? *Acta psychologica*, 107(1–3), pp.69–94.
- DeBettencourt, M.T. et al., 2015. Closed-loop training of attention with real-time brain imaging. *Nature Neuroscience*, 18(3), pp.1–9.
- DeCharms, R.C. et al., 2005. Control over brain activation and pain learned by using real-time functional MRI. *Proceedings of the National Academy of Sciences of the United States of America*, 102(51), pp.18626–31.
- DeCharms, R.C. et al., 2004. Learned regulation of spatially localized brain activation using real-time fMRI. *NeuroImage*, 21(1), pp.436–443.
- DeCharms, R.C., 2007. Reading and controlling human brain activation using real-time functional magnetic resonance imaging. *Trends in cognitive sciences*, 11(11), pp.473–481.
- Farah, M.J., 1989. The neural basis of mental imagery. *Trends in Neurosciences*, 12(10), pp.395–399.
- Friston, K.J. et al., 1998. Nonlinear event-related responses in fMRI. *Magnetic Resonance in Medicine*, 39(1), pp.41–52.
- Friston, K.J. et al., 1997. Psychophysiological and modulatory interactions in neuroimaging. *NeuroImage*, 6(3), pp.218–229.
- Goebel, R. et al., 1998. The constructive nature of vision: Direct evidence from functional magnetic resonance imaging studies of apparent motion and motion imagery. *European Journal of Neuroscience*, 10(5), pp.1563–1573.
- Graewe, B. et al., 2013. Impaired processing of 3D motion-defined faces in mild cognitive impairment and healthy aging: An fMRI study. *Cerebral Cortex*, 23(10), pp.2489–2499.
- Greer, S.M. et al., 2014. Control of nucleus accumbens activity with neurofeedback. *NeuroImage*, 96, pp.237–244.
- Hamilton, J.P. et al., 2011. Modulation of subgenual anterior cingulate cortex activity with real-time neurofeedback. *Human Brain Mapping*, 32(1), pp.22–31.
- Händel, B., Thier, P. & Haarmeier, T., 2009. Visual motion perception deficits due to cerebellar lesions are paralleled by specific changes in cerebro-cortical activity. *The Journal of Neuroscience*, 29(48), pp.15126–15133.
- Harmelech, T., Friedman, D. & Malach, R., 2015. Differential Magnetic Resonance Neurofeedback Modulations across Extrinsic (Visual) and Intrinsic (Default-Mode) Nodes of the Human Cortex. *Journal of Neuroscience*, 35(6), pp.2588–2595.
- Ignashchenkova, a et al., 2009. Normal spatial attention but impaired saccades and visual motion perception after lesions of the monkey cerebellum. *Journal of neurophysiology*, 102(6), pp.3156–3168.
- Ishai, A., 2010. Seeing faces and objects with the “mind’s eye.” *Archives Italiennes de Biologie*, 148(1), pp.1–9.
- Johnston, S.J. et al., 2010. Neurofeedback: A promising tool for the self-regulation of emotion networks. *NeuroImage*, 49(1), pp.1066–1072.
- Kaas, A. et al., 2010. Imagery of a moving object: The role of occipital cortex and human MT/V5+. *NeuroImage*, 49(1), pp.794–804.
- Kim, D.-Y. et al., 2015. The Inclusion of Functional Connectivity Information into fMRI-based Neurofeedback Improves Its Efficacy in the Reduction of Cigarette Cravings. *Journal of Cognitive Neuroscience*, 27(8), pp.1552–1572.
- Kosslyn, S.M. & Thompson, W.L., 2003. When is early visual cortex activated during visual mental imagery?

- Psychological bulletin*, 129(5), pp.723–746.
- Kourtzi, Z. & Kanwisher, N., 2000. Activation in human MT/MST by static images with implied motion. *Journal of cognitive neuroscience*, 12(1), pp.48–55.
- Kovács, G., Raabe, M. & Greenlee, M.W., 2008. Neural correlates of visually induced self-motion illusion in depth. *Cerebral Cortex*, 18(8), pp.1779–1787.
- Linden, D.E.J. et al., 2012. Real-time self-regulation of emotion networks in patients with depression. *PLoS ONE*, 7(6).
- Mechelli, A. et al., 2004. Where bottom-up meets top-down: Neuronal interactions during perception and imagery. *Cerebral Cortex*, 14(11), pp.1256–1265.
- Mellet, E. et al., 1998. Reopening the Mental Imagery Debate: Lessons from Functional Anatomy. *NeuroImage*, 8(2), pp.129–139.
- Mikami, A., Newsome, W.T. & Wurtz, R.H., 1986. Motion selectivity in macaque visual cortex. I. Mechanisms of direction and speed selectivity in extrastriate area MT. *Journal of neurophysiology*, 55(6), pp.1308–1327.
- Nagy, A. et al., 2008. Drifting grating stimulation reveals particular activation properties of visual neurons in the caudate nucleus. *European Journal of Neuroscience*, 27(7), pp.1801–1808.
- Nawrot, M. & Rizzo, M., 1995. Motion perception deficits from midline cerebellar lesions in human. *Vis. Res.*, 35, pp.723–31.
- Newsome, W.T. & Pare, E.B., 1988. A selective impairment of motion perception following lesions of the Middle Temporal visual area (MT). *Journal of Neuroscience*, 8(6), pp.2201–2211.
- O’Craven, K.M. & Kanwisher, N., 2000. Mental imagery of faces and places activates corresponding stimulus-specific brain regions. *Journal of cognitive neuroscience*, 12(6), pp.1013–23.
- O’Reilly, J.X. et al., 2012. Tools of the trade: Psychophysiological interactions and functional connectivity. *Social Cognitive and Affective Neuroscience*, 7(5), pp.604–609.
- Posse, S. et al., 2003. Real-time fMRI of temporolimbic regions detects amygdala activation during single-trial self-induced sadness. *NeuroImage*, 18(3), pp.760–768.
- Rebola, J. et al., 2012. Functional parcellation of the operculo-insular cortex in perceptual decision making: An fMRI study. *Neuropsychologia*, 50(14), pp.3693–3701.
- Romero, M.C. et al., 2008. Activity of neurons in the caudate and putamen during a visuomotor task. *Neuroreport*, 19(11), pp.1141–5.
- Rota, G. et al., 2009. Self-regulation of regional cortical activity using real-time fmri: the right inferior frontal gyrus and linguistic processing. *Human Brain Mapping*, 30(5), pp.1605–1614.
- Ruiz, S. et al., 2013. Acquired self-control of insula cortex modulates emotion recognition and brain network connectivity in schizophrenia. *Human Brain Mapping*, 34(1), pp.200–212.
- Scharnowski, F. et al., 2012. Improving Visual Perception through Neurofeedback. *Journal of Neuroscience*, 32(49), pp.17830–17841.
- Shibata, K. et al., 2011. Perceptual learning incepted by decoded fMRI neurofeedback without stimulus presentation. *Science*, 334(6061), pp.1413–5.
- Slotnick, S.D., Thompson, W.L. & Kosslyn, S.M., 2005. Visual mental imagery induces retinotopically organized activation of early visual areas. *Cerebral Cortex*, 15(10), pp.1570–1583.
- Subramanian, L. et al., 2011. Real-Time Functional Magnetic Resonance Imaging Neurofeedback for Treatment of Parkinson’s Disease. *The Journal of Neuroscience*, 31(45), pp.16309–16317.
- Sulzer, J. et al., 2013. Real-time fMRI neurofeedback: Progress and challenges. *NeuroImage*, 76, pp.386–399.
- Tootell, R.B. et al., 1995. Functional analysis of human MT and related visual cortical areas using magnetic resonance imaging. *Journal of Neuroscience*, 15(4), pp.3215–3230.
- Violante, I.R. et al., 2012. Abnormal brain activation in neurofibromatosis type 1: a link between visual processing and the default mode network. *PLoS One*, 7(6), p.e38785.
- Watson, J.D. et al., 1993. Area V5 of the human brain: Evidence from a combined study using positron emission tomography and magnetic resonance imaging. *Cereb Cortex*, 3(2), pp.79–94.
- Weiskopf, N. et al., 2003. Physiological self-regulation of regional brain activity using real-time functional magnetic resonance imaging (fMRI): methodology and exemplary data. *Neuroimage*, 19(3), pp.577–86.
- Weiskopf, N. et al., 2004. Self-regulation of local brain activity using real-time functional magnetic resonance imaging (fMRI). *Journal of Physiology Paris*, 98(4–6 SPEC. ISS.), pp.357–373.
- Williams, J. et al., 2013. Motor imagery skills of children with Attention Deficit Hyperactivity Disorder and Developmental Coordination Disorder. *Human Movement Science*, 32(1), pp.121–135.
- Zeki, S. et al., 1991. A direct demonstration of functional specialization in human visual cortex. *The Journal of Neuroscience*, 11(March), pp.641–649.
- Zotey, V. et al., 2011. Self-regulation of amygdala activation using real-time FMRI neurofeedback. *PLoS ONE*, 6(9).

APPENDIX

Chapter 2

A1. Experimental design

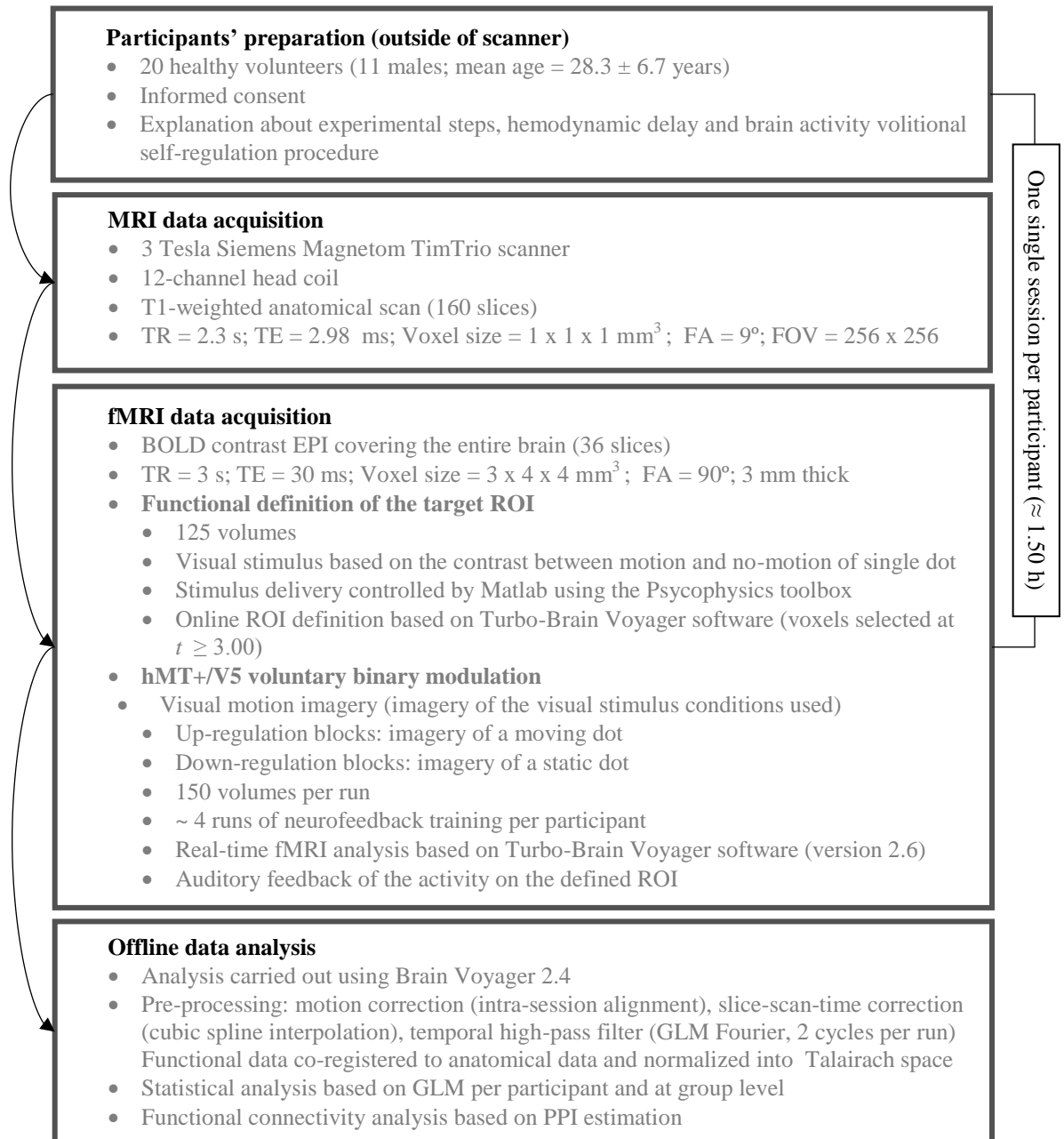


Figure 2.A1. Summary of the main steps of the experimental procedure followed in the study. Each participant took part of a single session lasting approximately about 1.50 h. First, clear instructions about the experimental steps and procedures were given to participants outside the scanner. Then, participants performed neurofeedback training based on fMRI signal and visual motion imagery to up- and down-regulate their hMT+/V5 activity. Anatomical data was also acquired to posterior co-registration of the functional data during offline analysis. The fMRI real-time analysis was performed on Turbo-Brain Voyager software and the offline analyses were performed using Brain Voyager Qx. The main analyses were based on general liner model (GLM) and psychophysiological interactions (PPI) approaches. *fMRI* – functional magnetic resonance imaging, *TR* – repetition time, *FA* – flip angle, *TE* – echo time, *FOV* – field of view, *ROI* – region of interest.

A2. Implemented neurofeedback system

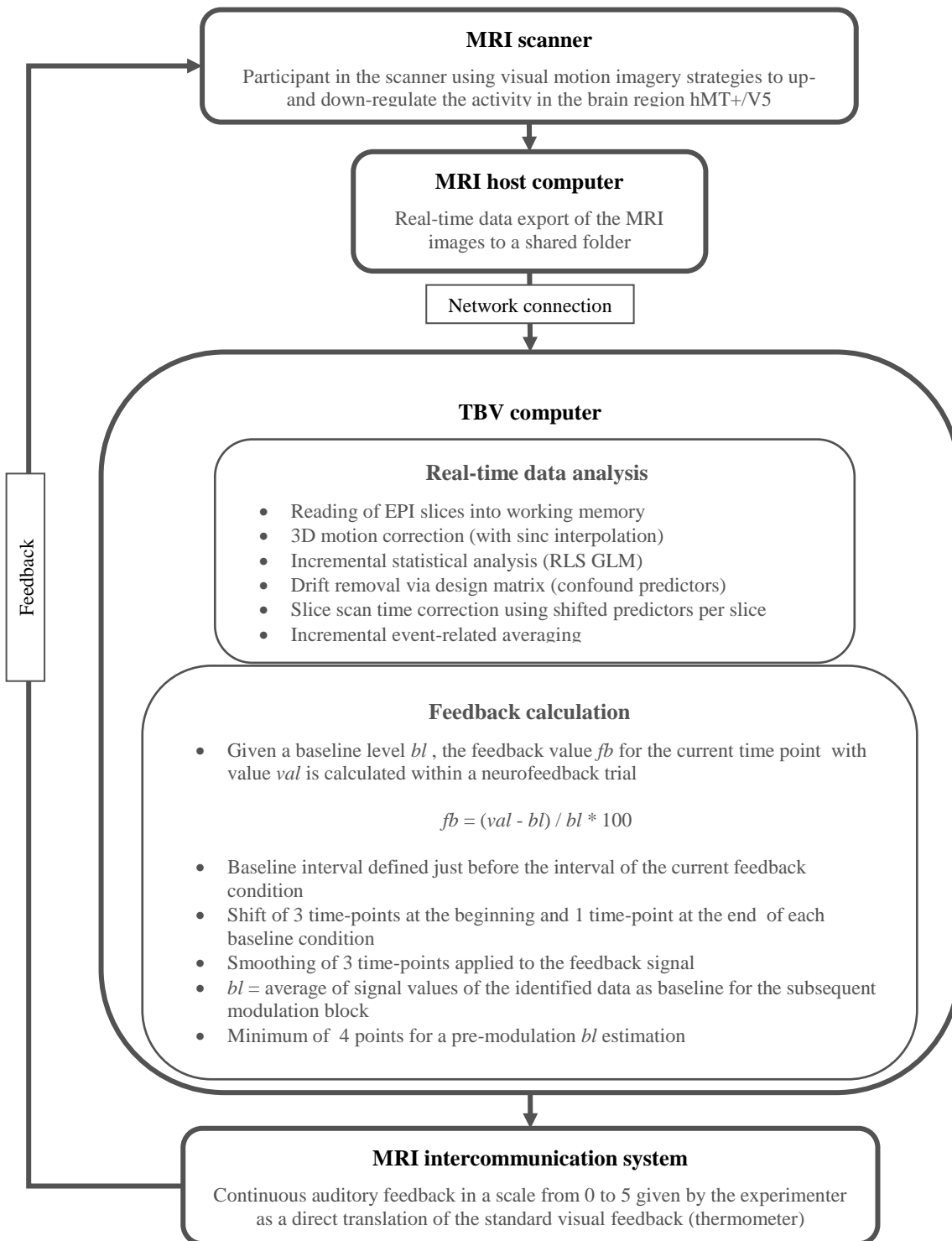


Figure 2.A2. Set-up of the implemented neurofeedback system. The participant was trying to up-regulate and down-regulate brain activity by applying strategies of visual motion imagery, inside the MRI scanner. The acquired fMRI data were analyzed in real-time and the level of brain activity was given as feedback to the participant. The Turbo-BrainVoyager (TBV) software was used for the real-time data processing. It was installed on a separate computer to ensure optimal hardware usage and, thereafter, best results in real-time processing. The TBV uses an incremental recursive least squares (RLS) based general linear model (GLM) to perform the statistical analysis.

CHAPTER 3

CONTROL OF BRAIN ACTIVITY IN HMT+/V5 AT THREE RESPONSE LEVELS USING fMRI-BASED NEUROFEEDBACK

Based on: Sousa, T., Direito, B., Lima, J., Ferreira, C., Nunes, U., Castelo-Branco, M., 2016. Control of brain activity in hMT+/V5 at three response levels using fMRI-based neurofeedback/BCI. *PLoS ONE*, 11(5).

We would like to thank the participants for their involvement with this study. We are also very grateful to João Pedro Marques for the help with real-time fMRI set up and scanning and, to Catarina Duarte and João Duarte for the help in offline analysis of the data.

Abstract

A major challenge in brain-computer interface research is to increase the number of command classes and levels of control. Brain-computer interface studies often use binary control level approaches (level 0 and 1 of brain activation for each class of control). Different classes may often be achieved but not different levels of activation for the same class. The increase in the number of levels of control in brain-computer interface applications may allow for larger efficiency in neurofeedback applications.

In this work we test the hypothesis whether more than two volitional modulation levels can be achieved in a single brain region, the hMT+/V5 complex. Participants performed three distinct imagery tasks during neurofeedback training: imagery of a static dot, imagery of a dot with two opposing motions in the vertical axis and imagery of a dot with four opposing motions in vertical or horizontal axes (imagery of 2 or 4 motion directions). The larger the number of motion alternations, the higher the expected hMT+/V5 response.

A substantial number (17 of 20) of participants achieved successful binary level of control and 12 were able to reach even three significant levels of control within the same session, confirming the whole group effects at the individual level. With this simple approach we suggest that it is possible to design a multilevel system of control based on volitional activity modulation of a specific brain region with at least three different levels. Furthermore, we show that particular imagery task instructions, based on different number of motion alternations, provide feasible achievement of different control levels in brain-computer interface and/or neurofeedback applications.

3.1. Introduction

Multivariate supervised learning methods combined with real-time functional magnetic resonance imaging (fMRI) have allowed for the development of approaches enabling decoding of brain states based on the blood-oxygenation-level-dependent (BOLD) signal (Formisano et al. 2008). The decoded brain states can be used as control signals for a brain-computer interface (BCI) and/or to provide neurofeedback (NF) to the subject (LaConte 2011; Weiskopf, Mathiak, et al. 2004; Weiskopf 2012).

NF systems represent a BCI variant which allow training of voluntary regulation of brain activity, by feeding back information based on users' brain activity (Weiskopf, Scharnowski, et al. 2004). It is known that healthy subjects can learn to self-regulate their local BOLD response with the help of real-time fMRI-based NF (Caria et al. 2007; Caria et al. 2010; DeCharms et al. 2004; Hamilton et al. 2011; Johnston et al. 2010; McCaig et al. 2011; Rota et al. 2009; Scharnowski et al. 2012; Yoo et al. 2007). Specific behavioral effects have been reported as a result of NF in line with the idea that it allows for useful self-regulation of neuronal activity (Caria et al. 2010; Johnston et al. 2010; Rota et al. 2009; Scharnowski et al. 2012). Accordingly, the potential importance of NF for learning self-regulation goes beyond what may be achieved by simple behavioral approaches based on the sole use of conscious cognitive strategies (Caria et al. 2007; DeCharms et al. 2005; Rota et al. 2009). Clinical results of real-time fMRI-based NF studies focused at behavioral modulation do support its role as a novel non-invasive treatment tool for neurological and psychiatric disorders (DeCharms et al. 2005; Haller et al. 2010; Linden et al. 2012; Ruiz et al. 2013; Sitaram et al. 2012; Subramanian et al. 2011).

The correspondence between distinct brain activity patterns and particular perceptual states are key factors in determining whether cognitive states can be decoded. One typical case of such separation is given when different cognitive states/commands are encoded in spatially distinct locations of the brain (Haynes & Rees 2006). In this case, BCI/NF studies are usually implemented using binary control level approaches. In other words, level 0 and 1 of brain activation are tested for a particular command. If multiple classes of control are aimed at, then multiple brain regions are needed to encompass several commands using this approach. Accordingly, a few studies have tested multiple classes of control based on a

variety of mental tasks, but critically, they recruited distinct brain areas for different commands, and not the same brain region (Lee et al. 2009; Yoo et al. 2004), or took advantage of different spatio-temporal aspects of the BOLD signal (Sorger et al. 2012). Different classes of control could be achieved but not different levels of up-regulation in the same region. Yoo et al. (2004) explored the possibility of using real-time fMRI to interpret the spatial distribution of brain activity as BCI commands. They asked participants to perform four different mental tasks ('right hand motor imagery', 'left hand motor imagery', 'mental calculation', and 'inner speech') that evoke differential brain activation in four distinct brain locations and were interpreted as four BCI commands (four classes of control, each with a binary up-regulation level). Lee et al. (2009) applied the same strategy to control a robotic arm movement. BOLD signals originating from the hand motor areas during right or left hand motor imagery tasks were translated into horizontal or vertical robotic arm movement (two classes of control with one upregulation level). More recently, Sorger et al. (2012) proposed a spelling device based on fMRI, by exploiting spatiotemporal characteristics of hemodynamic responses, evoked by performing differently timed mental imagery tasks (again, multiple commands, but only one up-regulation level).

When aiming to use real-time fMRI-based training for practical applications, it is relevant to demonstrate that training can produce beyond binary levels of control which might be advantageous as compared to those that can be achieved using conventional strategies. Therefore, it is of potential interest to assess multilevel/parametric BCI/NF (with more than one level of up-regulation) (Sorger 2010). The increase of the number of levels of control in BCI applications would allow for more powerful NF applications (different levels of volitional neuromodulation, i.e. more control levels over the activity of one particular brain region).

In this study we tested different visual imagery tasks with real-time fMRI-based NF in order to modulate the activity level of the same specific brain region, the hMT+/V5 complex, to verify whether more activation levels could be achieved than the typical binary case. We hypothesized that imagery tasks involving different numbers of imagined motion alternations, would lead to different levels of brain activity.

Pattern-based decoding of fMRI signals can successfully predict the perception of low-level perceptual features. For example, the orientation (Haynes & Rees 2005) and direction (Kamitani & Tong 2006) of a motion visual stimulus presented to an individual can be predicted by decoding spatially distributed patterns of signals from local regions in early

visual cortex. Decoding these patterns in imagery tasks is rather complex and none of these approaches alone has been successfully used to yield different levels of activation in imagery-based NF. Therefore, we decided to train the modulation of activity in the motion sensitive hMT+/V5 complex by exploring the alternative combination of multiple motion features, and to test three distinct visual imagery tasks based on those combinations.

We were inspired by the notion that strong and reliable fMRI responses are produced by the alternation of distinct grating orientations (Tootell et al. 1998) in primary visual cortex (V1) in humans. In the motion perception domain, conditions for which motion alternations occur more often lead to stronger responses due to a break in brain response adaptation and/or higher attentional deployment. We adapted this notion to design our approach by hypothesizing that a larger number of motion alternations during the imagery tasks would lead to higher activity levels in hMT+/V5 as compared to a lower number of imagined alternations. We tested two up-regulation tasks using visual imagery strategies, imagery of a dot with two opposing motions in the vertical axis (imagery of two motion directions) and imagery of a dot with four opposing motions in vertical or horizontal axes (imagery of four motion directions) and one additional condition of down-regulation through the imagery of a static dot (no motion). Our hypothesis is that three distinct levels of hMT+/V5 activity can be achieved based on these three imagery tasks with different number of motion alternations.

The visual region hMT+/V5 was chosen, since it is a well-studied motion sensitive area, at the intersection of the occipital, temporal and parietal lobes, often specified as located at the occipito-temporo-parietal pit, and easily identified through functional visual localizers with robust motion selective responses including imagery (Castelo-Branco et al. 2009; Goebel et al. 1998; Graewe et al. 2013). Response sensitivity to three-dimensional structure from motion is also well characterized in this region and in accordance with its monkey MT homologue (Kolster et al. 2010; Tootell et al. 1995).

3.2. Materials and methods

3.2.1. Ethics statement and participants

This work was approved by the Ethics Committee of the Faculty of Medicine of the University of Coimbra. Twenty human volunteers gave written informed consent to

participate in the experiment. The study has been conducted according to the principles expressed in the Declaration of Helsinki.

Twenty volunteers (fifteen male, between 20 and 53 years old, mean age = 28, $SD \pm 6.8$, all right handed) with normal or corrected-to normal vision participated in this study. None of them had a history of neurological, major medical, or psychiatric disorders.

3.2.2. Experimental design

First, participants were given instructions about the tasks and overall experiment. These included an explanation of the nature of feedback and recommendations concerning the regulation strategy (requiring imagery of different levels of movement direction alternation). We also explained the presence of a short time delay between the image acquisition and the feedback (which corresponds to the hemodynamic delay plus the real-time processing time). Then an anatomical scan was acquired. Participants performed a functional localizer task designed to identify the region-of-interest (ROI) hMT+/V5 over the left and right regions involved in visual motion processing. This ROI served as the subsequent signal source for NF runs.

Four imagery runs, each lasting nine minutes, with three different imagery tasks (visual imagery of the three types of stimuli shown during the previous localizer run) performed according to auditory instructions, were acquired. First, a passive imagery run (i.e. control run without feedback) was performed. In the two subsequent NF runs, participants attempted the up-regulation (during two motion imagery tasks) and down-regulation (during a static dot imagery task) of the selected ROI fMRI signals assisted by a real-time auditory feedback. Finally, participants tried self-regulation in the absence of feedback during the final transfer run. They were asked to close the eyes throughout the four imagery runs, to breathe steadily, and to remain as still as possible. For a complete overview of the experimental design please see the supplementary figure 3.A1 in appendix.

3.2.3. fMRI data acquisition

Scanning was performed using a 3 Tesla (3T) Siemens Magnetom TimTrio scanner, at the Portuguese Brain Imaging Network Central Facilities, using a 12-channel head coil. For each participant, scanning included the acquisition of five BOLD contrast echo-planar imaging (EPI) fMRI runs - one hMT+/V5 localizer experiment, one visual motion imagery run, two NF runs, and the final transfer run.

The recorded functional images consisted of 33 slices (field of view (FOV): 256 x 256 mm², voxel size 4.0 x 4.0 x 3.0 mm³, flip angle (FA): 90°) yielding a total coverage of the occipital and posterior temporal lobe. Repetition time (TR) was 2000 ms (echo time (TE): 30 ms). For each participant, 200 volumes were acquired for the localizer run and 275 volumes for each NF, imagery and transfer runs. The beginning of each run was synchronized with the acquisition of the fMRI volumes.

Each scanning session included the acquisition of a high-resolution magnetization-prepared rapid acquisition gradient echo (MPRAGE) sequence for co-registration of functional data (176 slices; TR: 2530 ms; TE: 3.42 ms; voxel size 1.0 x 1.0 x 1.0 mm³; FA: 7°; FOV: 256 x 256 mm²).

3.2.4. Real-time fMRI data processing

The fMRI setup used for real-time data processing was based on Turbo-BrainVoyager 3.0 (Brain Innovation, Maastricht, The Netherlands) (Goebel 2012) as previously described in (Weiskopf, Mathiak, et al. 2004). A scheme of the implemented NF system set-up is presented as supplementary figure 3.A2 in appendix.

Data were analyzed with real-time with Turbo-BrainVoyager software performing online 3D motion detection and correction, and drift removal. The statistical analysis was based on a parametric general linear model (GLM) and event-related averaging.

The feedback level was computed based on the mean activation level of the ROI of each incoming acquisition volume, i.e. at each TR the feedback was calculated based on percentage of ROI mean signal change in relation to the last baseline (down-regulation task) period. The feedback value was given to the participant using auditory instructions to prevent visual contamination/noise leading to additional signals in hMT+/V5 induced by motion in the visual field. The experimenter quantitatively forwarded the changes in mean activation level of the ROI, at each 2 TR, to the participant thus translating the exact levels of the standard visual “thermometer” scale of the Turbo Brain Voyager software (from level 0 - no activation to level 5 - max activation).

3.2.5. Functional definition of the target ROI (localizer experiments using visual stimulation)

Studies based on both single and multiple dots (Goebel et al. 1998; Mikami et al. 1986; Newsome & Pare 1988) have shown that a moving dot task reliably activates the hMT+/V5 complex (Graewe et al. 2013).

The NF target ROI, the hMT+/V5 complex, was determined using a functional localizer with 200 volumes. Participants were asked to fixate on a moving dot stimulus with two distinct motion conditions interleaved with a static dot. As described in figure 3.1, the moving stimulus is a white dot either oscillating up and down along a vertical trajectory or with a back/forward movement according to a horizontal trajectory, against a black background. Three different conditions with different number of motion alternations were used: zero motion (static dot), a dot with two opposing motions (in the vertical axis) and a dot with four opposing motions (either horizontal or vertical axes).

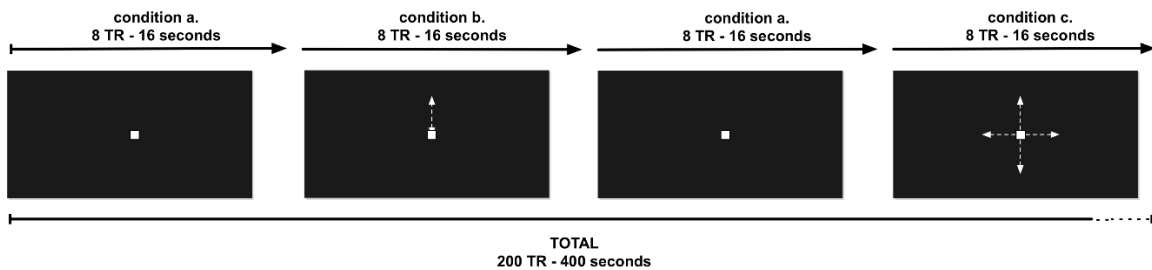


Figure 3.1. Functional localizer used to define the hMT+/V5 region-of-interest (ROI). (A) Static dot, condition used as baseline to the moving conditions depicted in (B) and (C). The arrows are here merely representing the dot motions used during the localizer. Each motion condition was repeated six times and randomly interleaved with the static dot condition. The duration of each block was 8 TR.

Sixteen seconds blocks of a moving dot (2.5 deg/s), were randomly interleaved with 16 seconds blocks of a static dot. The distance covered by the dot was 2 degrees of arc. The 2 blocks with motion were repeated 6 times, that resulted in a total of 25 blocks, 6 minutes and 40 seconds, 200 volumes. The point size was $0.5 \times 0.5 \text{ cm}^2$ and the stimulus was displayed at 44.5 cm (visual angle of the dot: 0.64 deg) from the subject at a screen of $24.1 \times 18.2 \text{ cm}^2$. Stimulus display was controlled by MATLAB (MathWorks) using the psychophysics toolbox. The ROI was defined by selecting on the occipito-temporo-parietal pit all significantly activated voxels at $P = 0.001$ during the functional localizer run. The bilateral ROI size was not fixed, given that it was only dependent on the defined threshold.

3.2.6. Neuromodulation runs (NF experiments using visual imagery)

After the anatomical and fMRI localizer scans, each subject performed four different real-time fMRI imagery runs: one control run of passive imagery, two NF runs and one control transfer run. Each run was composed by the three visual imagery tasks, matching the three visual stimulation conditions presented during the localizer run: imagery of a static dot, imagery of the dot with 2 opposing motions along the vertical axis and imagery of the dot with 4 opposing motions along either the horizontal or vertical axis. Instructions for each task/condition were provided as auditory cues and were coded as ‘A’, ‘B’ and ‘C’ respectively. Each run was composed of several up-regulation blocks (pseudo-randomly presented dot motion imagery tasks, 6 repetitions of each task) interleaved by down-regulation blocks (imagery of a static dot). The duration of each block was 22 seconds. Each run lasted 9 minutes and 10 seconds (i.e. a total of 275 volumes per run).

The passive imagery (imagery without feedback) run was acquired as a control. With the exception of the feedback component, all the other parameters of this run are similar to the NF runs during which participants performed different imagery tasks while trying to control the feedback value based on the activity of hMT+/V5. At the end of the NF training runs participants were instructed to modulate their ROI activity using the same strategies, but now without feedback (transfer run). All runs were performed consecutively on the same session.

Participants were not explicitly asked to try to achieve different levels of activation in the two different tasks of up-regulation (imagery of 2 or 4 motion directions). They were instructed to allocate similar effort (mere imagery) in the up-regulation conditions to achieve the highest level of activation possible. The goal was to achieve different activation levels depending on the used strategy (2 vs 4 motion directions) at a similar effort level. For the down-regulation condition (baseline) they were instructed to decrease as much as possible their ROI activity (imagery of static dot).

3.2.7. Offline data analysis

The BrainVoyager QX 2.8.4 software version (Brain Innovation, Maastricht, The Netherlands) (Goebel 2012) was used for fMRI offline post-processing and analysis.

Pre-processing of the functional data included temporal high-pass filtering (GLM Fourier) with 2 cycles per run, space domain 3D spatial smoothing with a Gaussian filter of 4 mm, 3D motion correction with intra-session alignment and slice scan time correction

with cubic spline interpolation. Functional data were co-registered to anatomical data per subject and subsequently normalized into Talairach coordinate space (Talairach & Tournoux 1988).

For each stimulus condition or imagery task presented to the subject, statistical maps were computed using a GLM (Kutner et al. 2004). The design matrix of the GLM was given by predictors encoding the stimulus conditions (localizer runs) and imagery task blocks (neuromodulation runs). The design matrixes were convolved with a double gamma hemodynamic response function in order to account for the hemodynamic delay and dispersion (Friston et al. 1998).

Statistical significant differences between each experimental motion condition and baseline (no motion condition), and between motion conditions were assessed using contrast (t) maps in each run. The contrasts β , t and P values were analyzed after correction for serial correlations (Kutner et al. 2004). This correction was performed using a second-order autoregressive, AR (2), method (Lenoski et al. 2008). A group random effect - RFX - analysis (with false discovery rate - FDR - correction for multiple comparisons) was performed to determine the ROI multi-subject cluster peak voxel resulting from the stimulation runs. Furthermore, supplementary whole-brain tests per imagery run were performed at the group level using fixed effects - FFX - analyses (with FDR correction for multiple comparisons) to list which other brain regions were recruited during the visual motion imagery (see supplementary table 3.A1 in appendix). These analyses were performed separately for each run due to the fact that we include control and NF runs, and that inter-run variability is a recognized feature (Sulzer et al. 2013) (either due to learning and/or fatigue).

In order to verify if there was a group overall significant difference between the three different stimulation conditions (localizer visual stimulation experiments) and also between the three imagery tasks (imagery experiments organized in two groups of runs: imagery with feedback and the two types of imagery runs without feedback), we performed group analyses using linear trend tests and repeated measures ANOVA. These statistical analyses were based on percentage of signal change for each experimental condition extracted from the event-related averaging of each participant and using as baseline the average of every value of each pre-period (2 TR of the beginning of each condition) over the whole time-course. We also performed post-hoc tests to verify between which conditions (static and 2 or 4 direction of motion imagery) occurred those differences. Furthermore, a two-way

ANOVA was conducted to examine the effect of feedback on ROI response level. Chi-square tests and Pearson correlation were computed as well to analyze the putative influence of gender or age, respectively. Effects were only accepted as significant when $P < 0.05$ (corrected for multiple comparisons).

3.3. Results

3.3.1. hMT+/V5 localization

The GLM statistical maps resulting from the localizer run, ($P < 0.05$, Bonferroni corrected), revealed significant activations in the hMT+/V5 complex for each participant motion contrast (figure 3.2, example from one participant), consistent with prior reports of its localization (Castelo-Branco et al. 2002; Castelo-Branco et al. 2009; Graewe et al. 2013). The ROI multi-subject cluster peak voxel center coordinates at $P = 0.001$ (RFX, q (FDR) = 0.05), were as follows (x, y, z): left (-44, -69, 2) and right (44, -68, 2).

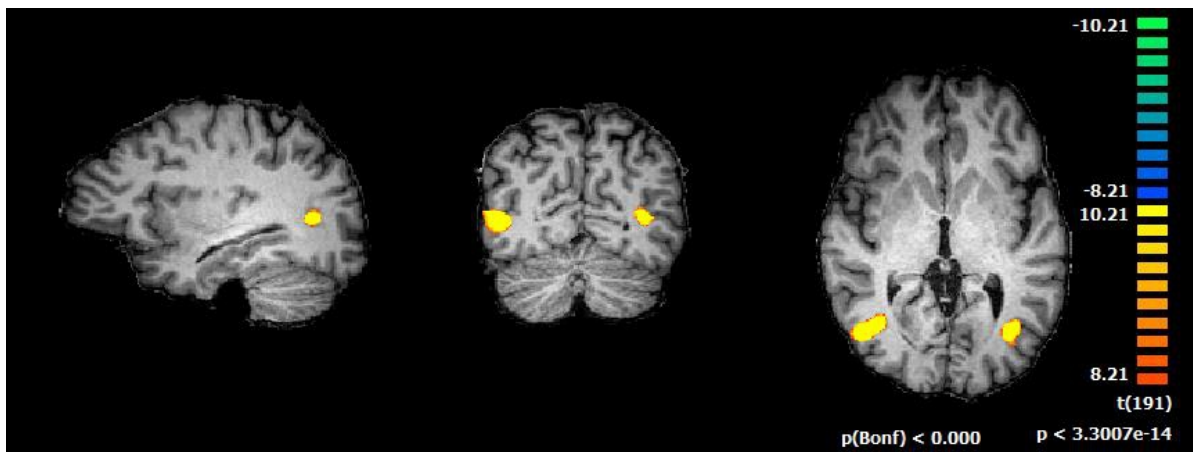


Figure 3.2. Example of hMT+/V5 identification using the defined localizer. General linear model (GLM) conjunction analysis (using the stringent criterion that all particular motion vs static blood-oxygenation-level-dependent (BOLD) signal contrasts had to be significant for a voxel to be considered positive) shows the resulting region-of-interest (ROI): hMT+/V5. Regions are shown at the same statistical threshold level ($P < 0.0001$, Bonferroni corrected).

Activation maps calculated in the offline analysis matched and validated activations maps observed in real-time using Turbo-Brain Voyager. This region was used as a ROI from which BOLD responses were extracted for each of the subsequent experimental conditions.

We predicted that different stimulation conditions with different quantity of motion alternation would lead to different levels of hMT+/V5 activity (for example 4 directions of motion lead to larger activity than 2 directions of motion). Accordingly, different ROI

activation levels were observed as response to the different stimulation conditions (figure 3.3). A repeated measures ANOVA determined that mean ROI activity differed significantly between stimulation conditions ($F(1.52, 22.80) = 51.35, P < 0.0001$). Post-hoc tests using the Bonferroni correction revealed that motion conditions evoked stronger hMT+/V5 activity than the zero motion condition (statistically significant at $P < 0.0001$). Furthermore, the two movement conditions evoked significantly different activity levels ($P = 0.045$), and larger activity was observed for the condition with 4 directions of motion.

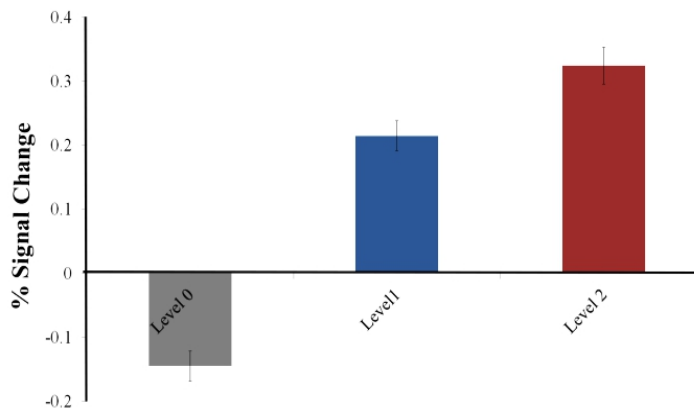


Figure 3.3. Mean blood-oxygenation-level-dependent (BOLD) activity within hMT+/V5 region-of-interest (ROI) during visual motion stimulation at different response levels. Group results for the localizer run, based on mean event-related BOLD response to the three stimulation conditions in the defined ROI per participant. Significant differences between all conditions were found at $P < 0.05$ (with Bonferroni correction for multiple comparisons). Values are presented as mean \pm s.e.m. Level 0 - static dot; level 1 - dot with two opposing motions; level 2 - dot with four opposing motions.

3.3.2. hMT+/V5 modulation: imagery based control of brain activity at 3 response levels

During the NF runs only three of the twenty participants were not able to modulate the hMT+/V5 activation. We considered that a participant was able to modulate the ROI activation when he/she showed an overall positive and statistically significant ROI response during at least one of the two up-regulation tasks in comparison to the down-regulation. From the remaining group, one participant achieved significant estimated effect (*beta* weight) for the 2 opposing motions imagery task, and sixteen participants were able to significantly increase (in relation to the down-regulation task) the defined ROI activity ($P < 0.05$) to both up-regulation tasks in at least one of the NF runs. Nevertheless, the contrast analysis between the ROI evoked responses during both up-regulation imagery strategies (with distinct number of imagined motion alternations), for each of these 16 participants, allowed us to verify that 12/20 participants showed not only a significant contrast between

the evoked response during each of up-regulation task and the down-regulation task, but also a significant contrast between the responses evoked by the both up-regulation strategies (hereafter, we refer to this group of participants as the successful neuromodulators group).

Globally, mean hMT+/V5 BOLD activity levels achieved during the up-regulation using the imagery of the dot with 4 opposing motion as strategy were higher than the mean activity resulting from the up-regulation using as strategy the imagery of the dot with 2 opposing motions. Figure 3.4 shows the mean group ($N = 20$) BOLD activity levels on the selected ROI for neuromodulation runs with and without feedback (separating the passive imagery and transfer runs) as result of the three imagery tasks. As illustrated, group results taking into account all the participants in the study show evidence for multilevel/parametric neuromodulation (responses levels 0, 1 and 2) according the number of motion alternations involved in each visual motion imagery strategy.

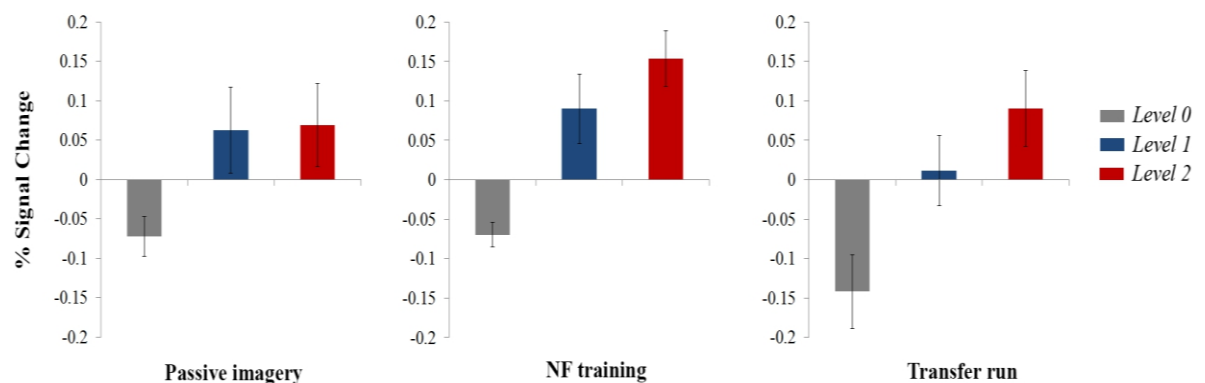


Figure 3.4. Mean blood-oxygenation-level-dependent (BOLD) activity within hMT+/V5 region-of-interest (ROI) during the neuromodulation runs with and without feedback. Group results ($N = 20$) based on mean event-related BOLD response to the three imagery tasks in the defined ROI per participant for neuromodulation runs with feedback (NF training) and for neuromodulation runs without feedback (prior passive imagery and transfer runs). Values are presented as mean \pm s.e.m. Three response levels were achieved depending on the applied imagery strategy (level 0: imagery of a static dot; level 1: imagery of a dot with two opposing motions; level 2: imagery of a dot with four opposing motions). A significant linear trend between response levels was found during the neurofeedback ($F(1, 57) = 20.74, P < 0.0003$) which persisted in the transfer run ($F(1, 57) = 11.86, P = 0.003$).

The comparison of the percentage of signal change achieved with distinct neuromodulation strategies using repeated measures ANOVA confirmed the main effect that mean ROI activity differed significantly between imagery tasks for all groups of runs: passive imagery ($F(1.20, 22.79) = 6.29, P = 0.02$), NF ($F(1.50, 28.44) = 14.90, P < 0.0001$) and transfer run ($F(1.40, 26.68) = 11.19, P = 0.001$). Furthermore, post-hoc comparisons between the 3 responses levels using Bonferroni correction revealed that differences between the response activity to the motion imagery strategies (level 1 and level

2) and the zero motion imagery (level 0) were significant for runs with ($P = 0.02$, $P < 0.0001$) and without feedback (passive imagery, $P = 0.05$ for both comparisons; transfer run, $P = 0.03$, $P = 0.004$). However, the differences between the level responses evoked by both up-regulation strategies were not significant, in particular passive imagery ($P = 1.00$) and NF ($P = 0.124$). Concerning the transfer run, a marginal effect was found ($P = 0.06$). In agreement with these findings, linear trend tests were not significant for the passive imagery run ($F(1, 57) = 4.40$, $P = 0.12$). Importantly, trend tests for level dependence were significant for the ROI response levels in the presence of NF ($F(1, 57) = 20.74$, $P < 0.0003$) and transfer run ($F(1, 57) = 11.86$, $P = 0.003$). A difference at the whole-group level of participants, concerning presence or absence of feedback and its effect on the difference in response levels, was further confirmed by a two-way ANOVA ($F(1, 19) = 5.22$, $P = 0.034$).

For the successful neuromodulators group we found a main effect for all neuromodulation runs (passive imagery ($F(1.38, 15.19) = 20.85$, $P < 0.0001$), NF ($F(2, 22) = 47.80$, $P < 0.0001$) and transfer run ($F(2, 22) = 22.46$, $P < 0.0001$). Furthermore, the post-hoc tests with Bonferroni correction revealed that level 0 differed from level 1 and from level 2 for all runs (passive imagery, $P = 0.004$, $P = 0.001$; NF, $P < 0.0001$, $P < 0.0001$; transfer, $P = 0.005$, $P < 0.0001$). Differences between all responses levels were significant only the in the feedback runs (passive imagery, $P = 0.97$; NF, $P = 0.002$; transfer, $P = 0.07$). A linear trend was also found for all runs, with stronger effect sizes during NF training (passive imagery ($F(1, 33) = 13.75$, $P = 0.003$), NF ($F(1, 33) = 51.23$, $P < 0.0003$) and transfer run ($F(1, 33) = 19.87$, $P = 0.0003$).

In order to understand if age and gender had an influence in the ability of neuromodulation, we ran a chi-square test that shown no statistically significant association between gender and success of neuromodulation ($\chi(1) = 1.11$, $P = 0.292$) and, a Pearson correlation was run to determine the relationship between individual's age and their performance in neuromodulation, which revealed no correlation between age and difference between maximal and minimal level of activity during the neuromodulation runs ($r = 0.072$, $N = 20$, $P = 0.763$).

The GLM results for group analyses per imagery run showed significant activations in the hMT+/V5 complex (FFX, q (FDR) = 0.05) during all performed neuromodulations runs. The recruited brain areas were similar in all runs (see supplementary table 3.1). We observed the typical imagery parieto-frontal network (Kaas et al. 2010; Mechelli et al. 2004) and the hMT+/V5 complex.

3.4. Discussion

We found evidence for the feasibility of BCI/NF applications with different levels of volitional modulation at the same brain location using the same strategy across participants. The possibility that multilevel neuromodulation based on the same brain region and using the same strategy across participants is feasible had so far not been explored in the literature, although some alternatives have been suggested (Sorger 2010). Previous studies have mainly tried to reach multiple commands by analyzing not one but instead multiple regions, or by exploring particular spatio-temporal aspects of the BOLD signal (Lee et al. 2009; Sorger et al. 2012; Yoo et al. 2004).

Here, multiple visual motion imagery strategies which take advantage of differential evoked brain responses according to the number of imagined motion alternations, allowed achieving up to three distinct levels of hMT+/V5 activity modulation. The larger number (4) of motion alternations during imagery tasks evoked higher activity levels in hMT+/V5 as compared to imagery tasks with a lower number of motion alternations (2) and static imagery. These results can be explained by the fact that in human visual cortex frequent movement or orientation changes lead to break in adaptation and increased fMRI responses. Lower signal adaptation does indeed occur as compared to brain responses evoked by a movement with less alternation (Tootell et al. 1998). Our results are also consistent with the previous visual stimulation studies of Huk & Heeger (2002) and Larsson et al. (2006) where the visual stimulus with the highest alternating rate evoked stronger brain activations. However, an alternative explanation is possible concerning the distinct levels of hMT+/V5 responses as a function of different imagery strategies. Accordingly, the different number of motion alternations may lead to distinct levels of attentional modulation which in turn impact on activity levels.

Trend analysis to the whole-group of participants revealed significant multilevel neuromodulation during NF runs. Furthermore, there was no significant trend on response levels during passive imagery runs (control run without feedback previous to NF training). In contrast, a significant trend was found during the transfer run (control run after NF training). These results suggest that the provided feedback contributed for successful neuromodulation and learning during NF training. The comparison between runs with feedback and runs without feedback shown a significant feedback effect on the achieved response levels in agreement with the effects identified by group trend analyses.

The significant difference in level of modulation achieved with the use of auditory feedback based on the BOLD signal changes, suggests that the participants effectively used neurofeedback strategies. It is important to point out that auditory feedback was used to avoid interferences that would have been induced by spurious brain activations due to the visual feedback and that would perturb the signals evoked by the imagery task.

Future studies should address how many sessions are necessary to achieve stable performance. Binary neuromodulation (successful up-regulation during the two motion imagery tasks, and successful down-regulation during non-motion imagery) was often obtained (17/20 participants) and three levels of modulation were documented in a substantial number of subjects (12/20 participants). Future studies beyond proof of concept should establish whether training can stabilize NF performance. We suggest that three levels of control of hMT+/V5 activity are possible but also imply that they may require a higher level of focused attention and training than the binary case.

We have shown that the same strategy can be efficiently used by different participants to achieve modulation of hMT+/V5, and that the type of instruction can be useful in BCI and NF applications. Thus, this approach could be useful in the future to dampen the variability due to ROI and subject-by-subject strategy definition, and to allow more effective neuromodulation training or at least improved BCI control. We postulate that the proposed approach is promising for future NF applications and even more for BCI applications, because it provides a simple way to achieve three control levels with simple instructions.

3.5. Conclusion

We demonstrated that both visual motion stimulation and imagery with different number of motion alternations lead to distinct activity levels in hMT+/V5, and this can be effectively used in a NF application. Up to three levels of volitional control of hMT+/V5 visual area by using real-time fMRI training could be achieved. The same imagery strategy was used by all participants, showing that the proposed novel methodology is of potential interest to implement in applications using level dependent multilevel BCI and/or NF.

References

- Caria, A. et al., 2007. Regulation of anterior insular cortex activity using real-time fMRI. *NeuroImage*, 35(3), pp.1238–1246.
- Caria, A. et al., 2010. Volitional control of anterior insula activity modulates the response to aversive stimuli. A real-time functional magnetic resonance imaging study. *Biological Psychiatry*, 68(5), pp.425–432.
- Castelo-Branco, M. et al., 2002. Activity patterns in human motion-sensitive areas depend on the interpretation of global motion. *Proceedings of the National Academy of Sciences of the United States of America*, 99(21), pp.13914–13919.
- Castelo-Branco, M. et al., 2009. Type of featural attention differentially modulates hMT+ responses to illusory motion aftereffects. *Journal of neurophysiology*, 102(5), pp.3016–3025.
- DeCharms, R.C. et al., 2005. Control over brain activation and pain learned by using real-time functional MRI. *Proceedings of the National Academy of Sciences of the United States of America*, 102(51), pp.18626–31.
- DeCharms, R.C. et al., 2004. Learned regulation of spatially localized brain activation using real-time fMRI. *NeuroImage*, 21(1), pp.436–443.
- Formisano, E., De Martino, F. & Valente, G., 2008. Multivariate analysis of fMRI time series: classification and regression of brain responses using machine learning. *Magnetic Resonance Imaging*, 26(7), pp.921–934.
- Friston, K.J. et al., 1998. Nonlinear event-related responses in fMRI. *Magnetic Resonance in Medicine*, 39(1), pp.41–52.
- Goebel, R., 2012. BrainVoyager: past, present, future. *NeuroImage*, 62(2), pp.748–56.
- Goebel, R. et al., 1998. The constructive nature of vision: Direct evidence from functional magnetic resonance imaging studies of apparent motion and motion imagery. *European Journal of Neuroscience*, 10(5), pp.1563–1573.
- Graewe, B. et al., 2013. Impaired processing of 3D motion-defined faces in mild cognitive impairment and healthy aging: An fMRI study. *Cerebral Cortex*, 23(10), pp.2489–2499.
- Haller, S., Birbaumer, N. & Veit, R., 2010. Real-time fMRI feedback training may improve chronic tinnitus. *European Radiology*, 20(3), pp.696–703.
- Hamilton, J.P. et al., 2011. Modulation of subgenual anterior cingulate cortex activity with real-time neurofeedback. *Human Brain Mapping*, 32(1), pp.22–31.
- Haynes, J.-D. & Rees, G., 2006. Decoding mental states from brain activity in humans. *Nature reviews. Neuroscience*, 7(7), pp.523–534.
- Haynes, J.-D. & Rees, G., 2005. Predicting the orientation of invisible stimuli from activity in human primary visual cortex. *Nature Neuroscience*, 8(5), pp.686–691.
- Huk, A.C. & Heeger, D.J., 2002. Pattern-motion responses in human visual cortex. *Nature Neuroscience*, 5(1), pp.72–75.
- Johnston, S.J. et al., 2010. Neurofeedback: A promising tool for the self-regulation of emotion networks. *NeuroImage*, 49(1), pp.1066–1072.
- Kaas, A. et al., 2010. Imagery of a moving object: The role of occipital cortex and human MT/V5+. *NeuroImage*, 49(1), pp.794–804.
- Kamitani, Y. & Tong, F., 2006. Decoding Seen and Attended Motion Directions from Activity in the Human Visual Cortex. *Current Biology*, 16(11), pp.1096–1102.
- Kolster, H., Peeters, R. & Orban, G. a., 2010. The retinotopic organization of the human middle temporal area MT/V5 and its cortical neighbors. *The Journal of neuroscience*, 30(29), pp.9801–20.
- Kutner, M.H. et al., 2004. *Applied Linear Statistical Models* 5th Ed., McGraw-Hill Companies.
- LaConte, S.M., 2011. Decoding fMRI brain states in real-time. *NeuroImage*, 56(2), pp.440–454.
- Larsson, J., Landy, M.S. & Heeger, D.J., 2006. Orientation-selective adaptation to first-and second-order patterns in human visual cortex. *Journal of Neurophysiology*, 95, pp.862–881.
- Lee, J.H. et al., 2009. Brain-machine interface via real-time fMRI: Preliminary study on thought-controlled robotic arm. *Neuroscience Letters*, 450(1), pp.1–6.
- Lenoski, B. et al., 2008. On the performance of autocorrelation estimation algorithms for fMRI analysis. *IEEE Journal on Selected Topics in Signal Processing*, 2(6), pp.828–838.
- Linden, D.E.J. et al., 2012. Real-time self-regulation of emotion networks in patients with depression. *PLoS ONE*, 7(6).
- McCaig, R.G. et al., 2011. Improved modulation of rostralateral prefrontal cortex using real-time fMRI training and meta-cognitive awareness. *NeuroImage*, 55(3), pp.1298–1305.
- Mechelli, A. et al., 2004. Where bottom-up meets top-down: Neuronal interactions during perception and

- imagery. *Cerebral Cortex*, 14(11), pp.1256–1265.
- Mikami, A., Newsome, W.T. & Wurtz, R.H., 1986. Motion selectivity in macaque visual cortex. I. Mechanisms of direction and speed selectivity in extrastriate area MT. *Journal of neurophysiology*, 55(6), pp.1308–1327.
- Newsome, W.T. & Pare, E.B., 1988. A selective impairment of motion perception following lesions of the Middle Temporal visual area (MT). *Journal of Neuroscience*, 8(6), pp.2201–2211.
- Rota, G. et al., 2009. Self-regulation of regional cortical activity using real-time fmri: the right inferior frontal gyrus and linguistic processing. *Human Brain Mapping*, 30(5), pp.1605–1614.
- Ruiz, S. et al., 2013. Acquired self-control of insula cortex modulates emotion recognition and brain network connectivity in schizophrenia. *Human Brain Mapping*, 34(1), pp.200–212.
- Scharnowski, F. et al., 2012. Improving Visual Perception through Neurofeedback. *Journal of Neuroscience*, 32(49), pp.17830–17841.
- Sitaram, R. et al., 2012. Acquired Control of Ventral Premotor Cortex Activity by Feedback Training: An Exploratory Real-Time fMRI and TMS Study. *Neurorehabilitation and Neural Repair*, 26(3), pp.256–265.
- Sorger, B. et al., 2012. A real-time fMRI-based spelling device immediately enabling robust motor-independent communication. *Current Biology*, 22(14), pp.1333–1338.
- Sorger, B., 2010. *When the brain speaks for itself: Exploiting hemodynamic brain signals for motor-independent communication*. Universitaire Pers Maastricht: Maastricht.
- Subramanian, L. et al., 2011. Real-Time Functional Magnetic Resonance Imaging Neurofeedback for Treatment of Parkinson's Disease. *The Journal of Neuroscience*, 31(45), pp.16309–16317.
- Sulzer, J. et al., 2013. Real-time fMRI neurofeedback: Progress and challenges. *NeuroImage*, 76, pp.386–399.
- Talairach, J. & Tournoux, P., 1988. *Co-Planar Stereotaxis Atlas of the Human Brain: 3-D Proportional System*, Thieme Medical Publisher.
- Tootell, R.B. et al., 1995. Functional analysis of human MT and related visual cortical areas using magnetic resonance imaging. *Journal of Neuroscience*, 15(4), pp.3215–3230.
- Tootell, R.B. et al., 1998. Functional analysis of primary visual cortex (V1) in humans. *Proceedings of the National Academy of Sciences of the United States of America*, 95(3), pp.811–817.
- Weiskopf, N., Mathiak, K., et al., 2004. Principles of a brain-computer interface (BCI) based on real-time functional magnetic resonance imaging (fMRI). *IEEE Transactions on Biomedical Engineering*, 51(6), pp.966–970.
- Weiskopf, N., 2012. Real-time fMRI and its application to neurofeedback. *NeuroImage*, 62(2), pp.682–692.
- Weiskopf, N., Scharnowski, F., et al., 2004. Self-regulation of local brain activity using real-time functional magnetic resonance imaging (fMRI). *Journal of Physiology Paris*, 98(4–6 SPEC. ISS.), pp.357–373.
- Yoo, S.-S. et al., 2004. Brain-computer interface using fMRI: spatial navigation by thoughts. *Neuroreport*, 15(10), pp.1591–1595.
- Yoo, S.-S. et al., 2007. Functional magnetic resonance imaging-mediated learning of increased activity in auditory areas. *Neuroreport*, 18(18), pp.1915–1920.

APPENDIX

Chapter 3

A1. Experimental design

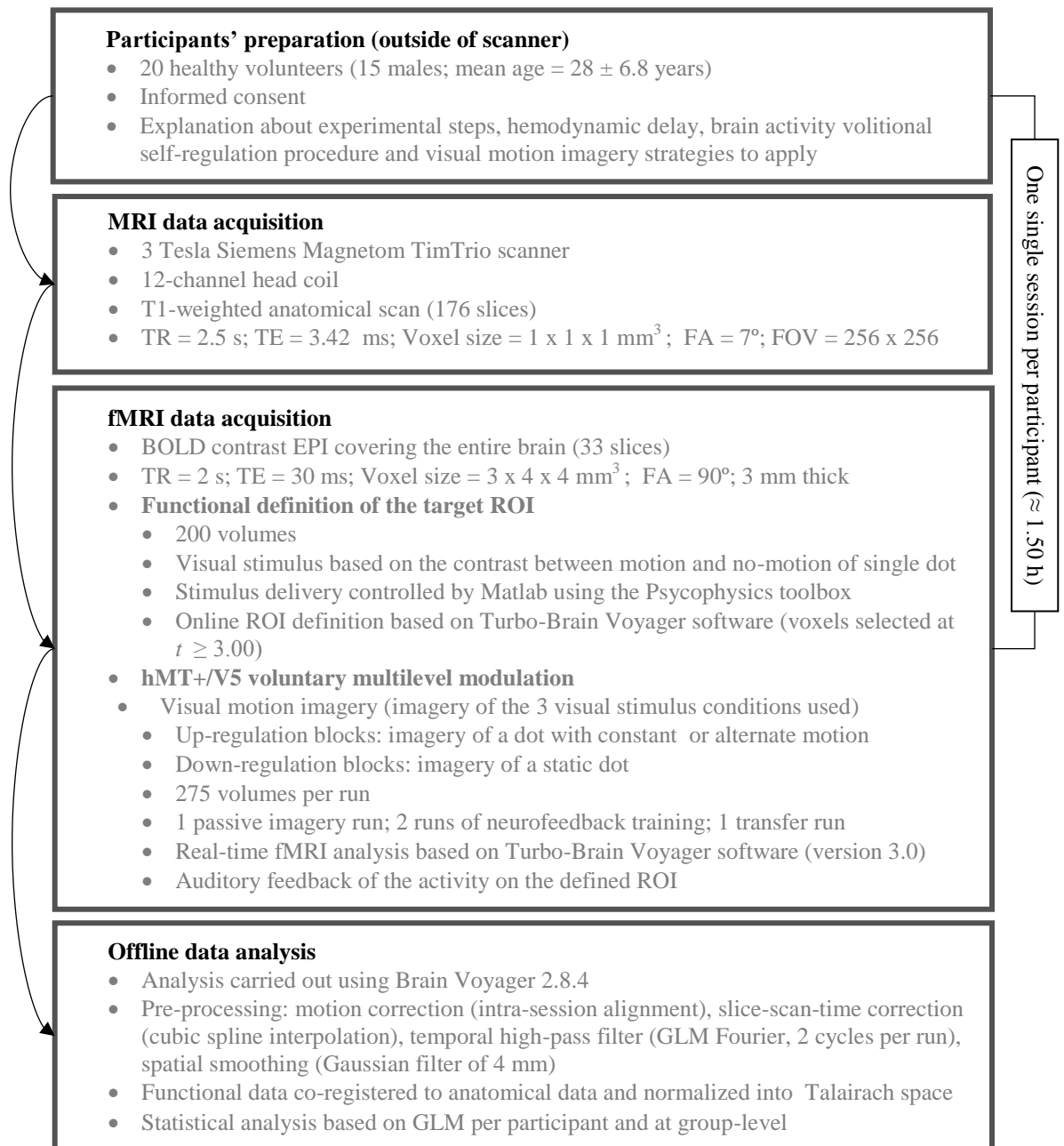


Figure 3.A1. Summary of the main steps of the experimental procedure followed in the study. Each participant took part of a single session lasting approximately 1.50 hour. First, a clear explanation about the fMRI based neurofeedback experiment procedures and visual motion imagery strategies was given to the participants outside of the scanner. Then, participants performed a passive imagery run (control run), two runs of neurofeedback training and a transfer run (to verify possible effects of learning after neurofeedback). Anatomical data were also acquired to posterior co-registration of the functional data during offline analysis. The fMRI real-time analysis was carried out on Turbo-Brain Voyager software and the offline analyses were performed using Brain Voyager Qx. All statistical analyses were based on general linear model (GLM) approaches. *fMRI* – functional magnetic resonance imaging, *TR* – repetition time, *FA* – flip angle, *TE* – echo time, *FOV* – field of view, *ROI* – region of interest.

A2. Implemented neurofeedback system

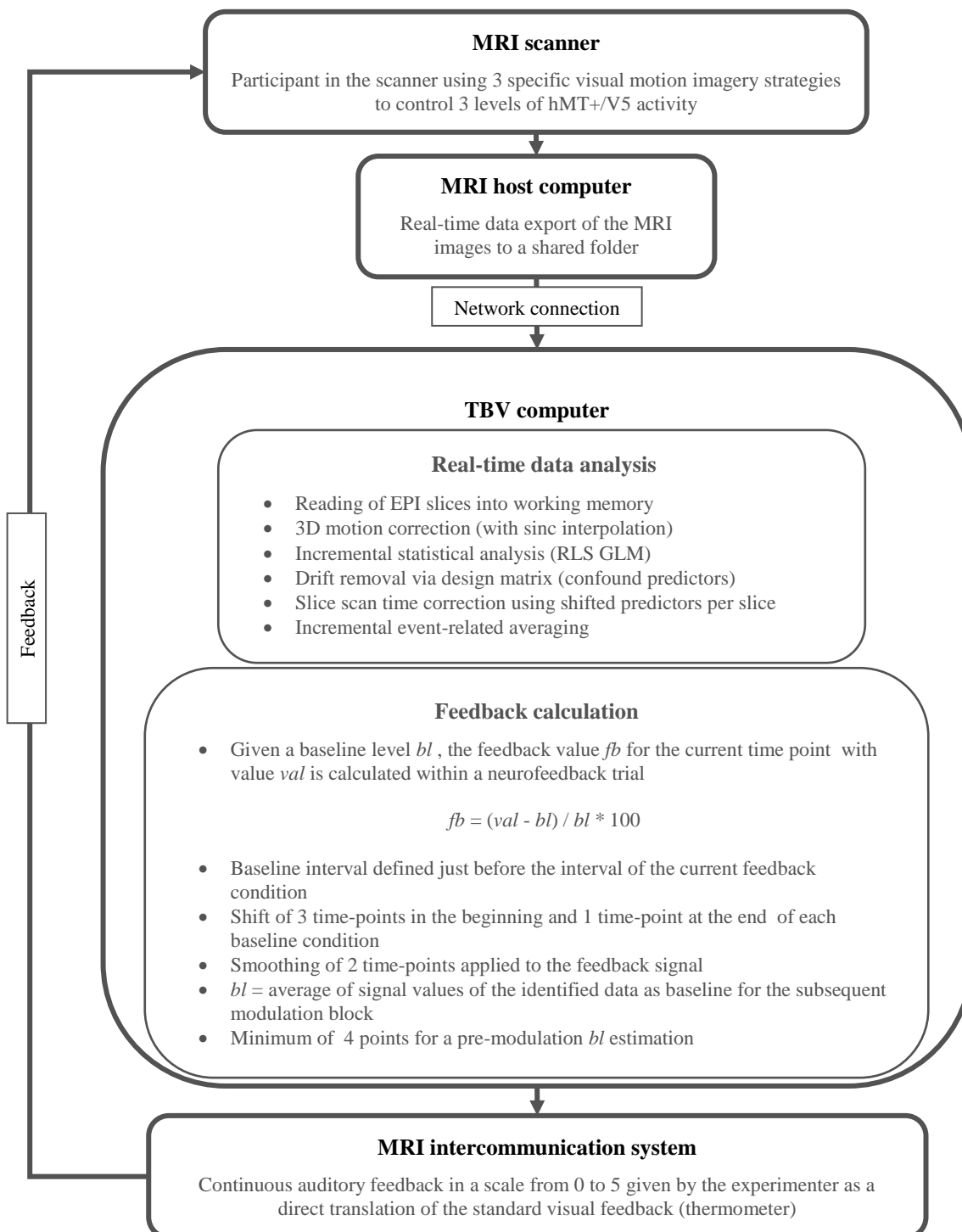


Figure 3.A2. Set-up of the implemented neurofeedback system. The participant was trying to up-regulate and down-regulate the hMT+/V5 brain activity, inside the MRI scanner. Three visual motion imagery strategies with different quantities of motion alternation were applied. The goal was to verify whether the different strategies would allow the voluntary regulation of 3 levels of brain activity, with the support of neurofeedback training. The acquired fMRI data were analyzed in real-time and the level of brain activity was given as feedback to the participant. The Turbo-BrainVoyager (TBV) software was used for the real-time data processing. It was installed on a separate computer to ensure optimal hardware usage and, therefore, best results in real-time processing. The TBV uses an incremental recursive least squares (RLS) based general linear model (GLM) to perform the statistical analysis.

A3. Whole-brain analysis

Table 3.A1. Summary of whole-brain regions activated during visual motion imagery. Peak voxels according Talairach coordinates and the number of used voxels (FFX, q (FDR) = 0.05 using the contrast up-regulation tasks versus down-regulation task. Results presented per imagery run: passive imagery run (control run without feedback), imagery runs with feedback (neurofeedback 1 and 2, NF1 and NF2) and transfer run.

Brain region		Passive imagery		NF1		NF2		Transfer run	
		Talairach coordinates (x, y, z)	Voxels	Talairach coordinates (x, y, z)	Voxels	Talairach coordinates (x, y, z)	Voxels	Talairach coordinates (x, y, z)	Voxels
hMT+/V5	Left	-49, -60, -1	1248	-44, -60, 0	5182	-47, -60, -2	2482	-48, -60, -1	1941
	Right	46, -59, -4	690	48, -57, -4	2029	47, -61, -5	244	50, -58, -5	409
Putamen	Left	-22, 1, 13	2335	-22, 1, 8	4203	-23, 2, 6	3398	-23, 1, 9	4448
	Right	21, 2, 12	1982	23, 1, 11	3093	21, 3, 10	3177	21, 4, 8	3502
Superior parietal lobule, Precuneus	Left	-21, -65, 48	3717	-21, -68, 47	2734	-21, -65, 46	3649	-22, -66, 46	2891
	Right	16, -67, 48	2666	15, -71, 46	2613	16, -66, 47	1957	14, -69, 42	2424
Inferior parietal lobule	Left	-37, -43, 43	5930	-34, -38, 37	4374	-39, -41, 42	4674	-38, -37, 38	4143
	Right	38, -42, 42	5587	30, -46, 40	3573	34, -42, 44	2842	35, -43, 38	4018
Precentral gyrus	Left	-49, -6, 40	3084	-50, 1, 29	3767	-51, 3, 22	3595	-50, 2, 25	4532
	Right	48, -4, 42	3430	52, 3, 27	3231	53, 3, 25	2945	50, 5, 24	4090
Medial frontal gyrus		5, 12, 43	972	-3, 4, 43	1745	-5, 1, 46	1169	-3, 10, 44	1178

CHAPTER 4

VISUAL MOTION IMAGERY AS A TOOL FOR MULTICLASS EEG-BASED BCI

Based on: Sousa, T., Amaral, C., Andrade, J., Gabriel, P., Nunes, U., Castelo-Branco, M., 2016. Visual motion imagery as a tool for multiclass EEG-based BCI. (*submitted*)

We would like to thank the participants for their involvement with this study. We are also very grateful to Gabriel Costa and Gilberto Silva for the help with data processing.

Abstract

The achievement of multiple instances of control with the same type of strategy represents a way to improve flexibility of brain-computer interface systems. In this study we test the hypothesis that visual motion imagery can be used as a tool to achieve electroencephalographic based brain-computer interfaces with three classes of control.

We hypothesize that different number of imagined motion alternations lead to distinctive signals, as predicted by distinct temporal motion modulation patterns and/or attentional deployment. Accordingly, distinct number of alternating sensory/perceptual signals would lead to distinct neural responses as previously demonstrated using functional magnetic resonance imaging. We anticipate that differential modulations, regardless of their polarity, should also be observed at the electroencephalographic domain. Electroencephalographic recordings were obtained from twelve participants during three tasks of visual imagery: imagery of a static dot, imagery of a dot with two opposing motions in the vertical axis (imagery of 2 motion directions) and imagery of a dot with four opposing motions in vertical or horizontal axes (imagery of 4 motion directions).

An increase of alpha-band power was found in frontal and central channels as a result of visual motion imagery tasks when compared with imagery of the static dot, in contrast with more posterior alpha decreases found during simple visual stimulation. The successful classification of the three imagery tasks using a support vector machine based on the power of this particular frequency-band and using a small group of six channels confirmed that three different classes of control based on visual motion imagery can be achieved. Patterns of alpha activity, as captured by classifier, closely reflected motion imagery properties, in particular the number of imagined motion alternations.

These results are consistent with the notion that frontal alpha synchronization is related with high internal processing demands, changing with the number of alternation levels during imagery. Our findings suggest the feasibility of visual motion imagery tasks as a strategy to achieve multiclass BCI systems and support the advantage of multivariate over univariate analysis methods.

4.1. Introduction

A brain-computer interface (BCI) is a system that acquires and analyzes brain signals to create a communication channel between the human brain and a computer or a machine. These systems measure and convert brain activity into artificial outputs (Farwell & Donchin 1988; Shih et al. 2012; Wolpaw & Wolpaw 2012).

In the last decades, many studies using BCI systems have been performed in the fields of motor rehabilitation and stroke with a particular emphasis in restoration of communication in paralyzed and locked-in patients (Birbaumer & Cohen 2007; Lopes et al. 2013; Pires et al. 2012). Furthermore, a BCI system can be applied as a neurofeedback (NF) approach allowing to train the self-regulation of a specific brain activity (Huster et al. 2014). Several studies have demonstrated that learned brain self-regulation gained through NF training can lead to specific behavioral modifications, and therefore a BCI could potentially be used, not only as a communication interface but also, as a cognitive neuroscience research tool and as therapeutic tool for neurological and psychiatric disorders (Friedrich et al. 2015; Ramirez et al. 2015; Strehl et al. 2006).

Effective BCI communication or device control based on electroencephalographic (EEG) signals – EEG-based BCI – has been demonstrated using slow cortical potentials (Birbaumer et al. 1999; Karim et al. 2006; Kubler et al. 2001), brain rhythms (McFarland et al. 2015; Ono et al. 2014; Pfurtscheller et al. 1997; Treder et al. 2011) or event-related potentials (Amaral et al. 2015; Baek et al. 2013; Combaz & Van Hulle 2015; Nijboer et al. 2008). The most used EEG-based BCI inputs are sensory-motor rhythms (Ge et al. 2014; Leeb et al. 2013; Maria et al. 2015; Ramos-Murguialday & Birbaumer 2015) and P300 evoked potentials (Amaral et al. 2015; Lopes et al. 2013; Pires et al. 2012). Due to the long learning process required for the participant, slow cortical potentials are not commonly used in BCI.

BCI studies often use binary control level approaches (level 0 and 1 of brain activation for each class of control). One of major goals of the current BCIs research is to increase the number of classes and the intrinsic number of levels of control, i.e. to increase the degrees of freedom in BCI applications. This would allow to increase communication efficiency and might favor more precise neurofeedback. Human brain functions can be at least in part

spatially localized, even in EEG, and thus separate commands can be encoded by taking advantage from information derived from different functional modules. This possibility is used in BCI systems based on motor imagery, where the imagery of different motor tasks (for example, leg or hand movement, right and left) produce spatially distributed brain activations (Ramos-Murguialday & Birbaumer 2015; Schlögl et al. 2005). Conventional P300 paradigms also allow to generate different BCI commands, e.g. to move a wheelchair (Lopes et al. 2013) or to generate a speller (Pires et al. 2012), when translating different user intentions. However, they require all the time a stimulus to encode the attentional focus.

Therefore, multilevel BCI approaches are still relatively incipient, and it remains difficult to go beyond binary levels of each class of control. Wolpaw and McFarland suggested a multidimensional point-to-point movement control based on the combination of mu or beta rhythm amplitude modulation over the right and left sensorimotor cortices (Wolpaw & McFarland 2004). They showed that people can learn to use scalp-recorded EEG rhythms to move a cursor in two dimensions, and recently also in 3 dimensions (McFarland et al. 2010). In another study, it was shown that self-regulation of slow cortical potentials can be reliably translated as two BCI commands (Karim et al. 2006). More recently, a BCI study proposed an approach where participants were able to switch between modulation of alpha-band and gamma-band oscillations in the visual cortex (Salari & Rose 2013). Although these studies attempted different levels of activity control, most only achieved two levels, and the proposed BCI approaches required some days of training.

In this work we test the possibility of obtaining three classes of brain activity control using visual motion imagery. To our best knowledge this is the first time that such approach is carried on. Our hypothesis is that focusing on a particular perceptual function, using visual motion imagery strategies with different number of motion alternations, it is possible to achieve different patterns of brain activity modulation allowing for simple self-regulation based multiclass control. We attempt to infer whether EEG can be used to test the notion that in visual motion perception domain the stimulus conditions or the imagery tasks for which motion alternations occur more often lead to stronger brain activations, as demonstrated using functional magnetic resonance imaging (fMRI) (Huk & Heeger 2002; Larsson et al. 2006; Tootell et al. 1998). This phenomenon occurs due to distinct temporal motion patterns and/or higher attentional deployment. Thus, our study is based on imagery of three stimulation conditions with different number of motion alternations: imagery of a static dot (no-motion), imagery of a dot with two opposing motions in the vertical axis

(imagery of two motion directions, constant orientation) and imagery of a dot with four opposing motions in the vertical and horizontal axes (imagery of four motions directions, alternate orientation). We test if using a reduced number of EEG channels, in a consistent way across participants, it is possible to classify three distinguishable patterns of brain activity according to the level of imagined motion alternation.

Our study is also based on the knowledge resulting from brain imaging studies which demonstrated that neural representations of visual motion imagery and perceptual images resemble one another (Banca et al. 2015; Emmerling et al. 2015; Goebel et al. 1998; Sousa et al. 2016). Mental imagery refers to the emergence of constructive representations and the accompanying experience of sensory information without a direct external stimulus. This process plays a core role in many mental health disorders and plays an increasingly important role in their treatment (Pearson et al. 2015). Therefore, we expect that this work might contribute to the discussion on feasibility of multiclass self-regulation control in BCI methods as well as in the potential usefulness of controlling mental imagery at a finer scale.

4.2. Methods

4.2.1. Participants

Twelve males participated in this study. On average, study participants were 28.9 years old ($SD = 3.8$ range 21-34 years). All participants were right-handed, had normal or corrected-to-normal vision and reported no medical or psychological disorders. Participants gave written informed consent prior to the EEG recording session. The procedure was approved by the Ethics Committee of the Faculty of Medicine of the University of Coimbra.

4.2.2. Experimental design

The experiments were composed of two sessions: visual motion stimulation and visual motion imagery. During the visual stimulation session, participants were asked to fixate a central cross. As illustrated on figure 4.1, three different conditions were used: (A) zero motion (static dot), (B) a dot moving in two opposing directions (with constant vertical orientation, less alternation, hereinafter referred as constant motion) and (C) a dot moving in four opposing directions (horizontal and vertical orientations, more alternation, hereinafter referred as alternate motion). Four second trials of a moving dot (5 deg/s) were randomly interleaved with 2 second trials of a static dot. The distance covered by the dot was 2.5

degrees of arc. The motion conditions were repeated 60 times divided in two parts. The point size was $0.5 \times 0.5 \text{ cm}^2$ (dot visual angle: 0.64 deg) and the stimulus was displayed at 44.5 cm from the participant at a screen of $24.1 \times 18.2 \text{ cm}^2$. Stimulus display and imagery instructions were controlled by MATLAB (MathWorks) using the Psychophysics toolbox (Brainard 1997).

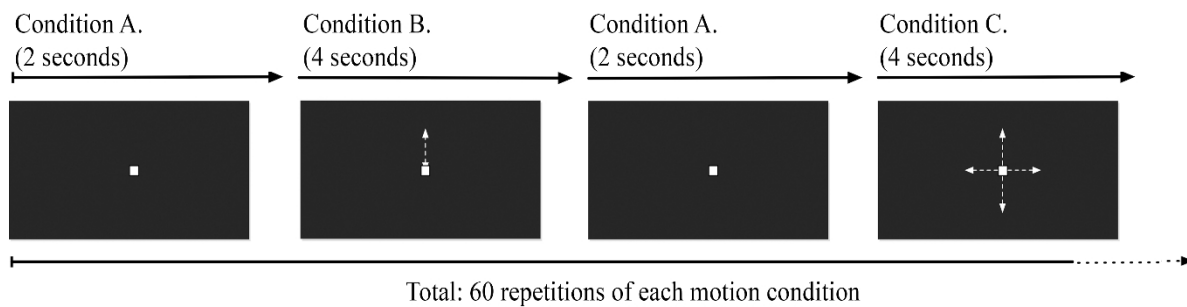


Figure 4.1. Stimulation conditions. (A) Static dot - static condition used as baseline to the motion conditions, (B) constant motion - moving dot alternating the direction, and (C) alternate motion - moving dot alternating the direction and the orientation. The arrows are here merely representing the dot motions. Each motion condition was repeated 60 times and randomly interleaved with the static dot condition. The duration of each motion condition was 4 seconds. Each static dot trial was presented only during 2 seconds.

In the visual motion imagery session, participants were asked to imagine the three previously presented stimulus conditions. The instruction for each imagery task was provided as an auditory cue coded as ‘A’, ‘B’ and ‘C’ respectively, and took one second. A beep sound was given to the participants 1.5 seconds after the beginning of each motion imagery task as a reminder of the spent imagery time.

The duration and number of repetitions of each task were equal to the stimulation session ones. The imagery session was divided in two parts intercalated with stimulation (also divided in two parts) in order to decrease fatigue effects. Participants were seated comfortably in the darkened sound-attenuating EEG recording room and, were asked to close the eyes throughout the imagery tasks, to breathe steadily, and to remain as still as possible without eyes movement. For a complete overview of the experimental design please see the supplementary figure 4.A1 in appendix.

4.2.3. Data acquisition

First, the participants scalp was cleaned using abrasive gel and then an actiCAP cap was placed on their heads. The EEG was recorded by means of a Brain Products Package (Brain Products, Germany) and sampled at a frequency of 1000 Hz. Ag/AgCl active electrodes (Brain Products), were located in 58 positions (according to the international 10-20 system

with interspaced positions, figure 4.2), a ground electrode was located on the forehead and, two reference electrodes were placed on the earlobes. The electrooculogram (EOG) was monitored via electrodes positioned at the standard positions (vertical and horizontal) to be used in the correction of artifacts due to blinking and eye movements. The signal was filtered between 0.1 Hz and 100 Hz and an additional 50 Hz notch filter was applied to avoid power line contamination. Electrode impedances were kept below 10 k Ω during the acquisitions. An overview of the acquisition system set-up is presented in supplementary figure 4.A2 in appendix.

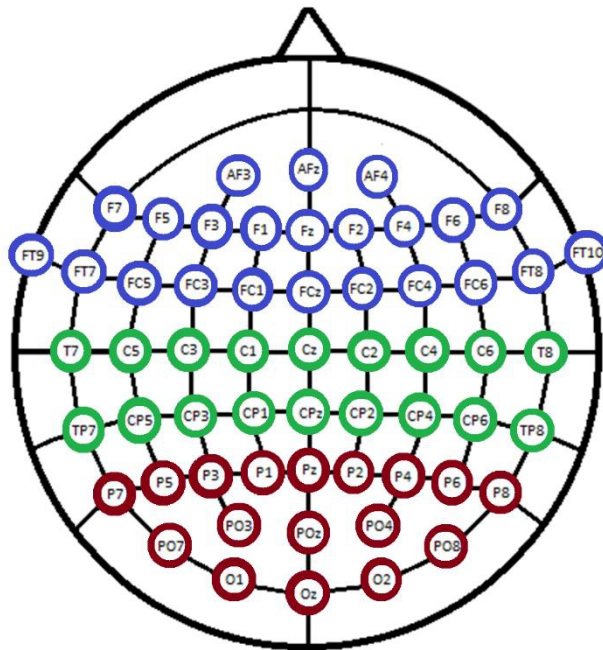


Figure 4.2. Layout of the EEG channel acquisition set up (58 EEG channels). The three channel clusters used in statistical data analysis are highlighted at different colors (frontal – blue, central – green, parieto-occipital – red).

4.2.4. Data analysis

The data analysis was made offline using Matlab (MathWorks) and the EEGLAB toolbox (version 13.5.4b) (Delorme & Makeig 2004). The signals were filtered between 0.5 Hz and 70 Hz, re-referenced to the average signal of the earlobes channels and segmented in epochs locked to each stimulation condition/imagery task onset. Then, it was applied an eye movement related artifacts correction based on independent component analysis (ICA) of all electrode data (including the EOG channels). Artifact components were identified based on their correlation with the EOG electrodes and on the scalp topography (increased activity distribution) and removed from the data (Keren et al. 2010). Signals were also corrected for

possible artifacts related to body movement or muscle tension, which were marked and excluded from further analysis. After artifact rejection we were able to keep more than 50 epochs for each stimulation condition/imagery task, except for the imagery data of one participant. For the data analysis of visual motion stimulation, we used a baseline taken from the last 500 ms of pre-stimulus time (last 500 ms of static dot condition before the motion conditions). For visual motion imagery data, the baseline was based on the last 500 ms of the static dot imagery period.

We performed time-frequency analyses of the stimulation and imagery data. Mean event-related changes in spectral power (from baseline) at each time during the epochs and at each frequency were analyzed using the event-related spectral perturbation (ERSP) method (Makeig 1993). ERSP analyses were performed for frequencies ranging from 3 to 50 Hz for all channels by applying Morlet wavelets with incremental cycles (2 cycles at 3 Hz, up to 27 at 50 Hz) resulting in 200 time points. To visualize power changes across the frequency range, the mean baseline log power spectrum from each spectral estimate was subtracted producing the baseline-normalized ERSP. Significance of deviations from baseline power was assessed using a bootstrap method. ERSP group results were analyzed at $P = 0.05$ (Delorme & Makeig 2004).

In order to understand the main differences for specific frequency bands between stimulation conditions and between imagery tasks, the mean power of EEG signal from all channels over the 500 ms and 1500 ms of all epochs was calculated for the three stimulation conditions and for the three imagery tasks. The power spectral density (PSD) was estimated via the Welch's method which uses the fast Fourier transform (FFT) (Welch 1967).

We also performed source localization of the EEG data based in sLORETA (standardized low resolution brain electromagnetic tomography) software package (Pascual-Marqui 2002). This method employs the current density estimate given by the minimum norm solution. The localization inference is based on standardized values of the current density estimates (Pascual-Marqui et al. 1994; Pascual-Marqui 2002). The source analysis was performed to infer about the biological significance of the most relevant frequency results found.

4.2.5. Imagery data classification

In order to verify if the three employed imagery tasks may successful achieve three classes of control in BCI applications, we attempted to classify these classes using a reduced number of channels and features.

We used pre-processed (filtered, re-referenced and with artifact correction) trials, with one second each (from 0.5 to 1.5 of each trial). The duration of the trials used for classification was chosen to be the same to the three conditions and to not include the reminder beep. The initial 0.5 seconds after the auditory instruction cue were also excluded.

The channels and features were selected based on group analysis of the imagery results. The relative spectral power (RSP) of the frequency band from 7 Hz to 15 Hz was extracted from 6 EEG channels (F3, F5, FC3, FC5, C3, C5). These 6 features from 50 trials of each imagery task were normalized and then classified using a support vector machine (SVM).

As shown in previous studies (Khalighi et al. 2013; Sousa et al. 2015), the RSP provides some of the most relevant information from the EEG signals to classification. The RSP of each frequency-band is given by the ratio between the band spectral power and the total spectral power (Mormann et al. 2007). The spectral power was calculated based on FFT. To avoid features in greater numeric ranges dominating those in smaller numeric ranges, each feature was independently normalized dividing its value by the difference between maximum and minimum of the feature across trials.

The classifier was trained and tested using leave-one out cross-validation (LOOCV). The libsvm toolbox (Chang & Lin 2011) with a sigmoid kernel was used in classification. The sigmoid degree and C parameter of SVM were optimized between 0 and 5 for each participant model classification. The classifier was trained and tested individually per participant. In order to characterize the trial-by-trial classification performance, some well-known measures such as balanced accuracy, sensitivity and specificity were used. The classification algorithm is presented in supplementary figure 4.A3 in appendix.

4.2.6. Statistical Analysis

Statistical analyses were performed to compare the group mean EEG power for the most relevant frequency-bands found in the evoked brain responses during the three stimulations conditions and during the three imagery tasks. The Friedman's test was applied to verify the presence of a main effect for each defined frequency band. Further, we computed pairwise comparisons for stimulation condition/imagery task per EEG channel cluster using Wilcoxon tests and applying the Dunn's correction for multiple comparisons. The EEG data were organized in three channel clusters: frontal (anterior-frontal, frontal, fronto-temporal and fronto-central channels), central (central, centro-parietal, temporal and tempo-parietal channels) and parieto-occipital (parietal, parieto-occipital and occipital channels). Statistical

analyses were performed with the IBM (Armonk, NY) SPSS Statistics 22.0 software package.

4.3. Results

4.3.1. Visual motion stimulation

Comparing the evoked brain activation by the motion conditions to the static dot condition brain response (used as baseline) we found a significant decrease of alpha-band power mainly on the parietal, parieto-occipital and occipital channels for visual moving stimuli conditions (figure 4.3).

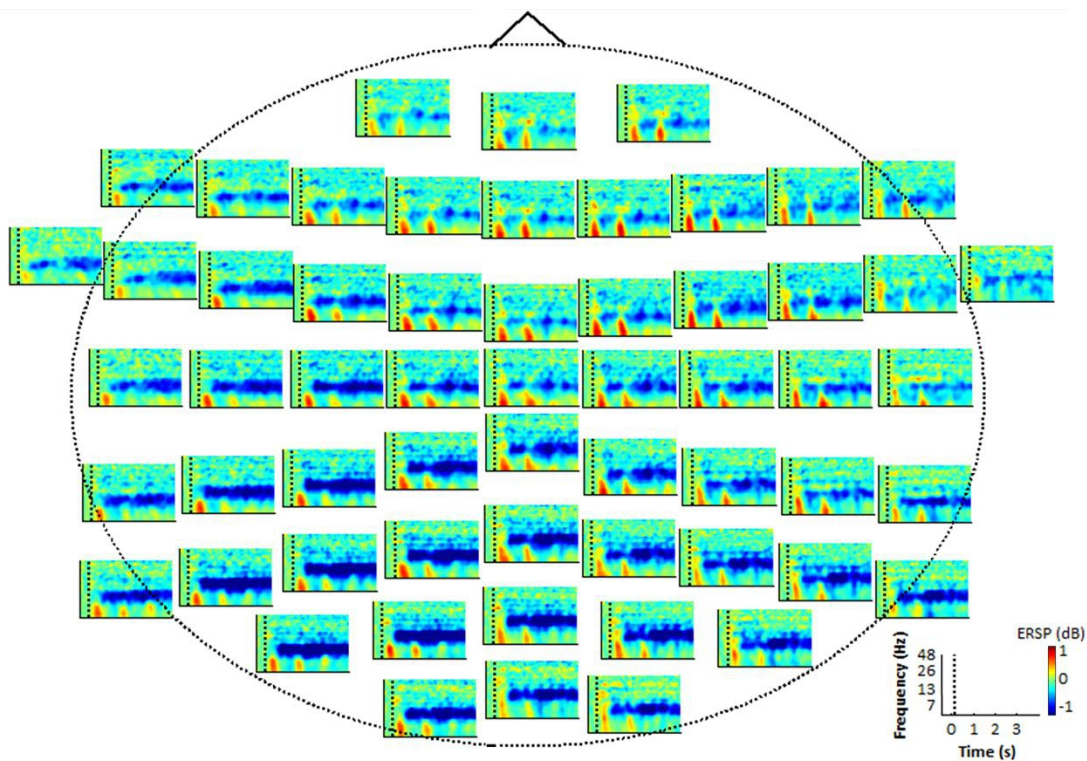


Figure 4.3. Brain responses to visual moving stimuli. Group event-related spectral perturbation (ERSP) for frequencies between 5 Hz and 50 Hz across entire trials (from -0.5 second to 4 seconds) pooled for moving stimuli when compared to a no-motion stimulation condition (baseline). All shown ERSP values different from zero are significant at $P = 0.05$.

For the parieto-occipital channels cluster we found statistically significant main effect differences between the evoked mean alpha-band power during the different stimulation conditions ($\chi^2_F(2) = 10.57$, $P = 0.005$). The peak power frequency (10 Hz) is consistent across the brain responses to the different stimulation conditions and is within the conventional alpha-band (figure 4.4). The alpha-band power was significantly lower during both moving stimulation conditions (CM and AM, $P = 0.01$, $P = 0.02$) than during the no-

motion stimulation (ST). Concerning the frontal and central channel clusters we found no significant differences. In the mean of participants and parieto-occipital cluster of channels, the power spectrum of the evoked brain activity during the constant motion stimulation and the alternate motion stimulation is similar.

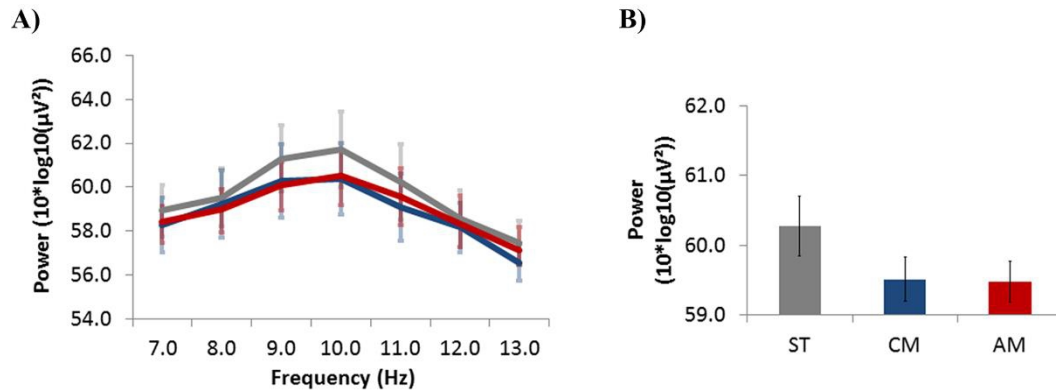


Figure 4.4. Group mean alpha-band power according to stimulation conditions (\pm SEM). Power spectrum of the evoked brain activity recorded in occipital channels cluster per stimulation condition (A) and its average from 8 Hz to 12 Hz (B). Color codes: red - alternate motion (AM), blue - constant motion (CM), gray - static dot (ST). The alpha-band power decreases significantly from no-motion to motion conditions (CM vs. ST, $P = 0.01$, corrected; AM vs. ST, $P = 0.02$, corrected).

4.3.2. Visual motion imagery

The time-frequency analyses of the visual motion imagery tasks revealed an increase of the alpha power activity when compared to the baseline (imagery of a static dot), starting after the participants received the specific imagery instruction (figure 4.5). This effect is mainly evident for the frontal and central EEG channels, suggesting that it is a different type of alpha activity as compared to the decreasing pattern seen for real stimulation conditions (figure 4.3).

The mean alpha power (figure 4.6) shows significant differences between the imagery tasks on the frontal channel cluster ($\chi^2_F(2) = 13.56$, $P = 0.001$). Post-hoc tests revealed the existence of statistically significant differences between the average of alpha-band power evoked by imagery of a static dot and by constant motion imagery ($P = 0.007$) and between the average of alpha-band power evoked by imagery of a static dot and by alternate motion imagery ($P = 0.003$). The peak power frequency (around 10 Hz) is consistent across the brain responses during the different imagery tasks. Although a classical statistical approach does not detect significant differences between both, the alpha-band power during the alternate motion imagery seems distinct from the pattern observed during constant motion imagery (see below a multivariate analysis strategy results based on SVM classification).

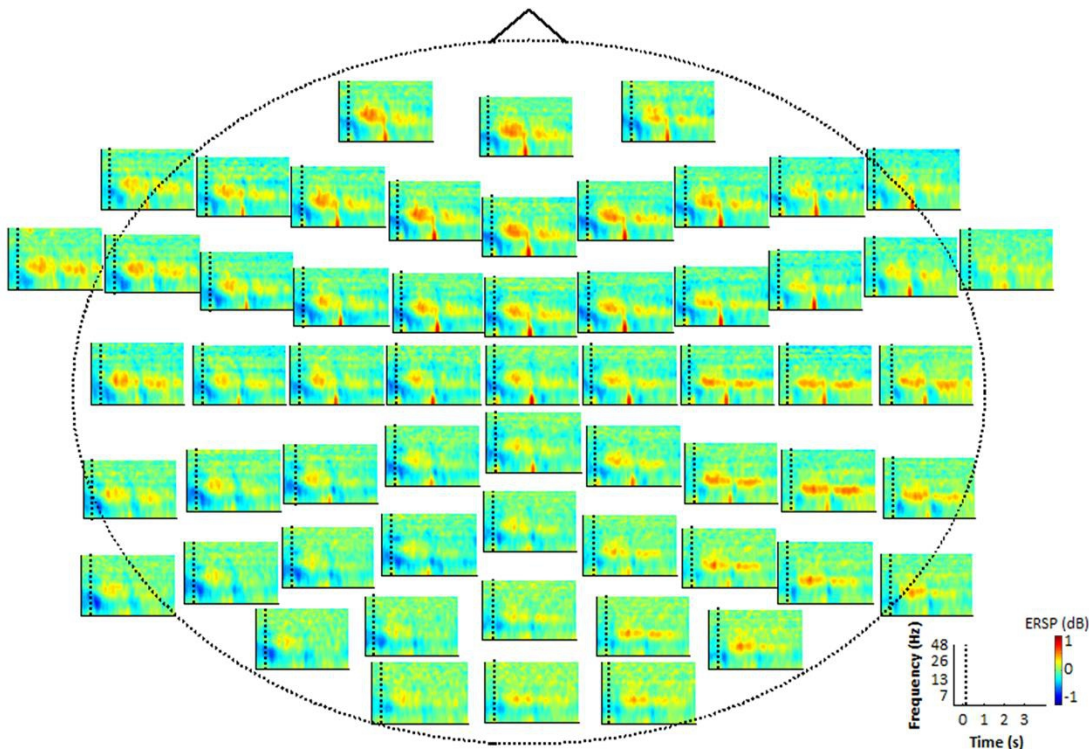


Figure 4.5. Brain responses to visual motion imagery. Group event-related spectral perturbation (ERSP) for frequencies between 5 Hz and 50 Hz across entire trials (from -0.5 second to 4 seconds) pooled for motion imagery tasks when compared to a no-motion imagery task (baseline). Time 0 corresponds to auditory instruction end. All shown ERSP values different from zero are significant at $P = 0.05$.

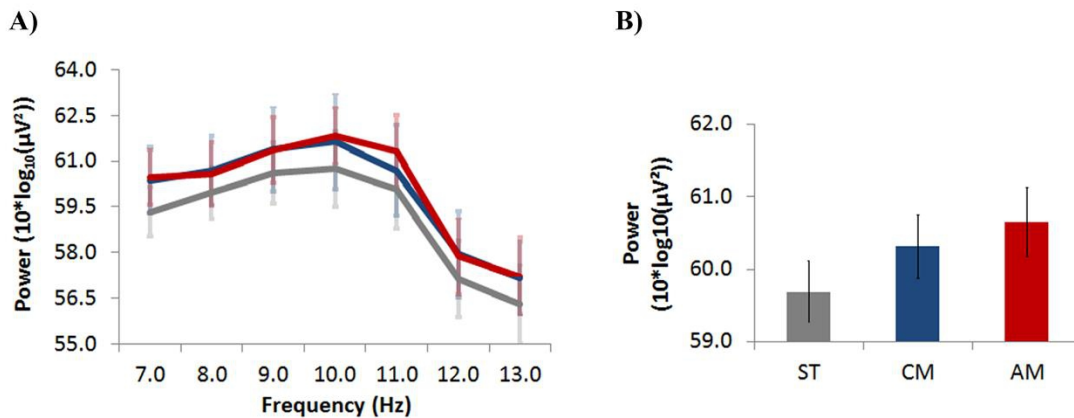


Figure 4.6. Group mean alpha-band power according to each imagery task (\pm SEM). Power spectrum of the evoked brain activity recorded in frontal channels cluster per imagery task (A) and its average from 10 Hz to 12 Hz (B). Color codes: red - alternate motion imagery (AM), blue - constant motion imagery (CM), gray - static dot imagery (ST). The alpha-band power of the evoked brain activity recorded in frontal channels cluster differs significantly between the moving stimuli and the no-motion stimulus (CM vs. ST, $P = 0.007$, corrected; AM vs. ST, $P = 0.003$, corrected).

In order to understand the origin of the alpha activity increasing during the visual imagery of motion when compared to the visual imagery of a static dot, the EEG source

localization for alpha-band (from 8 Hz to 12 Hz) and for two frequency sub-bands within the alpha range were examined (from 8 Hz to 10 Hz and from 10 to 12 Hz) applying the sLORETA method. The source localization of the alterations within this frequency-band during the visual stimulation was also performed for comparison. We used the comparison of visual moving stimuli (both motion conditions data combined) versus no-motion stimulus (figure 4.7, left) and the comparison of visual motion imagery (both visual motion imagery tasks data combined) versus no-motion visual imagery (figure 4.7, right), using the data time interval from 0.5 seconds to 1.5 seconds.

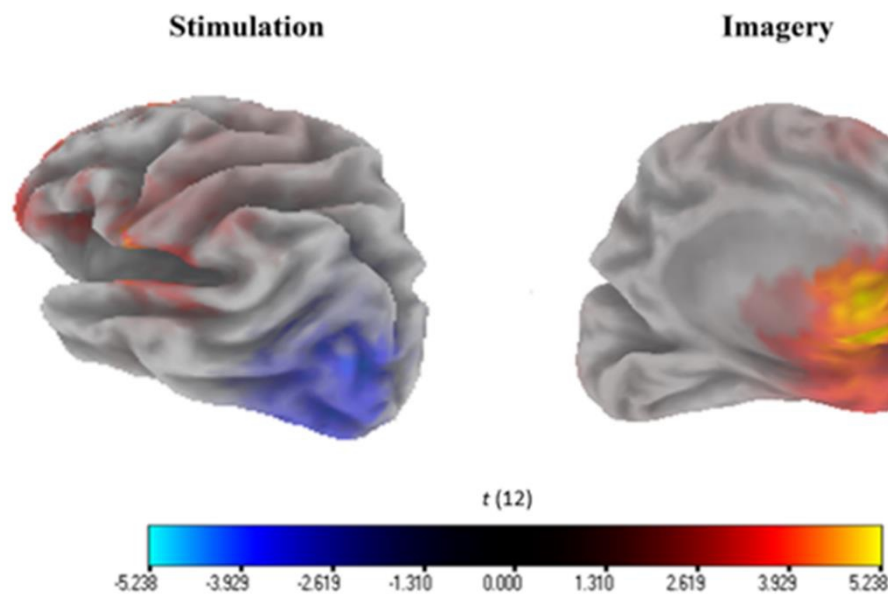


Figure 4.7. Source localization of the distinct alpha activity alterations during visual stimulation and visual imagery performed using sLORETA. The source found for the decrease in alpha during visual moving stimuli, when compared to non-moving stimulus, is shown at the left panel (maximum difference at the frequency-band from 8 Hz to 10 Hz). The right panel shows the identified dominant frontal source for the increase in alpha during visual motion imagery when compared to non-motion imagery (maximum difference at the frequency-band from 10 Hz to 12 Hz).

The highest level of alpha activity during the visual motion imagery in relation to the imagery of a static dot was found on the frontal lobe ($t = 5.24$, significant at $P = 0.05$ for two-tailed t test) at the frequency-band from 10 Hz to 12 Hz. During the visual moving stimulation the lowest recorded level of alpha activity in relation to the non-moving stimulus evoked brain activity was found in the occipital lobe at the frequency-band from 8 Hz to 10 Hz ($t = -4.52$, significant at $P = 0.05$ for two-tailed t test).

4.3.3. Visual motion imagery classification

The data were classified on trial-by-trial basis and using the relative spectral power of the frequency band from 7 Hz to 15 Hz of 6 selected EEG anterior channels (F3, F5, FC3, FC5, C3, and C5).

On average the three imagery tasks were classified with 87.64 % of accuracy: 88.68 % on the classification of static dot imagery, 88 % on the classification of constant motion imagery, and 86.23 % on the classification alternate motion imagery (table 4.1). The mean accuracy of classification was above the chance level for all participants (group results significant at $P = 0.001$ as revealed by a 2-tailed binomial test). From the eleven tested participants, only two were classified with accuracy lower than 80 %. On those cases, the misclassifications were mainly between the static dot imagery and the alternate motion imagery.

Table 4.1. Group classification performance \pm SEM. Sensitivity (Sens), specificity (Spec) and balanced accuracy (bACC) are presented as the group classification performance evaluation results for the imagery of a static dot (ST), imagery of a dot with constant motion (CM) and imagery of a dot with alternate motion (AM).

	Sens	Spec	bACC
ST	83.45 \pm 4.20	93.91 \pm 1.41	88.68 \pm 2.72
CM	84.55 \pm 2.47	91.45 \pm 1.96	88.00 \pm 2.07
AM	82.55 \pm 3.16	89.91 \pm 1.93	86.23 \pm 2.32
<i>Total</i>	83.52 \pm 2.99	91.76 \pm 1.49	87.64 \pm 2.24

In the group confusion matrix (table 4.2), it can be seen that the best performance of the classification algorithm was in the distinction of constant motion imagery from no-motion imagery. On the other hand, the classifier presented the highest number of misclassifications in distinguishing between constant motion imagery trials and alternate motion imagery trials.

Table 4.2. Confusion matrix of the classified EEG trials. Classification results of 550 trials from each imagery task - static dot imagery (ST), constant motion imagery (CM) and alternate motion imagery (AM).

		Classification		
		ST	CM	AM
Imagery trials	ST	459	38	53
	CM	27	465	58
	AM	40	56	454

4.4. Discussion

In this study we tested the hypothesis that visual motion imagery can induce different discriminable classes (at least 3) of EEG signal modulation. We tested three visual stimulation conditions with different number of motion alternations and the imagery of each visualized condition. We were motivated by findings showing that a different number of alternating sensory/perceptual signals (real or imagined) lead to distinct neural responses (Huk & Heeger 2002; Larsson et al. 2006; Sousa et al. 2016; Tootell et al. 1998).

Stimulation conditions and imagery strategies evoked different patterns and sources of alpha activity and, the spectral power of this frequency-band seems to reflect the complexity of the imagined visual motion. Importantly, only single-trial classification approaches were successful in differentiating the 3 imagery strategies while standard statistical measures failed. The visual motion stimulation evoked an alpha pattern different than the visual motion imagery: in the first case we found a decrease of alpha activity on the parieto-occipital channels while for the second case it was found an increase of alpha activity on the fronto-central channels. That is, we have identified different functional forms of alpha activity for evoked brain responses by visual motion stimulation and visual motion imagery.

It is well known that visual stimulation elicits an occipital alpha power decrease, reflecting a functional mechanism by which information is selected or gated in visual cortex (Foxye & Snyder 2011; Klimesch 2012; Klimesch et al. 2011; Schomer & Lopes Da Silva 2011). We found similar alpha power suppression, mainly on the parieto-occipital region, during both visual motion conditions presentation. However, a significant increase of alpha activity was found on the frontal channels cluster during both visual motion imagery tasks. Some studies have suggested an increasing of frontal alpha activity during high internal processing demands as top-down processing and working memory (Benedek et al. 2011; Sauseng et al. 2005) and processes requiring imagination of stimulus sequences (Cooper et al. 2003). According to Klimesch et al. (2007) and Schomer & Lopes Da Silva (2011) the functional state where frontal alpha oscillations are dominant reflects a state of reduced external information processing that is referred as a 'modulation gate', and the decrease of occipital alpha power corresponds to a situation in which attention to external stimuli is enabled. Moreover, previous studies suggest that mean frontal alpha amplitudes are enhanced for more complex tasks (Cooper et al. 2003). Thus, there are some evidences that the differences found between the different visual motion imagery tasks results on the frontal

alpha activity, with frequency peak above 10 Hz, can be related with the process of recovering the different visualized motion sequence conditions.

The source for the highest difference between the no-motion conditions/tasks and the motion conditions/tasks differs on the alpha sub-band frequency and location. These results are in agreement with previous studies that have shown different patterns of alpha desynchronization/synchronization subdividing the alpha frequency-band into different sub-bands (Klimesch 1999; Klimesch et al. 2007). The source localization results for the frontal alpha power increase during visual motion imagery can be related with the frontal lobe role on memory processes (Lenartowicz & McIntosh 2005). In animal studies similar observations could be reported for memory tasks involving temporally complex visual information (Gaffan & Wilson 2008).

EEG studies using non-visual imagery modulation strategies, for example focused on mental calculation, also reported increased frontal activity and suggested that it would be associated with the frontal lobe role in memory and cognitive challenges (Harmony et al. 1999; Harmony et al. 2004). However, they reported increased delta and theta activity instead of alpha activity. Thus, more research is needed to understand the relation of the frontal alpha increase with visual motion imagery.

Although a more classical statistical approach could not discern between the motion imagery tasks with different number of alternations, the applied classification algorithm performed a successful distinction between all visual motion imagery strategies supporting the advantage of multivariate data analysis approaches (Lemm et al. 2011). The high performance achieved by the classifier reveals potentially distinguishable brain activity patterns according to each imagery tasks, which suggests that visual motion imagery can be used as simple strategy to BCI multiclass control. Yet, real-time tests need to be carried on to confirm this proof-of-concept result. Furthermore, according to the number of classification errors related to the differentiation of constant motion imagery and alternate motion imagery, some participants had difficulties in achieving distinct patterns of brain activity during the motion imagery tasks.

4.5. Conclusion

This study provides a proof-of-concept showing that it is possible to achieve up to three classes of volitional brain activity using visual motion imagery. Results show that the imagery and stimulation of a single dot motion evokes different alpha activity patterns (with

distinct neural sources). While for the visual motion stimulation the parieto-occipital alpha activity showed a decrease, the frontal alpha increased during imagery with distinguishable patterns of activity (by means of a classifier) depending on the motion imagery strategy.

EEG data collected from visual motion imagery were used to test its applicability for BCI. A 3-class classifier was learned, using only a few channels, achieving 87.64 % offline accuracy, which shows the potential relevance of frontal alpha activity in imagery processes and their applications in BCI research.

References

- Amaral, C.P., Simões, M. a. & Castelo-Branco, M.S., 2015. Neural Signals Evoked by Stimuli of Increasing Social Scene Complexity Are Detectable at the Single-Trial Level and Right Lateralized. *Plos One*, 10(3), p.e0121970.
- Baek, H.J. et al., 2013. Brain-computer interfaces using capacitive measurement of visual or auditory steady-state responses. *Journal of neural engineering*, 10, p.24001.
- Banca, P. et al., 2015. Visual motion imagery neurofeedback based on the hMT+/V5 complex: evidence for a feedback-specific neural circuit involving neocortical and cerebellar regions. *Journal of Neural Engineering*, 12(6), p.66003.
- Benedek, M. et al., 2011. EEG alpha synchronization is related to top-down processing in convergent and divergent thinking. *Neuropsychologia*, 49(12), pp.3505–3511.
- Birbaumer, N. et al., 1999. A spelling device for the paralysed. *Nature*, 398(6725), pp.297–298.
- Birbaumer, N. & Cohen, L.G., 2007. Brain-computer interfaces: communication and restoration of movement in paralysis. *The Journal of physiology*, 579(Pt 3), pp.621–36.
- Brainard, D.H., 1997. The Psychophysics Toolbox. *Spatial vision*, 10(4), pp.433–436.
- Chang, C. & Lin, C., 2011. LIBSVM: A Library for Support Vector Machines. *ACM Transactions on Intelligent Systems and Technology (TIST)*, 2, pp.1–39.
- Combaz, A. & Van Hulle, M.M., 2015. Simultaneous detection of P300 and steady-state visually evoked potentials for hybrid brain-computer interface. *PloS one*, 10(3), p.e0121481.
- Cooper, N.R. et al., 2003. Paradox lost? Exploring the role of alpha oscillations during externally vs. internally directed attention and the implications for idling and inhibition hypotheses. *International Journal of Psychophysiology*, 47, pp.65–74.
- Delorme, A. & Makeig, S., 2004. EEGLAB: An open source toolbox for analysis of single-trial EEG dynamics including independent component analysis. *Journal of Neuroscience Methods*, 134(1), pp.9–21.
- Emmerling, T. et al., 2015. Decoding the direction of imagined visual motion using 7T ultra-high field fMRI. *NeuroImage*, 125, pp.61–73.
- Farwell, L.A. & Donchin, E., 1988. Talking off the top of your head: toward a mental prosthesis utilizing event-related brain potentials. *Electroencephalography and Clinical Neurophysiology*, 70(6), pp.510–523.
- Foxe, J.J. & Snyder, A.C., 2011. The role of alpha-band brain oscillations as a sensory suppression mechanism during selective attention. *Frontiers in Psychology*, 2(JUL).
- Friedrich, E.V.C. et al., 2015. An Effective Neurofeedback Intervention to Improve Social Interactions in Children with Autism Spectrum Disorder. *Journal of autism and developmental disorders*.
- Gaffan, D. & Wilson, C.R.E., 2008. Medial temporal and prefrontal function: Recent behavioural disconnection studies in the macaque monkey. *Cortex*, 44(8), pp.928–935.
- Ge, S., Wang, R. & Yu, D., 2014. Classification of Four-Class Motor Imagery Employing Single-Channel Electroencephalography. *PLoS ONE*, 9(6), p.e98019.
- Goebel, R. et al., 1998. The constructive nature of vision: Direct evidence from functional magnetic resonance imaging studies of apparent motion and motion imagery. *European Journal of Neuroscience*, 10(5), pp.1563–1573.
- Harmony, T. et al., 1999. Do specific EEG frequencies indicate different processes during mental calculation? *Neuroscience Letters*, 266(1), pp.25–28.
- Harmony, T. et al., 2004. Specific EEG frequencies signal general common cognitive processes as well as specific task processes in man. *International Journal of Psychophysiology*, 53(3), pp.207–216.
- Huk, A.C. & Heeger, D.J., 2002. Pattern-motion responses in human visual cortex. *Nature neuroscience*, 5(1), pp.72–75.
- Huster, R. et al., 2014. Brain-computer interfaces for EEG neurofeedback: Peculiarities and solutions. *International Journal of Psychophysiology*, 91(1), pp.36–45.
- Karim, A. et al., 2006. Neural Internet: Web Surfing with Brain Potentials for the Completely Paralyzed. *Neurorehabilitation and Neural Repair*, 20(4), pp.508–515.
- Keren, A.S., Yuval-Greenberg, S. & Deouell, L.Y., 2010. Saccadic spike potentials in gamma-band EEG: Characterization, detection and suppression. *NeuroImage*, 49(3), pp.2248–2263.
- Khalighi, S. et al., 2013. Automatic sleep staging: A computer assisted approach for optimal combination of features and polysomnographic channels. *Expert Systems with Applications*, 40(17), pp.7046–7059.
- Klimesch, W., 2012. Alpha-band oscillations, attention, and controlled access to stored information. *Trends in Cognitive Sciences*, 16(12), pp.606–617.
- Klimesch, W., 1999. EEG alpha and theta oscillations reflect cognitive and memory performance: A review

- and analysis. *Brain Research Reviews*, 29(2–3), pp.169–195.
- Klimesch, W., Fellinger, R. & Freunberger, R., 2011. Alpha oscillations and early stages of visual encoding. *Frontiers in Psychology*, 2(MAY).
- Klimesch, W., Sauseng, P. & Hanslmayr, S., 2007. EEG alpha oscillations: The inhibition-timing hypothesis. *Brain Research Reviews*, 53(1), pp.63–88.
- Kubler, A. et al., 2001. Brain-computer communication: Self-regulation of slow cortical potentials for verbal communication. *Archives of Physical Medicine and Rehabilitation*, 82(11), pp.1533–1539.
- Larsson, J., Landy, M.S. & Heeger, D.J., 2006. *Orientation-selective adaptation to first- and second-order patterns in human visual cortex.*
- Leeb, R. et al., 2013. Transferring brain-computer interfaces beyond the laboratory: Successful application control for motor-disabled users. *Artificial Intelligence in Medicine*, 59, pp.121–132.
- Lemm, S. et al., 2011. Introduction to machine learning for brain imaging. *NeuroImage*, 56(2), pp.387–399.
- Lenartowicz, A. & McIntosh, A.R., 2005. The role of anterior cingulate cortex in working memory is shaped by functional connectivity. *Journal of cognitive neuroscience*, 17(7), pp.1026–42.
- Lopes, A.C., Pires, G. & Nunes, U., 2013. Assisted navigation for a brain-actuated intelligent wheelchair. *Robotics and Autonomous Systems*, 61(3), pp.245–258.
- Makeig, S., 1993. Auditory event-related dynamics of the EEG spectrum and effects of exposure to tones. *Electroencephalography and clinical neurophysiology*, 86(92), pp.283–293.
- Maria, A.-V.L., Antonio, S.-R.R. & A., R.-M.R., 2015. Motor Imagery based Brain-Computer Interfaces: An Emerging Technology to Rehabilitate Motor Deficits. *Neuropsychologia*, pp.1–10.
- McFarland, D., Sarnacki, W.A. & R, W., 2015. Effects of training pre-movement sensorimotor rhythms on behavioral performance. *Journal of Neural Engineering*, 12(6), p.66021.
- McFarland, D.J., Sarnacki, W. a & Wolpaw, J.R., 2010. Electroencephalographic (EEG) control of three-dimensional movement. *Journal of neural engineering*, 7(3), p.36007.
- Mormann, F. et al., 2007. Seizure prediction: the long and winding road. *Brain*, 130, pp.314–333.
- Nijboer, F. et al., 2008. A P300-based brain-computer interface for people with amyotrophic lateral sclerosis. *Clinical neurophysiology*, 119(8), pp.1909–16.
- Ono, T. et al., 2014. Brain-computer interface with somatosensory feedback improves functional recovery from severe hemiplegia due to chronic stroke. *Frontiers in neuroengineering*, 7(July), p.19.
- Pascual-Marqui, R.D., 2002. Standardized low-resolution brain electromagnetic tomography (sLORETA): technical details. *Methods and findings in experimental and clinical pharmacology*, 24 Suppl D, pp.5–12.
- Pascual-Marqui, R.D., Michel, C.M. & Lehmann, D., 1994. Low resolution electromagnetic tomography: a new method for localizing electrical activity in the brain. *International Journal of Psychophysiology*, 18(1), pp.49–65.
- Pearson, J. et al., 2015. Mental Imagery: Functional Mechanisms and Clinical Applications. *Trends in Cognitive Sciences*, 19(10), pp.590–602.
- Pfurtscheller, G. et al., 1997. EEG-based discrimination between imagination of right and left hand movement. *Electroencephalography and Clinical Neurophysiology*, 103(6), pp.642–651.
- Pires, G., Nunes, U. & Castelo-Branco, M., 2012. Comparison of a row-column speller vs. a novel lateral single-character speller: Assessment of BCI for severe motor disabled patients. *Clinical Neurophysiology*, 123(6), pp.1168–1181.
- Ramirez, R. et al., 2015. Musical neurofeedback for treating depression in elderly people. *Frontiers in Neuroscience*, 9(October), pp.1–10.
- Ramos-Murguialday, A. & Birbaumer, N., 2015. Brain oscillatory signatures of motor tasks. *Journal of Neurophysiology*, 7, p.jn.00467.2013.
- Salari, N. & Rose, M., 2013. A Brain-Computer-Interface for the Detection and Modulation of Gamma Band Activity. *Brain Sciences*, 3(4), pp.1569–1587. Available at: <http://www.mdpi.com/2076-3425/3/4/1569/>.
- Sauseng, P. et al., 2005. EEG alpha synchronization and functional coupling during top-down processing in a working memory task. *Human Brain Mapping*, 26(2), pp.148–155.
- Schlögl, A. et al., 2005. Characterization of Four-Class Motor Imagery EEG Data for the BCI-Competition 2005. *Journal of Neural Engineering*, 2(4), pp.L14–L22.
- Schomer, D. & Lopes Da Silva, F., 2011. *Niedermeyer's Electroencephalography: Basic Principles, Clinical Applications, and Related Fields* 6th Ed., Lippincott Williams & Wilkins.
- Shih, J.J., Krusienski, D.J. & Wolpaw, J.R., 2012. Brain-computer interfaces in medicine. *Mayo Clinic Proceedings*, 87(3), pp.268–279.
- Sousa, T. et al., 2015. A two-step automatic sleep stage classification method with dubious range detection. *Computers in Biology and Medicine*, 59, pp.42–53.
- Sousa, T. et al., 2016. Control of Brain Activity in hMT+/V5 at Three Response Levels Using fMRI-Based

- Neurofeedback/BCI. *Plos One*, 11(5), p.e0155961.
- Strehl, U. et al., 2006. Self-regulation of slow cortical potentials: a new treatment for children with attention-deficit/hyperactivity disorder. *Pediatrics*, 118(5), pp.e1530-40.
- Tootell, R.B. et al., 1998. Functional analysis of primary visual cortex (V1) in humans. *Proceedings of the National Academy of Sciences of the United States of America*, 95(3), pp.811–817.
- Treder, M.S. et al., 2011. Brain-computer interfacing using modulations of alpha activity induced by covert shifts of attention. *Journal of neuroengineering and rehabilitation*, 8, p.24.
- Welch, P., 1967. The use of fast Fourier transform for the estimation of power spectra. *Audio and Electroacoustics, IEEE Transactions on*, 15(2), pp.70–73.
- Wolpaw, J. & Wolpaw, E.W., 2012. *Brain-Computer Interfaces: Principles and Practice.*, Oxford University Press.
- Wolpaw, J.R. & McFarland, D.J., 2004. Control of a two-dimensional movement signal by a noninvasive brain-computer interface in humans. *Proceedings of the National Academy of Sciences of the United States of America*, 101(51), pp.17849–54.

APPENDIX

Chapter 4

A1. Experimental design

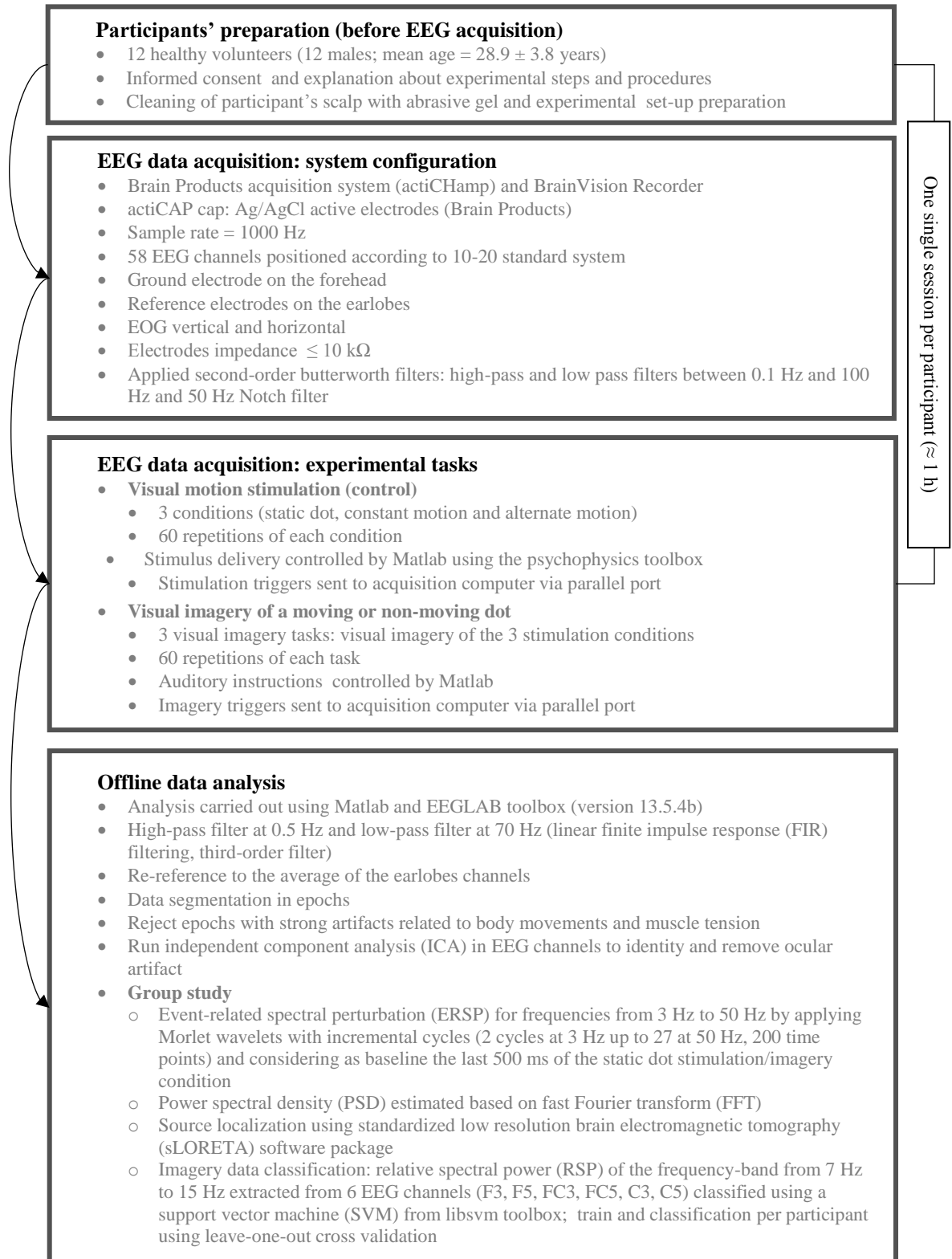


Figure 4.A1. Summary of the main experimental steps. The visual motion stimulation was used as a control study and as a guide for the visual motion imagery tasks. Participants were asked to imagine alternately the 3 visual conditions, based on different quantities of motion variation. The data analyses were performed offline.

A2. Acquisition system set-up

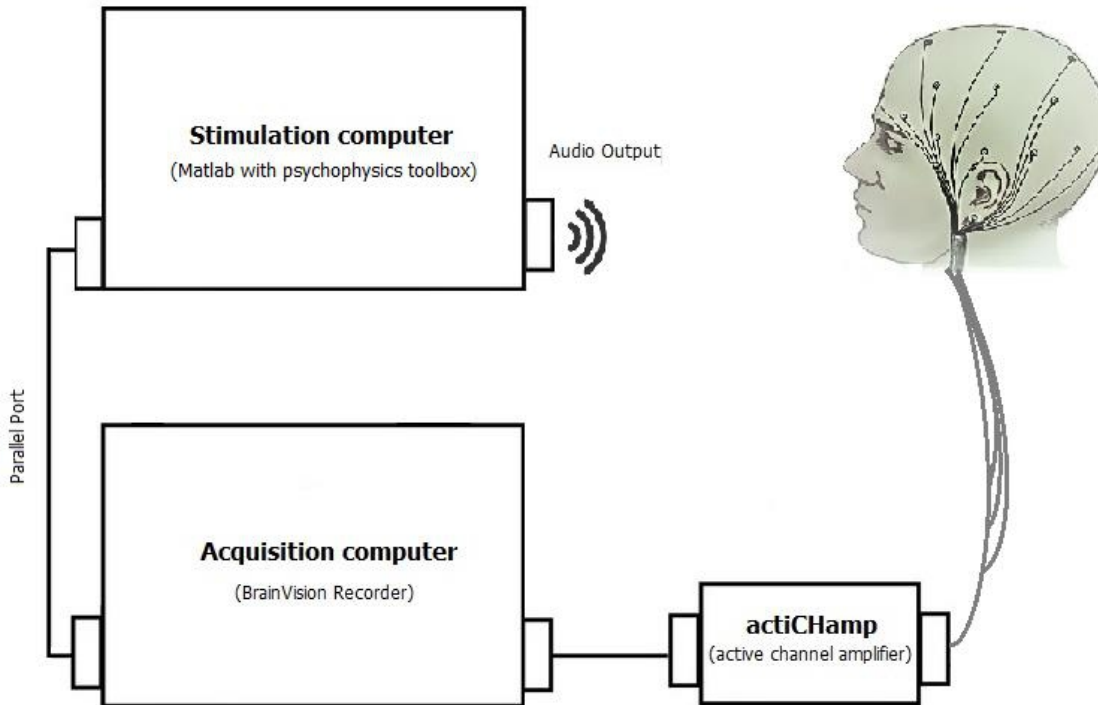


Figure 4.A2. Schematic diagram of acquisition set-up. The EEG data were acquired during visual motion stimulation and during visual motion imagery. The stimulation conditions and the imagery instruction (auditory) were controlled using the Matlab and its psychophysics toolbox. The stimulation computer sent the triggers to the acquisition computer via parallel port. The EEG data were recorded using active electrodes and the actiCHamp system from Brain Products.

A3. Classification algorithm

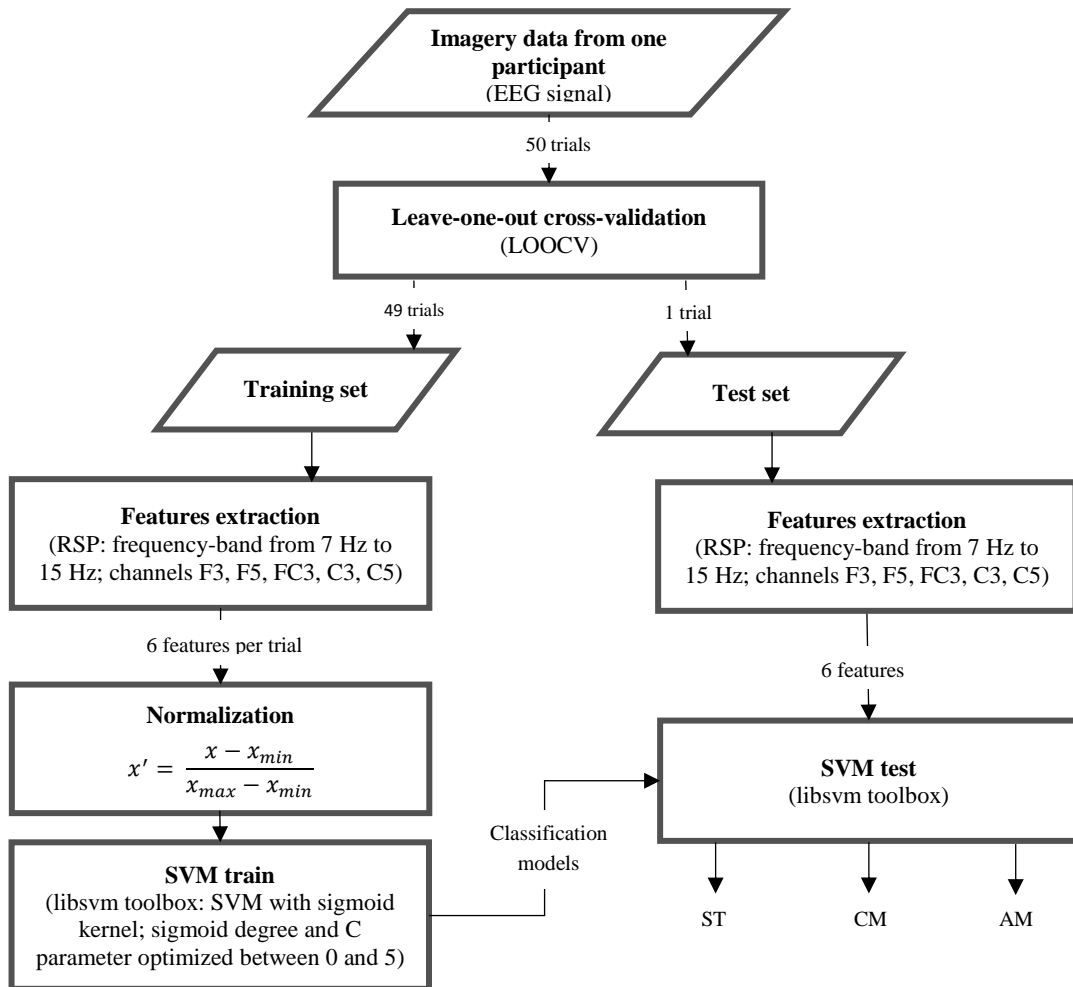


Figure 4.A3. Classification algorithm. The EEG data acquired during each imagery task – imagery of a static dot (ST), imagery of a dot with constant motion (CM) and, imagery of a dot with alternate motion (AM) – were classified per participant using a support vector machine (SVM), based on the relative spectral power (RSP) of a small number of channels.

CHAPTER 5

PERCEPTUAL INTERPRETATION OF VISUAL MOTION REVEALED AT HIGH-RESOLUTION 7T fMRI

Based on: Sousa, T., Kemper, V., Duarte, J. V., Costa, G., Martins, R., Goebel, R., Castelo-Branco, M., 2016. Perceptual interpretation of visual motion revealed at high-resolution 7T fMRI in functional domains within visual area hMT+/V5. *(In preparation)*

Abstract

It has been suggested that activity in hMT+/V5 reflects global motion interpretation of perceptual bistability. The multistability in perceptual decision in the presence of an unchanging stimulus can arise from a variety of stimulus types, involving alterations in a pattern's perceived depth, direction of motion, or visibility. These perceptual phenomena are extensively used in the visual sciences as a tool for investigating mechanisms of perceptual organization, but fine grained studies of the respective neural dynamics are still lacking.

Here we took advantage of high resolution seven tesla functional magnetic resonance imaging to investigate how bistable perceptual integration/segmentation of interhemispheric 1D directional cues is mapped in hMT+/V5 functional sub-domains. To achieve this goal we used a paradigm in which 2D motion coherence requires interhemispheric integration of line gratings and incoherence breaks such binding across hemispheres.

We found evidence for the existence of perception related sub-domains in the hMT+/V5 region. These domains responded preferentially either to coherent or incoherent motion and have showed preferred axes of motion that matched the perceptual reports. Accordingly, an interaction between the type of perceptual sub-domain and the axes of motion preference was found, suggesting columnar-level neural correlates of perceptual content in area hMT+/V5. Moreover, our results suggest that hMT+/V5 also has a functional role in integrating interhemispheric representations of bistable percepts. Finally, these findings suggest that both the transition of perceptual states and the content of perception can be read-out directly from the activity patterns across perceptual sub-domains in hMT+/V5 area.

5.1. Introduction

During continuous observation of an unchanging stimulus, visual perception may alternate between competing interpretations, switching over time between alternative dominant percepts. This phenomenon is called multistable visual perception (Leopold & Logothetis 1999; Kornmeier & Bach 2012) and is generated by stimuli commonly referred to as ambiguous perceptual stimuli. It is in general possible to study the temporal dynamics of perceptual oscillations using simple functions that may be useful to infer about putative neural mechanisms underlying perceptual decision. The study of multistable perception can offer powerful insights into mechanisms of visual awareness, perceptual organization, and decision (Pomerantz & Kubovy 1981; Crick & Koch 1998; Blake & Logothetis 2002; Blake et al. 2014). Low level explanations of multistable visual phenomena suggest that the spontaneous perceptual switches are due to antagonistic connectivity within the visual system and adaptation phenomena. However, the origin of perceptual reversals is still highly under debate and the role of high level regions is also relevant (Leopold & Logothetis 1999; Long & Toppino 2004; Kornmeier et al. 2009; Kornmeier & Bach 2012).

The inherent ambiguity of the direction of motion of a line is known for a long time (Wallach 1935). This is because collinear line patterns (gratings) only define one dimension in velocity space. Perceptually, a line is always seen to move in the direction perpendicular to its orientation, in spite of the inherent ambiguity of 1D stimuli. Because of this fact, when the line moves behind an aperture, the perceived direction changes from the perpendicular direction and is affected by the shape of aperture. If instead of a single line we have a group of lines as a grating pattern, the single lines together constitute a new object that is characterized by its perceived motion as a whole (Wallach 1935; Movshon et al. 1985; Wuerger et al. 1996).

There are several studies using two line grating patterns combined, exploring how full integration of multiple globally moving surfaces is achieved within the visual system, such as plaid stimuli, made by superimposing two gratings of different orientations (Adelson & Movshon 1982; Burke et al. 1994; Castelo-Branco et al. 2000; Castelo-Branco et al. 2002; Castelo-Branco et al. 2009; Kozak & Castelo-Branco 2009). Even when physically constant, this type of stimulus produces perceptual bistability, in which observers spontaneously

switch perception between two independent moving objects or one single object moving coherently. A close relation was found between the activity changes in the the human motion complex (hMT+/V5), known to be involved in motion perception (Tootell et al. 1995; Kolster et al. 2010), and the perceptual switches involving differential binding of stimulus components moving in different directions (Castelo-Branco et al. 2002). Thus, it has been suggested that activity in this brain area reflects global motion interpretation in relation to perceptual bistability. However, it remains to be established whether functional domains related to visual perception can be identified in hMT+/V5.

Ultra-high field functional magnetic resonance imaging (fMRI) provides higher spatial specificity (Uğurbil et al. 2003; Uludağ et al. 2009), signal-to-noise ratio (Vaughan et al. 2001) and functional specificity (Shmuel et al. 2007) than conventional 3 Tesla fMRI. These advances in fMRI have led to the possibility of detecting small neuronal ensembles that constitute fundamental computational units in the brain, down to the columnar or quasi-columnar level. The study of the functional organization of the human visual system close to these levels may allow to understand early visual integration mechanisms and beyond (Menon et al. 1997; Cheng et al. 2001; Yacoub et al. 2007; Yacoub et al. 2008), particularly in the hMT+/V5 complex (Zimmermann et al. 2011). More recently, also perceptual tasks have been investigated at this detailed level of organization, revealing columnar-level neural correlates of perceptual switches in area hMT+/V5 using plaid stimuli (see preliminary report by Goebel et al. 2014).

Here we have used a previously described ambiguous moving stimulus in a non-overlapping configuration whereby 1D components are presented to each hemisphere (Wallach 1935; Wuerger et al. 1996) thereby requiring long range integration. Accordingly, the motion coherence requires interhemispheric binding and incoherence interhemispheric segregation. We took advantage of high resolution 7 Tesla (7T) fMRI to explore the relation between hMT+/V5 spatial and temporal activity patterns and perceptual oscillations related to bistable perception. We aimed to map functional sub-domains in the hMT+/V5 region responding specifically for each type of global motion percept (coherent or incoherent). Moreover, we aimed to test if these perceptual sub-domains have different axes of motion preferences and if they matched the type of perceived global motion. With this study, we attempted to provide new insights about the relation between putative perceptual domains and global direction-selective responses in hMT+/V5.

5.2. Material and Methods

5.2.1. Participants

Ten healthy participants (six males; mean age \pm standard deviation: 28.4 ± 8.0 years; 9 right-handed and 1 left-handed) with normal or corrected-to-normal vision participated in this study. Participants gave informed consent and were paid for their participation.

All experimental procedures were conducted with approval from the Ethical Committees of Coimbra University and the Faculty of Psychology and Neuroscience at Maastricht University.

5.2.2. Experimental design overview

All the recruited participants performed a familiarization session outside of the scanner (twelve minutes per day – two runs of ambiguous stimulation, during five days in the week before of the scanning session). During the familiarization session the participants should get used to the ambiguous stimulus and to report perceptual alternations, which after these sessions should have stabilized in terms of their dynamics. The ambiguous stimulus was presented with the same parameters of the scanning session (see stimulus description below). In order to be able to use an efficient block design in our analyses, only participants with minimum average duration of six seconds per each motion percept were selected for the study.

The scanning session included the acquisition of anatomical data for co-registration of functional data, two runs of an hMT+/V5 functional localizer for the correct slice positioning of the subsequent high-resolution functional images, two control runs (unambiguous stimulation), four runs of ambiguous stimulation (each two interleaved with one control run) and three runs of a functional localizer of the hMT+/V5 sub-domains with different axes of motion preference. The total of the scanning session took two hours. Participants were asked to breathe steadily and to remain as still as possible.

The experimental design is further detailed in the next subsections and its complete overview is given as supplementary figure 5.A1 in appendix.

5.2.3. Stimuli

The stimuli were created with MATLAB (The Mathworks, Inc.), using the Psychophysics Toolbox (Brainard 1997; Pelli 1997). In the scanner, they were projected on a screen located

at 99 cm away from the participant (screen size: 17.2 deg x 10.4 deg (horizontal x vertical); stimuli size: 11 deg x 10 deg; projected display: resolution of 1920 x 1080 and refresh rate of 60 Hz). Responses were collected through an MR compatible button box (Current Designs, 4-button response device, Philadelphia, USA).

A) Ambiguous Stimulation

The ambiguous stimulus was designed based on the original description of Wallach (Wallach 1935; Wuerger et al. 1996). The roof shaped stimulus consisted of continuously moving downward oblique black lines forming an inverted V-shape, on a white background (orientation: ± 25 deg relative to x-axis; contrast: 100 %; motion speed: 3 deg/s; duty cycle: 6%; spatial frequency: 0.6 cycle/deg; stimulus visual angle: 11 deg x 10 deg - horizontal x vertical). A central blue cross (visual angle: 0.2 deg) was present as a fixation target at the visual midline. The lines terminations on the stimulus border were smoothed using a mask, with a central aperture (9.9 deg x 10 deg), superimposed to the Wallach stimulus. The mask was prepared using a bi-dimensional squared Gaussian kernel (width and height: 0.6 deg) with an identical standard-deviation (0.3 deg) on both dimensions.

In spite of the absence of physical change in the moving stimulus, participants spontaneously exhibited perceptual alternations between coherent motion (the lines were perceived moving downward as a single roof-like object – figure 5.1-A) or incoherent motion (the lines were perceived as two separate objects, one in each visual hemi-field, moving inward – figure 5.1-B). Participants indicated their perceived motion pattern through a button press.

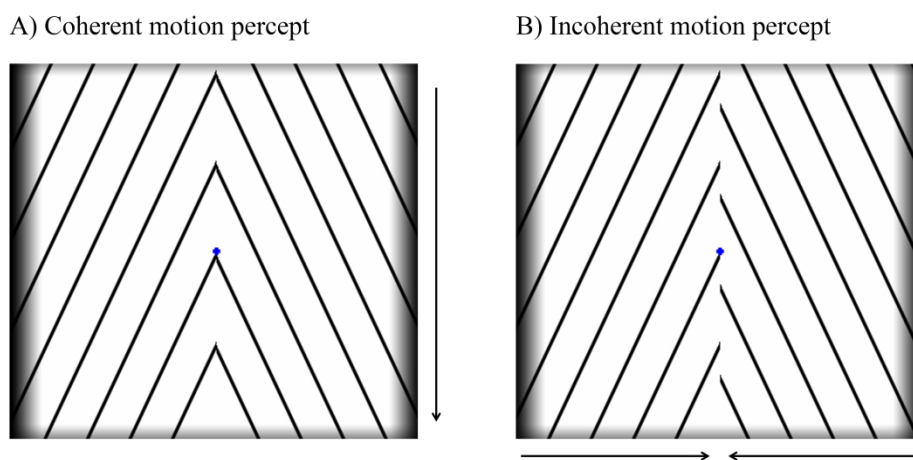


Figure 5.1. Patterns of motion perceived during ambiguous stimulation. The bistable percept resulting from ambiguous stimulation was reflected on the alternation of two patterns of motion perceived by each participant: one roof-like object moving downward - coherent motion percept (A) or two separate objects

moving inward - incoherent motion percept (**B**). The arrows are representing the perceived direction of motion. The blue cross was used as central fixation point. The line offset in right panel does not necessarily physically exist and maybe virtually perceived.

In order to facilitate more stable percepts we performed pilot tests where we varied features of stimulus. By offsetting the lines between the two hemi-fields participants reported larger and more balanced perceptual durations, thus the stimuli were prepared with a slight offset of 0.06 deg. The ambiguous stimulation was run in four separated runs with 180 volumes each, completing a total of 20 trials of motion (60 seconds each) interleaved with no-motion periods (static figure of the inverted V-shaped lines presented during 15 seconds).

B) Unambiguous Stimulation

The unambiguous stimulation was used as control test for the brain response to the coherent and incoherent motion. We added background moving dots (600 dots randomly distributed with contrast of 40 % and visual angle of 0.1 deg) to the ambiguous stimulus biasing the participants to unambiguously perceive each kind of motion. With all dots moving inward simultaneously on each hemi-field the participants were induced to perceive the incoherent motion pattern (figure 5.2-B) and with all dots moving simultaneously downward on each hemi-field the participants were induced to perceive the coherent motion pattern (figure 5.2-A). The dots were moving at the same speed as the inverted V-shaped lines (3 deg/s).

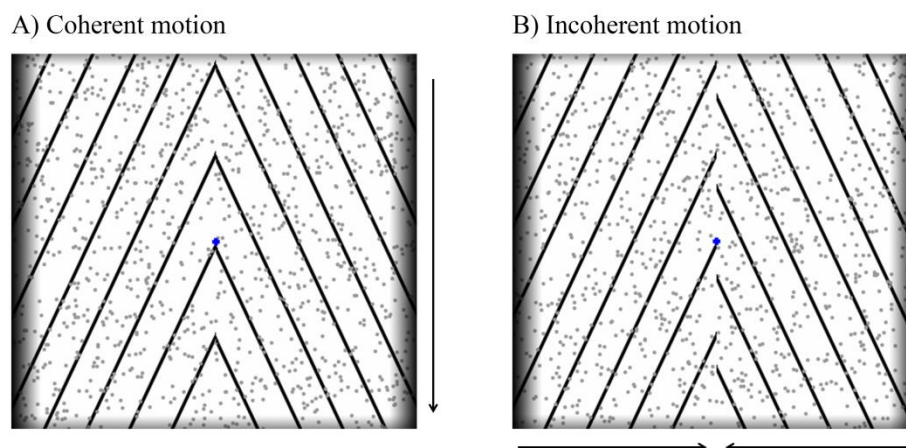


Figure 5.2. Motion conditions during unambiguous stimulation (control). By disambiguating the stimulus with additional moving dots the participants were biased to unambiguously perceive each kind of motion, as induced by dot motion pattern: dots moving downward - coherent motion (**A**), dots moving inward - incoherent motion (**B**). The arrows are representing the perceived direction of motion. The blue cross was used as central fixation point.

The unambiguous stimulation was performed in two runs of 180 volumes each. The duration of each motion condition varied between 6 and 9 seconds. Per run, each motion condition was repeated 10 times and randomly interleaved with no-motion condition (static figure of the inverted v-shaped lines with the added dots presented during 15 seconds). In order to confirm the perceived pattern of motion, we asked to the participants to indicate via a button press their perceptual content.

C) Axes of motion preference mapping

To explore the relation between bistable perception and axis of motion preference, we designed a stimulus to functionally localize direction of motion tuned columnar like features in hMT+/V5. We showed participants moving conditions in different axes of motion (0 deg, 45 deg, 90 deg and 135 deg) randomly interleaved with a no-motion condition (figure 5.3).

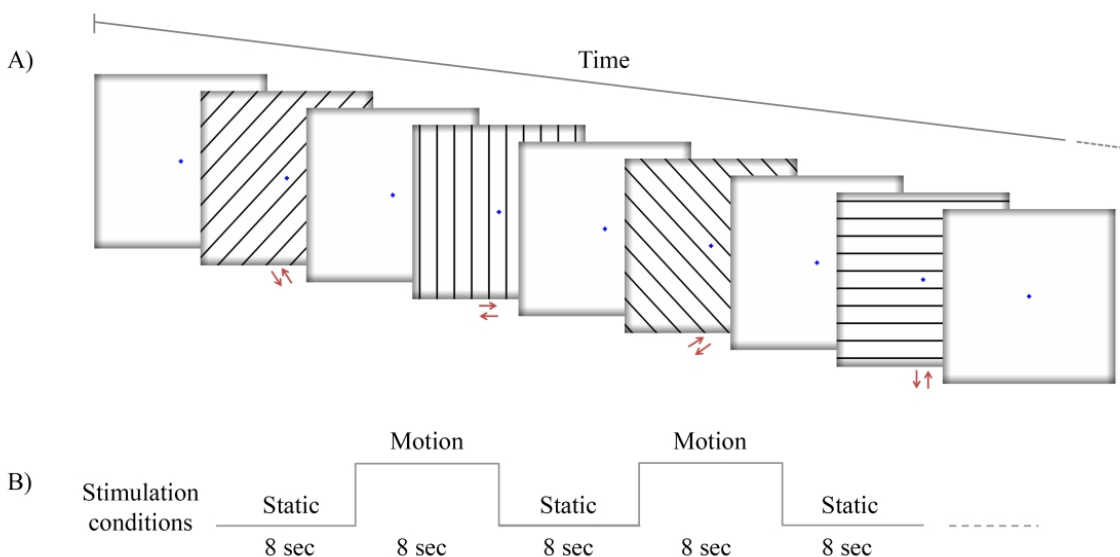


Figure 5.3. Stimulation conditions used for axes of motion preference mapping. **A)** Each axis of motion (45 deg, 0 deg, 135 deg or 90 deg) was defined pooling together stimulation conditions with opposing directions. The red arrows are indicating the motion directions of each stimulation condition. The motion conditions were randomly interleaved with a no-motion condition (18 trials of each motion orientation). **B)** Each trial (motion or no-motion) lasted 8 seconds. The blue cross was used as central fixation point.

As previously demonstrated axis of motion columns are referred as aggregated functional clusters responding to opposing motion directions (Zimmermann et al. 2011). Therefore we pooled responses to motion conditions with opposing directions to select functional domains with preference for a specific orientation. The stimulus was composed by 8 motion conditions and 1 no-motion condition, all with the duration of 8 seconds. All the motion conditions consisted of black moving lines on a white background with the same parameters

as the ambiguous and the unambiguous stimuli (with the exception of the axis of motion). Each condition with different motion direction was repeated 9 times across 3 stimulation runs with 196 volumes each (3 trials of each motion direction per run) totaling a total of 18 trials of each motion orientation in this study.

5.2.4. Imaging data acquisition

Images were acquired with a Siemens MAGNETOM 7T scanner (Siemens; Erlangen, Germany) and a 32-channel head-coil (Nova Medical Inc.; Wilmington, MA, USA).

Structural images were acquired for anatomical reference using a T1-weighted magnetization prepared rapid acquisition gradient echo (3D-MPRAGE) (256 sagittal slices; isotropic resolution of 0.6 mm; repetition time (TR) = 3100 ms; echo time (TE) = 2.52 ms; flip angle = 5°; matrix = 384 × 384; generalized partially parallel acquisitions (GRAPPA) acceleration factor = 3). To correct for intensity inhomogeneities additional gradient echo proton-density (GE-PD) images (same parameters as 3D-MPRAGE, except TR = 1440 ms) were acquired.

High-resolution functional images were obtained using a gradient echo (T2-weighted) echo-planar imaging (2D GE-EPI) (28 slices; isotropic resolution of 0.8 mm; TR = 2000 ms; TE = 25.6 ms; flip angle = 69°; matrix = 186 × 186; GRAPPA acceleration factor = 3). To correct for EPI distortions additional functional volumes (five volumes with a reversed encoding direction) were acquired right after the GE-PD images. The field-of-view included a very restricted functional coverage (figure 5.4). In order to ensure that functional images with isotropic resolution of 0.8 mm would be in the correct position to cover the bilateral ROI, two hMT+/V5 functional localizer runs were first acquired for slice positioning (39 coronal slices; isotropic resolution of 1.6 mm; TR = 2000 ms; TE = 17.2 ms; flip angle = 70°; matrix = 88 × 88; GRAPPA acceleration factor = 2). The hMT+/V5 localizer protocol was based on studies of Huk & Heeger (2002) as used by Zimmermann et al. (2011) and Emmerling et al. (2015).

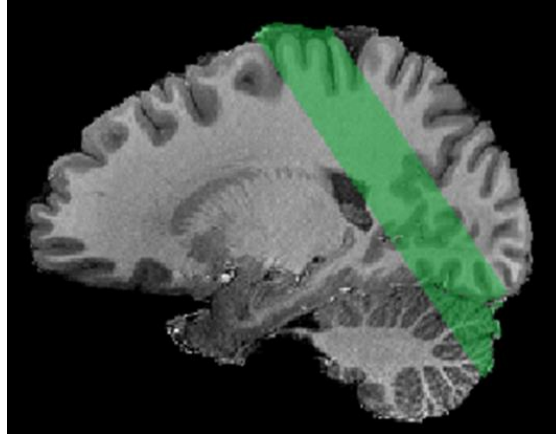


Figure 5.4. Functional field-of-view. Example from one participant showing the restricted functional coverage of the high-resolution functional magnetic resonance imaging (fMRI) data acquired.

5.2.5. Offline data analyses

The offline data analyses were performed using BrainVoyager QX (BV QX) software (version 2.8.4; Brain Innovation; Maastricht, The Netherlands) (Goebel et al. 2006) and with the IBM (Armonk, NY) SPSS Statistics 22.0 software package.

A) Behavioral data analysis

Aiming to understand the temporal distribution of bistable perception during the ambiguous stimulation we calculated the mean duration of each percept and the number of perceptual switches per participant. Furthermore, we estimated the probability of occurrence of a particular duration for each percept using the probability density function. The gamma and the lognormal distributions, commonly used for fitting perceptual duration data of ambiguous stimuli (Borsellino et al. 1972; Leopold & Logothetis 1999; Zhou et al. 2004), were fitted to the data using the maximum likelihood method to estimate the parameters. The maximum likelihood estimates of α and β (gamma distribution) or σ and μ (lognormal distribution) parameters were calculated for each participant using a time-window from zero to the longest percept duration that occurred, and the goodness of fit was assessed using the Kolmogorov-Smirnov test ($P > 0.05$).

B) Imaging data pre-processing

First, spatial intensity inhomogeneities of the anatomical images were corrected based on proton density (PD) measurement information. The PD scan acts as a coarse estimation of

spatial intensity inhomogeneities allowing to remove them from the corresponding T1 data by dividing the T1 data by the PD data (Van de Moortele et al. 2009). In order to further improve the homogeneity of the data, was also applied a standard correction which uses low-order polynomials to model low-frequency variations across the 3D image space. The polynomials were fitted to a subset of voxels that have been labeled as belonging to white matter. After estimating the low-frequency intensity fluctuations, they were removed from the data producing voxels with more homogeneous intensities that improved visualization and were also better starting points for subsequent functional co-registration steps (Hou et al. 2006; Sled et al. 1997).

After inhomogeneity corrections the anatomical data were normalized to the AC-PC space. Like native space, AC-PC space reflects the true shape of an individual brain since this rigid body transformation only translates and rotates the brain in a canonical orientation (Talairach & Tournoux 1988). Moreover, using a sinc-weighted interpolation the anatomical images were up-scaled to an isotropic resolution of 0.8 mm to match the resolution of the functional data.

The functional data were corrected for 3D rigid body motion (aligning all subsequent runs to the closest functional run of the anatomical scans) and high-pass filtered using a general linear model (GLM) Fourier basis set of two cycles sine/cosine per run (including linear trend removal). Furthermore, as EPI images suffer from geometric distortions due to non-zero off-resonance fields, a correction method based on opposite phase encoding was applied (Andersson et al. 2003). The susceptibility-induced off-resonance field was estimated from the pairs of images with distortions in opposite directions (recorded functional volumes of normal and reversed phase encoding).

Finally, functional images were co-registered to the 3D anatomical data and resampled at the original resolution using a sinc interpolation. The functional images with 0.8 mm isotropic resolution matched the final resolution of the anatomical data.

C) Imaging data analysis

First, a standard GLM was used to assess the functional activation pattern (Kutner et al. 1996). The condition predictors were created by convolving the activation blocks with a standard hemodynamic response function (Friston et al. 1998). For each stimulation protocol (ambiguous, unambiguous and axes of motion preference mapping), all runs were analyzed together on a single subject-by-subject basis using the motion parameters as

confound predictors. Then, we defined the hMT+/V5 region of interest (ROI) per participant using the axes of motion preference mapping data. The ROI was defined for each hemisphere including all voxels significantly activated at $q(\text{FDR}) = 0.05$ contrasting all motion stimulation conditions with the baseline. This ROI served as base for the subsequent analysis steps.

The ambiguous evoked responses were analyzed as a function of presence of coherent or incoherent percepts and compared with the evoked responses during unambiguous stimulation. Importantly, we asked whether perceptually selective ROIs could be discovered based on the ambiguous stimulation data (incoherent perceptual ROI and coherent perceptual ROI). Then we asked whether preferred responses to given axes of motion also matched the direction of the preferred type of percept. Our goal was to investigate whether an interaction between the motion preference of each functional domains and preference for each kind of percept. The axes of motion preference mapping stimulus included motion conditions tuned for the coherent or incoherent percept due to their different orientations (figure 5.5). The resulting axis of motion of the perceived coherent pattern after integration is vertical despite the diagonal lines. On the other hand, for incoherent percepts the axis of motion of each object is diagonal.

A) Coherent and incoherent patterns of motion



B) Stimulus for axes of motion preference mapping

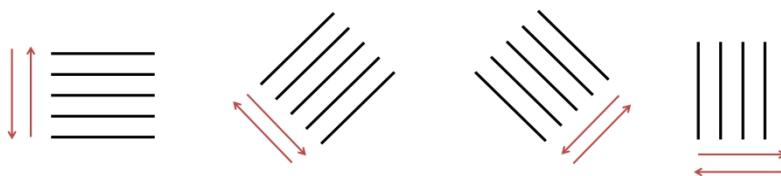


Figure 5.5. Correspondence between patterns of motion perceived during ambiguous stimulation and the studied axes of motion. The red arrows in the figure represent the motion direction. Due to the different axes of motion perceived during ambiguous stimulation (A) we asked whether a matched occurred between the functional domains with preference for each kind of percept and axes of motion preference (B).

The perceptual ROIs were defined based on the contrast between the hMT+/V5 responses to the incoherent and coherent percept. For each ROI were selected the significant

voxels of the contrast ($P < 0.05$) with preference for each percept. The ROIs were defined with equal size, which was determined by the percept recruiting the lower number of specific voxels.

The beta values of the evoked responses on each perceptual ROI (from each hemisphere and from each participant) according the moving simulation conditions on different axes of motion were extracted. A two-tailed t test was used to verify if there were significant differences in the responses of each perceptual ROI to the different stimulus conditions at the group level. Furthermore, we ran a mixed ANOVA in which the within-subjects factor was the type of moving condition (tuned for axis of motion identical to the coherent percept or tuned for axes corresponding to incoherent percept) and the between-subjects factor was the type of perceptual ROI (coherent or incoherent) to understand if there was an interaction between these two factors on the dependent variable (measured brain activity).

In order to validate our approach we performed the axes of motion preference mapping. The ROIs mapping voxels with different axes of motion preferences were defined using the winner maps tool from BV QX restricted to the defined hMT+/V5 ROI. Following previous studies that have reliably mapped axes of motion, we pooled responses with opposing directions (Zimmermann et al. 2011). First, a probabilistic map for each stimulus motion orientation (0° , 45° , 90° and 135°) was created using the contrast of each motion orientation versus baseline. Second, the maps were combined and the winner map was determined and finally, a ROI restricted to the localized hMT+/V5 region was defined per each orientation preference winner. The responses of each ROI to the different motion orientations were registered and the tuning curves of each functional domain represented by these ROIs were traced.

All analyzed beta values on offline processing of the data were extracted after correction for serial correlations performed according to a second-order autoregressive method (Lenoski et al. 2008). Furthermore, all averaged results are presented as mean \pm standard error of the mean (SEM).

5.3. Results

5.3.1. Behavioral analysis results

Concerning bistable perceptual dynamics, mean percept duration and the number of perceptual switches per participant during ambiguous stimulation are presented in figure

5.6. In general all participants showed a sufficiently large number of switches for analysis, the same holding true for perceptual durations, which were relatively balanced for each percept type.

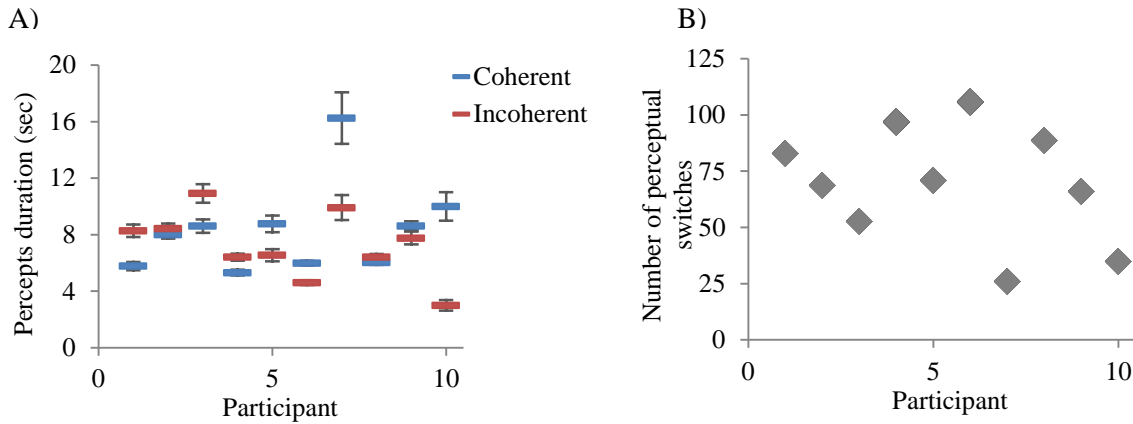


Figure 5.6. Percepts duration and number of perceptual switches during ambiguous stimulation per participant. The mean duration of the perceived coherent pattern of motion is represented by the blue rectangles and the mean duration of the perceived incoherent motion is represented by the red rectangles (A). Error bars represent \pm SEM. In (B) are plotted the number of perceptual switches reported per participant.

The mean group results are plotted in figure 5.7. During ambiguous stimulation participants perceived the coherent condition for 8.35 ± 1.01 seconds, on average, while the mean duration of the incoherent condition was 7.25 ± 0.75 seconds. Furthermore, 69.50 ± 7.50 perceptual switches per participant were found.

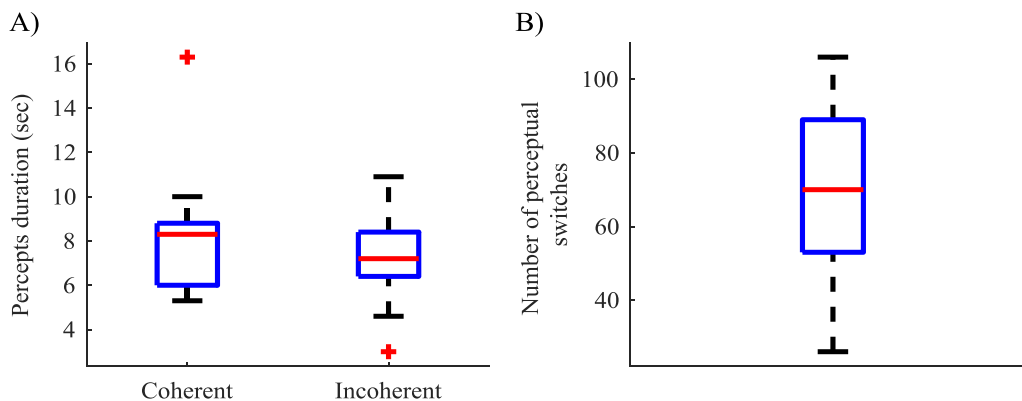


Figure 5.7. Group mean percepts duration and number of perceptual switches occurred on ambiguous stimulation. Each box presents the group mean duration of the perceived coherent pattern of motion and of the incoherent pattern of motion (A), and the average of perceptual switches occurred during ambiguous stimulation (B).

For each percept, the probability distribution of perceptual durations was estimated per participant and the gamma and lognormal distributions were fitted to the resulting histogram. In figure 5.8 is presented one example from one participant. For this particular example, both distributions fit similarly the percepts duration histogram (coherent motion

percept duration distribution (figure 5.8-A) and incoherent motion percept durations distribution (figure 5.8-B)).

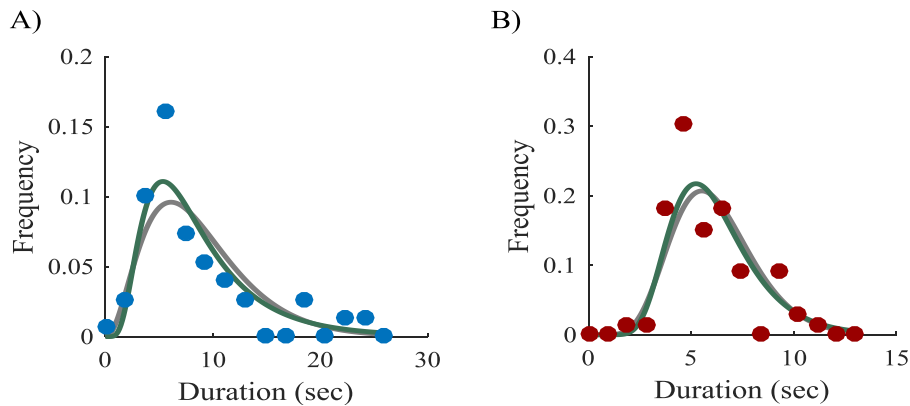


Figure 5.8. Data from one participant exemplifying the distribution of percepts durations during the ambiguous stimulation runs. The dots are representing the coherent (A) and incoherent (B) motion percepts duration histograms from one participant. The gray and green lines are illustrating the gamma and the lognormal distributions, respectively, fitted to the data.

In agreement with previous bistable perception studies (Borsellino et al. 1972; Zhou et al. 2004) the Kolmogorov-Smirnov test group results demonstrated no significant deviation between the fitted distributions and each percept duration histogram ($P > 0.05$). Additionally, both distributions fitted similarly the data and both percepts duration histograms.

According to the participants reports the unambiguous stimulus clearly produced unequivocal coherent or incoherent percepts following the pattern of motion of the background dots. Moreover, participants reported that the perceived patterns of motion were similar to the ones perceived during the ambiguous stimulation.

5.3.2. hMT+/V5 localization

The hMT+/V5 ROI definition by the localizer was the first imaging analysis step and the base of all subsequent steps. The contrast between the evoked brain activity during localizer stimulus conditions moving in different directions and the no-motion condition produced statistical maps with clear bilateral activations (figure 5.9, example from one participant). The defined ROIs included on average 512.89 ± 84.29 voxels from right hemisphere and 811.33 ± 102.45 voxels from left hemisphere.

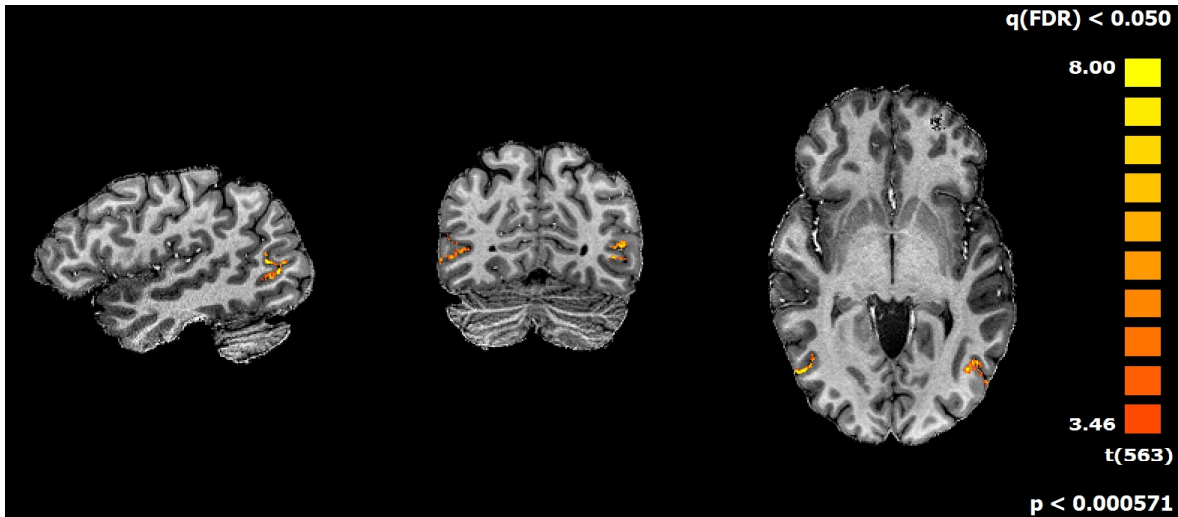


Figure 5.9. Example of bilateral hMT+/V5. Activation map resulting from the contrast between motion conditions and static condition during the localizer experiment. The hMT+/V5 left and right are shown at the same statistical threshold level (q (FDR) = 0.05).

5.3.3. Stimulus validation for axes of motion preference mapping

In order to verify if the used 1D component stimuli can be related to different axes of motion preferences, the hMT+/V5 evoked responses during the localizer moving stimulus were analyzed. As expected the hMT+/V5 voxels were differentially activated according the moving stimulus axis of motion. Therefore, the different motion orientations of the stimulus conditions allowed to map per participant functional hMT+/V5 sub-domains with specific preference for the diagonal, vertical or horizontal axis of motion. The defined ROIs included on average 54.89 ± 8.46 voxels from the right hemisphere and 95.11 ± 14.19 voxels. As illustrated on the tuning curves of figure 5.10 each mapped hMT+/V5 sub-domain responded significantly more to the stimulus moving with a preferred orientation than to the stimulus with other motion orientations ($P < 0.0001$, adjusted for multiple comparisons using Bonferroni correction).

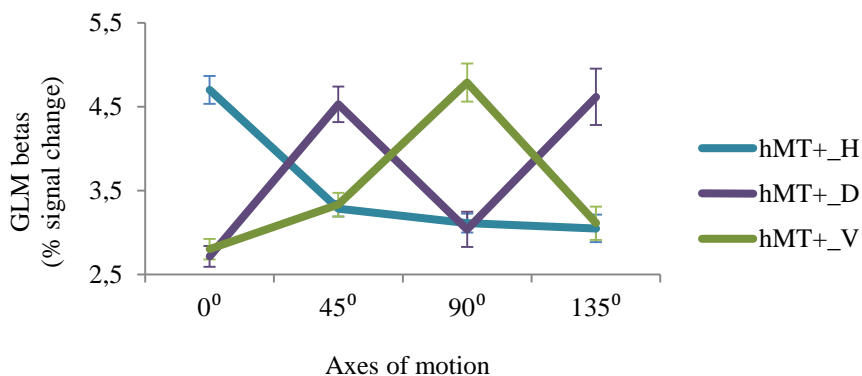


Figure 5.10. Tuning curves resulting from axes of motion preference mapping. Average response results of hMT+/V5 functional sub-domains (regions-of-interest - ROIs - represented by the lines) with different axes

of motion preference to stimulation conditions with different motion orientations (0 deg, 45 deg, 90 deg or 135deg). hMT+_H: ROIs with preference for horizontal motion; hMT+_D: ROIs with preference for diagonal motion; hMT+_V: ROIs with preference for vertical motion. Error bars represent \pm SEM.

5.3.4. Ambiguous and unambiguous imaging analysis results

During ambiguous and unambiguous stimulation both left and right hMT/V5 were recruited. The evoked responses were significantly higher ($P < 0.0001$, as revealed by mean of a t test) during the incoherent motion percept than during the coherent motion percept for both types of stimulation (figure 5.11). Accordingly, during ambiguous stimulation, the beta value of coherent percept evoked hMT+/V5 response was on average 2.71 ± 0.18 and the incoherent percept evoked a response of 3.48 ± 0.22 . Similarly, the unambiguous stimulation evoked hMT+/V5 response during the coherent motion was of 2.95 ± 0.14 and during the incoherent motion was 4.14 ± 0.25 .

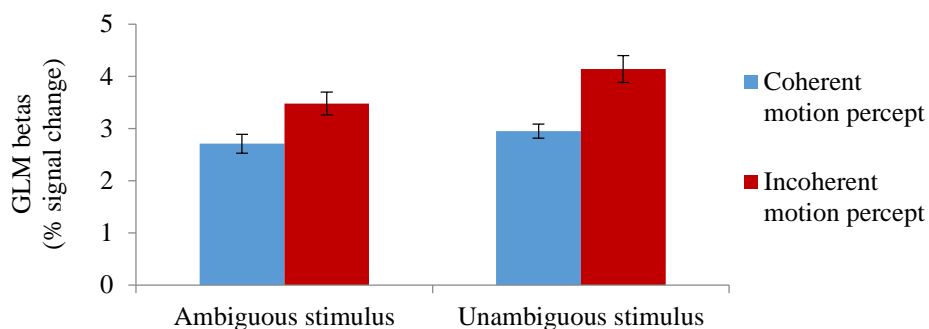


Figure 5.11. hMT+/V5 evoked activation during coherent and incoherent motion perception. Group average of general linear model (GLM) beta values of responses to each kind of percept during ambiguous and unambiguous stimulation at hMT+/V5. Error bars represent \pm SEM.

5.3.5. hMT+/V5 shows domains that are selective for the type of percept

We found that it is possible to identify hMT+/V5 domains that are selective for the type of percept. Such perceptually defined ROIs were found per participant and per hemisphere based on hMT+/V5 significantly activated voxels at $P \leq 0.05$ for the contrast between coherent and the incoherent motion percepts elicited by ambiguous stimuli.

The identified domains with preference for the coherent percept are now labelled as coherent perceptual ROIs and likewise for incoherent perceptual ROIs. The mean size of the perceptual ROIs from right and from left hemispheres was 17.67 ± 6.09 and 19.0 ± 4.19 , respectively. The clear perceptual preferences of the defined ROIs are depicted for visual purposes in figure 5.12.

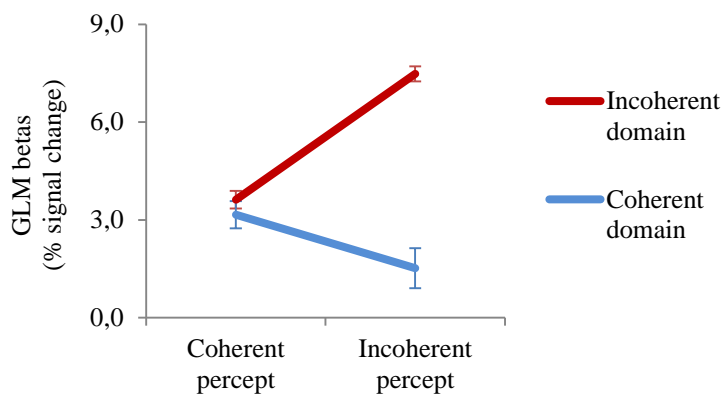


Figure 5.12. Perception related functional domains for the coherent and incoherent percepts. Group average of general linear model (GLM) beta values of evoked responses to each kind of percept (coherent or incoherent) during ambiguous stimulation are shown (for visualization purposes) in the discovered perception related hMT+/V5 functional sub-domains. Error bars represent \pm SEM.

We then tested whether the responses of the perception selective domains were tuned to axes of motion that matched each type of percept. One participant was excluded from this analysis due to excessive movement artifacts in the data. The responses of these domains were organized in two groups (figure 5.13): responses to the stimulus with axis of motion tuned for the coherent percept (moving along the vertical axis) and responses to the stimulus with axis of motion tuned for the incoherent percept (moving along diagonal axes).

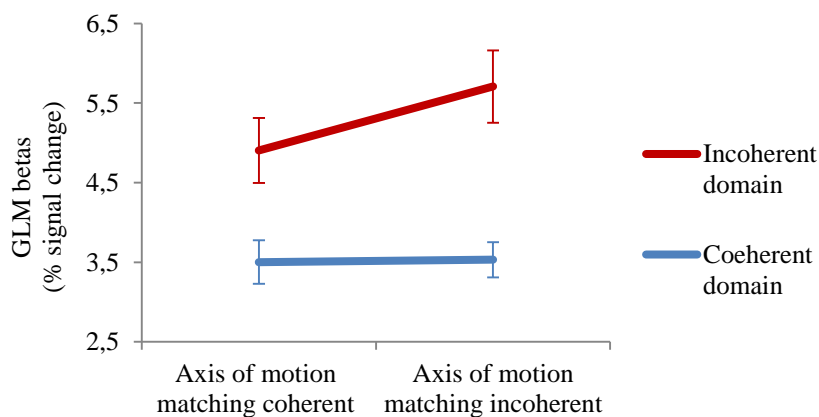


Figure 5.13. Responses of domains selective to perception type (coherent or incoherent). Group average of GLM beta values of perceptual ROIs responses to stimulus conditions moving on different orientations tuned for coherent or incoherent percept. The perceptual ROIs with preference for incoherent motion percept responded significantly more to the stimulus with motion orientation tuned for incoherent percept than to the stimulus with motion orientation tuned for coherent percept ($P = 0.009$). Error bars represent \pm SEM.

We found that the domains selective to incoherent perception showed responses that were on average significantly stronger for stimuli with axis of motion matching the incoherent percept (5.71 ± 0.46) than for stimuli with axis of motion matching the coherent percept (4.90 ± 0.41) (significant differences at $P = 0.009$, see ANOVA below). The

coherent perceptual ROIs responded similarly during both type of motion conditions (3.50 ± 0.27 for stimuli with axis of motion matching the coherent percept and 3.53 ± 0.22 for stimuli with axis of motion matching the incoherent percept, no significant differences).

We had hypothesized that the hMT+/V5 functional sub-domains with preference for one kind of percept (coherent or incoherent) during ambiguous stimulation (no physical changes on moving stimulus) would be differentially modulated by moving stimulus in different axes of motion (moving stimulus with real physical changes). A mixed way ANOVA revealed a significant interaction between the type of perceptual ROI (coherent or incoherent) and the stimulus motion orientation (tuned for coherent or incoherent percept) on the measured brain activity ($F(1, 34) = 5.64, P = 0.023$). This interaction can be appreciated in figure 5.13. Domains selective for the incoherent percept showed stronger activation for stimuli with axis of motion matching such incoherent percept, suggesting a clear interaction between percept type and motion tuning in these domains.

5.4. Discussion

Here we took advantage of high resolution fMRI to investigate if functional sub-domains related to perceptual content exist in hMT+/V5 and if they reflect preference for axes of motion matching the perception. To answer these questions we used a bistable perception paradigm, and assessed neural responses during ambiguous stimulation (yielding coherent motion or incoherent motion percept). A critical test to this hypothesis was whether an interaction between perception and axis of motion tuning could be found.

All these predictions were found to hold true. Moreover we also found that incoherent motion percept induced higher hMT+/V5 activity, on average, than the coherent motion percept, in line with previous findings (Castelo-Branco et al. 2002). The perception of incoherent motion involves two moving objects, whereas the perception of coherent motion involved only one moving object. Moreover, incoherent percepts may activate a larger number of component selective neurons (which respond to the 1D stimulus components). This notion is consistent with data showing that 40 % of the neurons in primate MT are component direction selective and only 25 % are pattern direction selective (Movshon et al. 1985). Therefore, perceiving incoherent motion may be associated with activation of a larger pool of neurons than perceiving coherent motion, and this could account for a higher BOLD signal.

It has been suggested that overall activity in the hMT+/V5 reflects global motion interpretation of perceptual bistability (Castelo-Branco et al. 2002). The current work goes a substantial step further by showing with high resolution fMRI that it is possible to identify hMT+/V5 functional sub-domains which activity is modulated according to the visual motion perception content. Our results show that the bistable perception is reflected not only at the global level of hMT+/V5 region but also at the level of perception related functional sub-domains. Importantly, these perceptual sub-domains presented different axes of motion preference. During the stimulation with different motion conditions the sub-domains selective for incoherent perception had also selective responses to axes of motion matching the incoherent percept. These results suggest that the tuning of the hMT+/V5 functional sub-domains is for the interpretation of the perceptually relevant motion features irrespective of real physical stimulation. This finding was corroborated by interaction analysis and found to be true in particular for sub-domains selective for incoherent percepts. Future studies should elucidate the reason for this asymmetry. A parsimonious explanation would be that only component neurons regions in the first stage of global motion computation are sensitive to perceptual modulation by feedback signals at the level of hMT+/V5.

The interaction found between the type of perceptual sub-domain and the axes of motion preference support the reports of previous studies that suggested quasi columnar-level neural correlates of perceptual switches in area hMT+/V5 (Goebel et al. 2014). Importantly, our findings show that the identified hMT+/V5 functional sub-domains related to bistable perception emerge even when 1D representations have to be bound/segregated inter-hemispherically.

The results of the present study greatly encourage the development of a new application for a multilevel neuromodulation approach using visual motion strategies. We hypothesize that the self-regulation of the functional connectivity between different hMT+/V5 perceptual sub-domains could allow to train our perception of external stimuli. Moving from the macroscopic level neuroimaging (3Tesla) to the mesoscopic level (7Tesla) might lead e.g. to more natural brain-computer interface systems.

5.5. Conclusion

We demonstrated that not only the transition of perceptual states but also the content of perception can be read-out directly from the activity patterns across perceptual sub-domains

in hMT+/V5 area. We found an interaction between the content of bistable perception of motion and the axes of motion preference within the identified perception related subdomains. Furthermore, our results showed that neural responses in hMT+/V5 functional sub-domains reflect perceptual interpretation of global motion matching local tuning and not strict physical stimulus properties.

References

- Adelson, E.H. & Movshon, J. a., 1982. Phenomenal coherence of moving visual patterns. *Nature*, 300(5892), pp.523–525.
- Andersson, J.L.R., Skare, S. & Ashburner, J., 2003. How to correct susceptibility distortions in spin-echo echo-planar images: Application to diffusion tensor imaging. *NeuroImage*, 20(2), pp.870–888.
- Blake, R., Brascamp, J. & Heeger, D.J., 2014. Can binocular rivalry reveal neural correlates of consciousness? *Philosophical transactions of the Royal Society of London. Series B, Biological sciences*, 369(1641), p.20130211..
- Blake, R. & Logothetis, N.K., 2002. Visual competition. *Nature reviews. Neuroscience*, 3(1), pp.13–21.
- Borsellino, A. et al., 1972. Reversal time distribution in the perception of visual ambiguous stimuli. *Kybernetik*, 10(3), pp.139–144.
- Brainard, D.H., 1997. The Psychophysics Toolbox. *Spatial vision*, 10(4), pp.433–436.
- Burke, D., Alais, D. & Wenderoth, P., 1994. A Role for a low level mechanism in determining plaid coherence. *Vision Research*, 34(23).
- Castelo-Branco, M. et al., 2002. Activity patterns in human motion-sensitive areas depend on the interpretation of global motion. *Proceedings of the National Academy of Sciences of the United States of America*, 99(21), pp.13914–13919.
- Castelo-Branco, M. et al., 2000. Neural synchrony correlates with surface segregation rules. *Nature*, 405, pp.685–689.
- Castelo-Branco, M. et al., 2009. Type of featural attention differentially modulates hMT+ responses to illusory motion aftereffects. *Journal of neurophysiology*, 102(5), pp.3016–3025.
- Cheng, K., Waggoner, R. a & Tanaka, K., 2001. Human ocular dominance columns as revealed by high-field functional magnetic resonance imaging. *Neuron*, 32(2), pp.359–374.
- Crick, F. & Koch, C., 1998. Feature Article Consciousness and Neuroscience. *Cerebral Cortex*, 8(2), pp.97–107.
- Emmerling, T. et al., 2015. Decoding the direction of imagined visual motion using 7T ultra-high field fMRI. *NeuroImage*, 125, pp.61–73..
- Friston, K.J. et al., 1998. Nonlinear event-related responses in fMRI. *Magnetic Resonance in Medicine*, 39(1), pp.41–52.
- Goebel, R. et al., 2014. Revealing columnar level neural correlates of perceptual switches in area hMT using fMRI at 7 Tesla. In *Society For Neuroscience (SfN) Annual meeting*.
- Goebel, R., Esposito, F. & Formisano, E., 2006. Analysis of Functional Image Analysis Contest (FIAC) data with BrainVoyager QX: From single-subject to cortically aligned group General Linear Model analysis and self-organizing group Independent Component Analysis. *Human Brain Mapping*, 27(5), pp.392–401.
- Hou, Z. et al., 2006. A fast and automatic method to correct intensity inhomogeneity in MR brain images. *Medical image computing and computer-assisted intervention : MICCAI ... International Conference on Medical Image Computing and Computer-Assisted Intervention*, 9(Pt 2), pp.324–31.
- Huk, A.C. & Heeger, D.J., 2002. Pattern-motion responses in human visual cortex. *Nature neuroscience*, 5(1), pp.72–75.
- Kolster, H., Peeters, R. & Orban, G.A., 2010. The retinotopic organization of the human middle temporal area MT/V5 and its cortical neighbors. *The Journal of neuroscience : the official journal of the Society for Neuroscience*, 30(29), pp.9801–9820.
- Kornmeier, J. & Bach, M., 2012. Ambiguous figures - what happens in the brain when perception changes but not the stimulus. *Frontiers in human neuroscience*, 6(March), p.51
- Kornmeier, J., Hein, C.M. & Bach, M., 2009. Multistable perception: When bottom-up and top-down coincide. *Brain and Cognition*, 69(1), pp.138–147.
- Kozak, L.R. & Castelo-Branco, M., 2009. Peripheral influences on motion integration in foveal vision are modulated by central local ambiguity and center-surround congruence. *Investigative Ophthalmology and Visual Science*, 50(2), pp.980–988.
- Kutner, M.H. et al., 1996. *Applied Linear Statistical Models*,
- Lenoski, B. et al., 2008. On the performance of autocorrelation estimation algorithms for fMRI analysis. *IEEE Journal on Selected Topics in Signal Processing*, 2(6), pp.828–838.
- Leopold, D.A. & Logothetis, N.K., 1999. Multistable phenomena: Changing views in perception. *Trends in Cognitive Sciences*, 3(7), pp.254–264.
- Long, G.M. & Toppino, T.C., 2004. Enduring interest in perceptual ambiguity: alternating views of reversible figures. *Psychological bulletin*, 130(5), p.748.
- Menon, R.S. et al., 1997. Ocular dominance in human V1 demonstrated by functional magnetic resonance

- imaging. *Journal of Neurophysiology*, 77(5), pp.2780–2787.
- Van de Moortele, P.-F. et al., 2009. T1 weighted brain images at 7 Tesla unbiased for Proton Density, T2* contrast and RF coil receive B1 sensitivity with simultaneous vessel visualization. *NeuroImage*, 46(2), pp.432–46.
- Movshon, J. et al., 1985. The analysis of moving visual patterns. *Pattern Recognition Mechanisms*, pp.117–151.
- Pelli, D.G., 1997. The VideoToolbox software for visual psychophysics: transforming numbers into movies. *Spatial Vision*, 10(4), pp.437–442.
- Pomerantz, J.R. & Kubovy, M., 1981. Perceptual organization: An overview. In *Perceptual Organization*. pp. 423–456.
- Shmuel, A. et al., 2007. Spatio-temporal point-spread function of fMRI signal in human gray matter at 7 Tesla. *NeuroImage*, 35(2), pp.539–552.
- Sled, J., Zijdenbos, a & Evans, a C., 1997. A comparison of retrospective intensity non-uniformity correction methods for MRI. In *Information Processing in Medical Imaging*, pp.459–464.
- Talairach, J. & Tournoux, P., 1988. *Co-Planar Stereotaxis Atlas of the Human Brain*,
- Tootell, R.B. et al., 1995. Functional analysis of human MT and related visual cortical areas using magnetic resonance imaging. *Journal of Neuroscience*, 15(4), pp.3215–3230.
- Uğurbil, K. et al., 2003. Ultrahigh field magnetic resonance imaging and spectroscopy. *Magnetic Resonance Imaging*, 21(10), pp.1263–1281. Available at: <http://www.scopus.com/inward/record.url?eid=2-s2.0-10744228692&partnerID=40&md5=9e396455b382979b6ef5be05e621f148>.
- Uludağ, K., Müller-Bierl, B. & Uğurbil, K., 2009. An integrative model for neuronal activity-induced signal changes for gradient and spin echo functional imaging. *NeuroImage*, 48(1), pp.150–165.
- Vaughan, J.T. et al., 2001. 7T vs. 4T: RF power, homogeneity, and signal-to-noise comparison in head images. *Magnetic Resonance in Medicine*, 46(1), pp.24–30.
- Wallach, H., 1935. Über visuell wahrgenommene Bewegungsrichtung. *Psychologische Forschung*, (20), pp.325–380.
- Wuerger, S., Shapley, R. & Rubin, N., 1996. “On the visually perceived direction of motion” by Hans Wallach: 60 years later. *Perception*, 25(11), pp.1317–1367.
- Yacoub, E. et al., 2007. Robust detection of ocular dominance columns in humans using Hahn Spin Echo BOLD functional MRI at 7 Tesla. *NeuroImage*, 37(4), pp.1161–1177.
- Yacoub, E., Harel, N. & Ugurbil, K., 2008. High-field fMRI unveils orientation columns in humans. *Proceedings of the National Academy of Sciences of the United States of America*, 105(30), pp.10607–12..
- Zeki, S.M., 1974. Cells responding to changing image size and disparity in the cortex of the rhesus monkey. *The Journal of physiology*, 242(3), pp.827–41..
- Zhou, Y.H. et al., 2004. Perceptual dominance time distributions in multistable visual perception. *Biological Cybernetics*, 90(4), pp.256–263.
- Zimmermann, J. et al., 2011. Mapping the organization of axis of motion selective features in human area mt using high-field fmri. *PLoS ONE*, 6(12), pp.1–10.

APPENDIX

Chapter 5

A1. Experimental design

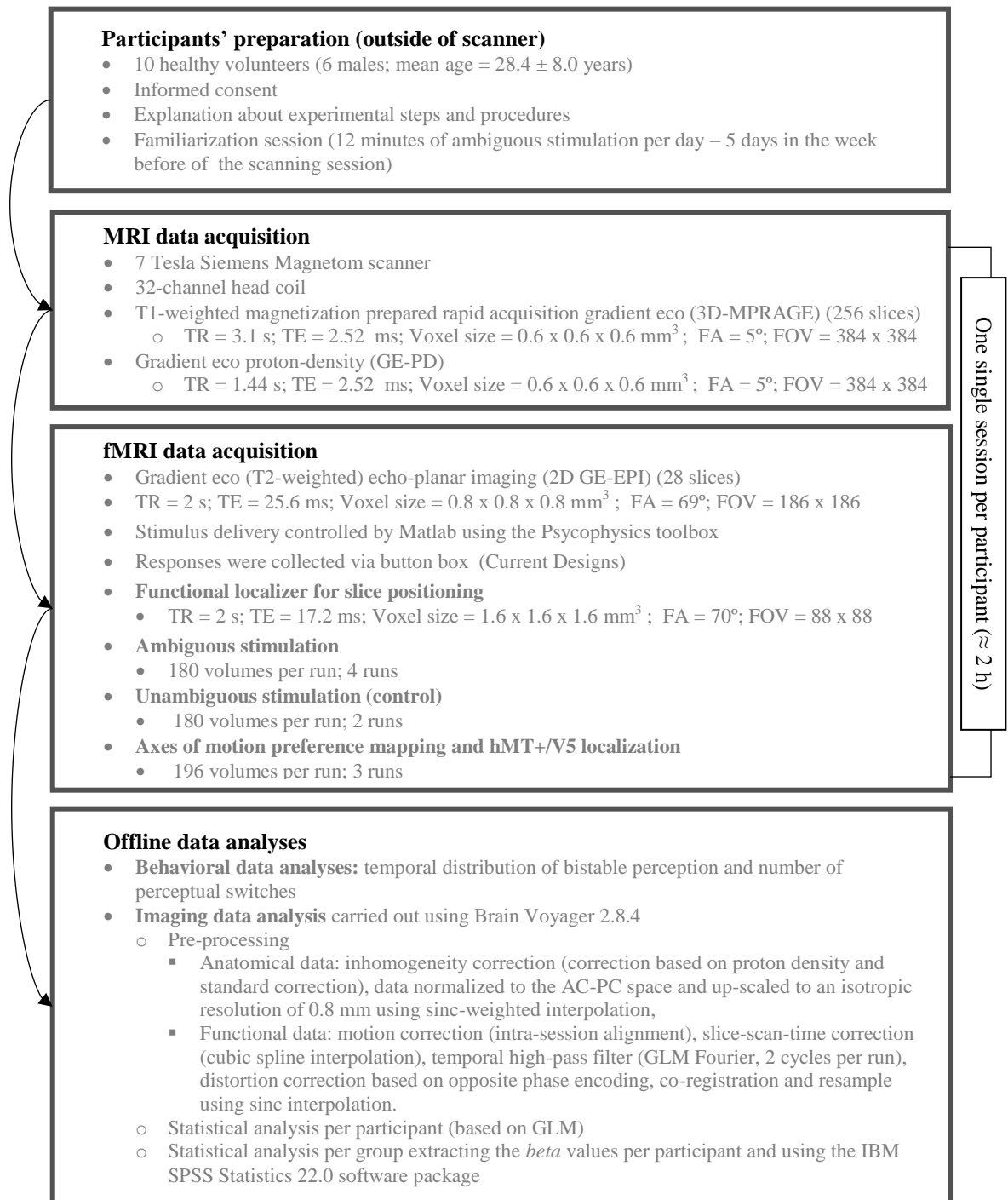


Figure 5.A1. Summary of the main steps of the experimental procedure followed in the study. Each participant took part of a familiarization session with the ambiguous stimulus during the week before the fMRI acquisition session. The hMT+/V5 sub-domains preferring each type of motion percept during the ambiguous stimulation were mapped and their response to different axes-of-motion was compared. The functional data were acquired using the 7T fMRI and offline analyzed using a general linear model (GLM) approach to assess the functional activation patterns. *fMRI* – functional magnetic resonance imaging, *TR* – repetition time, *FA* – flip angle, *TE* – echo time, *FOV* – field of view.

CHAPTER 6

GENERAL DISCUSSION AND CONCLUSIONS

6.1. General discussion

Current neuroimaging technology offers the opportunity to non-invasively investigate detailed brain anatomy and structural connectivity, but more importantly, to also monitor brain function in real-time, beyond simple localization. If a subject can observe in real-time his own brain activity, he may potential learn how to control it. Based on this concept, the neurofeedback (NF) training comes up as an alternative to the currently used methods (neurosurgery, pharmacology and psychotherapy) to change brain function (Thibault et al. 2016). As we form thoughts they generate distributed patterns of brain activity and complex functional interactions in our brain, between identifiable regions. Thus, the training of brain activity self-regulation with NF approaches is based on mental strategies to voluntarily increase (up-regulate) or decrease (down-regulate) specific brain activity either from a single region or a network of areas. In this thesis we present some proof-of-concept studies suggesting possible advances volitional brain activity control. Based on visual motion imagery strategies we explored the hypothesis of volitional parametric/multilevel control of brain activity.

There are many different paradigms that might endow the brain with the power to control an external device through a brain-computer interface (BCI) (McFarland & Wolpaw 2011; Shih et al. 2012; Wolpaw et al. 2002). We explored approaches that are active, i.e. that require the engagement of the subject in controlling a device, and where the subject controlling the device develops a sense of agency, i.e. knowledge or awareness that he is controlling. The visual motion imagery was chosen to take advantage of the specific recruitment of hMT+/V5 brain region during the visualization or imagery of moving stimuli (Goebel et al. 1998; Tootell et al. 1995). Thus, we were able ensure that the measured activity during the performed mental tasks was due to specific imagery processes. Furthermore, contrarily to for example motor imagery, a commonly used strategy to self-regulation of brain activity, visual motion imagery is still a non-explored strategy to volitional brain activity control (Ruiz et al. 2014; Thibault et al. 2016).

Although it has been demonstrated that focusing on default-mode network (DMN) may yield powerful NF approaches (Harmelech et al. 2015), we opted for an early visual area because of our interest in NF potential to clinical applications, as the attentional disorders

ADHD and Neurofibromatosis type 1, in which a ‘failure to deactivate the DMN’ has been postulated (Violante et al. 2012). We defend that ‘BCI-eligibility’ might not only depend on ‘learning’ abilities but also on the particular clinical condition to be treated. Thus, the research work presented on this thesis can contribute to the debate on the relative potential of sensory versus DMN brain regions in the clinical application of NF paradigms.

We started with studies based on functional magnetic resonance imaging (fMRI) data and then we probed similar paradigms using electroencephalography (EEG) in order to try the “real-life transfer” of the proposed brain activity control approach. An EEG-based BCI approach is desirable due its low-cost and portability (Huster et al. 2014). However, EEG offers only a low spatial resolution and ambiguous localization of neural activity, since underlying electric sources need to be reconstructed from the distribution of electric potentials across the scalp (Niedermeyer & Lopes Da Silva 2005). Therefore, fMRI studies are helpful to effectively map and understand the underlying brain functions. The technical progresses in real-time fMRI allowed to observe the ongoing brain activity while a subject is scanned and select specific brain regions for NF due to its high spatial resolution (Weiskopf et al. 2007) and may enable a subject to learn greater explicit control over his/her own cognitive and neural activities by self-regulation of desired brain states (DeCharms 2007; Weiskopf 2012).

In the first step of the developed research work, presented on chapter 2, we trained healthy participants to achieve self-driven hMT+/V5 activity modulation using fMRI-based NF. In our first experiment, two levels of brain activity control based on self-regulation strategies were tested and successfully achieved by seventy five percent of our participants (15/20 participants). We show that the hMT+/V5 activity up-regulation is possible through visual imagery of a moving dot and the down-regulation is possible based on visual imagery of a static dot. These strategies allowed reliable self-regulation of the target area already during the first two NF runs in most participants, demonstrating that hMT+/V5 is at least as effective as other brain regions used as targets of NF approaches, as for example the somatomotor cortex (DeCharms et al. 2004) and amygdala (Zotев et al. 2011). Furthermore, our results converges with the previous report of effective hMT+/V5 activation with visual motion imagery (Goebel et al. 1998) and corroborate the possibility of a single-day training with fMRI-based NF training to be enough to achieve learning (Caria et al. 2007; DeCharms et al. 2005; Weiskopf et al. 2004).

Although, the few previous studies that have targeted the visual cortex for NF training encompassed several early visual areas (Scharnowski et al. 2012; Shibata et al. 2011), we proposed a brain activity self-regulation approach focused on a single ROI functionally defined. By this way, all participants are forced to the use of a similar mental strategy. Focused visual motion imagery showed to be relatively simple to learn and to instruct in a generalized way. Thus, we suggest that the single ROI choice can be an advantage and potentially renders group effects more homogeneous.

A specific neural circuitry was found to be involved in successful hMT+/V5 neuromodulation, which includes regions known to contribute to visual motion perception and imagery (putative V6, putamen, cerebellum and hMT+/V5), attention (striatum) (DeBettencourt et al. 2015) and to decision making, such as the anterior insula (Rebola et al. 2012). These results may indicate that this whole circuit might be used as a target for future NF studies based on functional connectivity. The use of functional connectivity based NF instead of the more classical region based approach may be advantageous. Kim et al. (2015) recently demonstrated that NF training based on functional connectivity facilitates greater volitional control over brain activity and greater modulation of mental function than NF training based on simple measures of brain activity. Importantly, the analysis of the core circuit found to be involved in visual motion imagery based NF contributed for a better understanding of the neural correlates of cognitive processes, establishing, for example, for the first time a direct functional link between the hMT+/V5 and the cerebellum.

After we have shown that operant control over brain activity can be achieved using visual motion imagery, in a subsequent experiment we attempted to train subjects to go beyond binary control using three different visual motion imagery strategies. This research work, presented in chapter 3, took advantage of differential evoked brain responses according to the number of imagined motion alternations. In human visual cortex frequent motion or orientation changes lead to break in adaptation and increased fMRI responses (Tootell et al. 1998). Furthermore, the different number of motion alternations may lead to distinct levels of attentional modulation which in turn impact on activity levels. We show that using three mental strategies consisting on visual imagery of a static point, motion in opposing directions and motion in four alternating directions is possible to achieve up to three distinct levels of hMT+/V5 activity self-regulation. Our approach was inspired by literature addressing the physiological basis of visual motion processing: the visual stimulus with the

higher rate of motion alternation evoked stronger brain activations than the stimulus with less motion alternation (Huk & Heeger 2002; Larsson et al. 2006).

We also found evidence that the provided feedback contributed for successful neuromodulation and learning during NF training. The three modulation levels were only achieved during NF training or after it. Furthermore, we suggest that multilevel neuromodulation may require a higher level of focused attention and training than the binary case, but future studies beyond proof-of-concept should establish whether training can stabilize NF performance and how many sessions would be necessary. Moreover, it is important to point out that the ability to learn NF strategies is known to be variable in the population (learners versus non-learners) (Coben & Evans 2010; Enriquez-Geppert et al. 2013; Neumann & Birbaumer 2003; Wan et al. 2014).

The new brain activity self-regulation approach presented on this thesis provides a simple way to achieve up to three control levels with simple instructions and can be efficiently used by different subjects, which is of potential interest for future assistive BCI systems and also for NF applications. Our approach can be useful to dampen the variability due to ROI and subject-by-subject strategy definition and to allow more effective neuromodulation training or at least improved BCI control. Our work present a novel contribution to operant BCI control because for our best knowledge, although the parametric/multilevel neuromodulation has been suggested (Goebel et al. 2004; Sorger et al. 2004; Sorger 2010), this is the first report in the literature demonstrating that multilevel neuromodulation based on the same brain region and using the same strategy across participants is feasible. The previous studies that report more than two classes of control using BOLD signal self-regulation attempted mainly to achieve multiple classes and not multilevels of the same class of control (Lee et al. 2009; Sorger et al. 2012; Yoo et al. 2004).

In a follow-up part of the research work presented in this thesis (chapter 4) we investigated the EEG activity patterns induced by the three visual stimulation and imagery tasks with different number of motion alternations previously studied with fMRI. We attempted to transfer the proposed new methodology of brain activity self-regulation from the fMRI basis to EEG.

We found different functional forms of alpha activity for evoked brain responses by visual motion stimulation and visual motion imagery. A decrease of alpha activity on the parieto-occipital channels was found during visual stimulation with moving stimuli and an increase of alpha activity on the fronto-central channels was found during visual motion

imagery. The occipital alpha decrease during visual stimulation reflects a functional mechanism by which information is selected or gated in visual cortex (Foxe & Snyder 2011; Klimesch et al. 2011; Klimesch 2012; Schomer & Lopes Da Silva 2011). The functional state where frontal alpha oscillations are dominant reflects a state of reduced external information processing that is referred as a ‘modulation gate’ (Klimesch et al. 2007; Schomer & Lopes Da Silva 2011). It has been reported during high internal processing demands as top-down processing and working memory (Benedek et al. 2011; Sauseng et al. 2005) and processes requiring imagination of stimulus sequences (Cooper et al. 2003). EEG studies using non-visual imagery modulation strategies, as mental calculation, reported also increase of frontal delta and theta rhythms related to neural processes associated with the frontal lobe role in memory and cognitive challenges (Harmony et al. 1999; Harmony et al. 2004). In any case, we found a frontal activation pattern possibly evoked by brain functions under memory and planning processes subjacent to imagery.

The spectral power of alpha activity seems to reflect the complexity of the imagined visual motion. As previous studies described that mean frontal alpha amplitudes are enhanced for more complex tasks (Cooper et al. 2003), we suggest that the differences found between the different visual motion imagery tasks results on the frontal alpha activity, can be related with the process of recovering the different visualized motion sequence conditions. Although a more classical statistical approach could not discern between the motion imagery tasks with different number of alternations, the applied classification algorithm performed a successful distinction between all visual motion imagery strategies supporting the advantage of multivariate data analysis approaches (Lemm et al. 2011). Based on the high classification accuracy achieved, we propose the visual motion imagery as a simple strategy to BCI multiclass control. However, real-time tests need to be carried on to confirm this proof-of-concept result.

The volitional multilevel neuromodulation was not achieved in the EEG study, only 3 different classes not linearly related, but it is important to point out that we were only using passive imagery. The participants did not have the opportunity to be aware of their brain activations. We were still searching for the evoked brain activity patterns by the different visual motion imagery strategies.

Recent advances in magnetic resonance imaging technology allow recording fMRI signals with sub-millimeter spatial resolution (Harel 2012), offering the opportunity to go into the mesoscopic level of the hMT+/V5 functional organization (Emmerling et al. 2015;

Zimmermann et al. 2011). Taking advantage of high-resolution fMRI we investigated hMT+/V5 functional sub-domains related to perception of different patterns of motion. This study, described in chapter 5, gave us a detailed functional account of the brain region that we have been targeting during the NF training, which might potentially contribute for the development of new research works focused on neural correlates of perceptual decision making and cognitive control. We aimed to evaluate the possibility of a new multilevel neuromodulation approach based on the connectivity between the functional hMT+/V5 region sub-domains to train visual motion perception, specifically in cases of ambiguous moving stimuli. In short, if participants can influence their own perceptual decision making, this would allow for a novel form of NF.

Using 7 Tesla (7T) fMRI and a bistable perception paradigm we assessed to the hMT+/V5 activity during ambiguous stimulation (yielding coherent motion or incoherent motion percepts). In line with previous findings (Castelo-Branco et al. 2002) we found higher hMT+/V5 activity during the perception of incoherent motion, than during the perception of coherent motion. When a participant reported the incoherent motion pattern, he was perceiving two moving objects/surfaces, whereas during the coherent motion he was perceiving only one moving object, which can explain the differences on hMT+/V5 responses during the ambiguous stimulation: the higher number of perceived moving surfaces evokes stronger responses. These differential hMT+/V5 responses can be also related with the types of neurons contributing for its activity. It is described in the literature that 40% of the neurons in primate MT (the equivalent to the human hMT+/V5 region) are component direction selective and only 25 % are pattern direction selective (Movshon et al. 1985). Thus, due to the two 1D motion objects the component neurons should be mainly active during the perception of incoherent motion (in addition to the 2 pattern populations responding to the inwardly moving surfaces) and then a larger pool of hMT+/V5 neurons are recruited leading to higher activations.

The 7T fMRI allowed to identify hMT+/V5 functional sub-domains which activity is modulated according to the visual motion perception content. We demonstrate that the motion perception is reflected not only at the global level of hMT+/V5 region (Castelo-Branco et al. 2002) but also at the level of perception related functional sub-domains. Furthermore, the hMT+/V5 functional sub-domains presented different axes of motion preference, which allowed to verify that the tuning of these sub-domains is for the interpretation of the perceptually relevant motion features irrespective of real physical

stimulation. Our results support the reports of previous studies that suggested quasi columnar-level neural correlates of perceptual switches in area hMT+/V5 (Goebel et al. 2014).

The finding that activity levels in hMT+/V5 region depend on the perceptual interpretation paves the way for the design of NF paradigms based on perception decision dependent activity or connectivity modulation down to the quasi-columnar level, which should be followed up in future studies.

6.2. Conclusions

BCI research features a rapidly developing area that benefits from research on the basic cognitive neuroscience in a cross-fertilizing dialogue. The research work presented in this thesis, focusing on multilevel brain activity control, provides the basis for future projects aiming more direct and flexible assistive BCI systems and more precise NF approaches. The developed studies focused on mental strategies to multilevel self-regulation of brain activity that were successful in particular for fMRI. Visual motion imagery was proposed as a new mental strategy for BCI control. fMRI experiments consisting of visual imagery of a static point, constant motion and alternate motion showed the possibility of a multilevel discrimination in the visual cortex and, EEG only for multiclass non-level dependent control. These findings suggest the feasibility of visual motion imagery for multiclass EEG-based BCI control and for multilevel fMRI-based NF.

First, we showed that the volitional binary control of hMT+/V5 is possible and simple to learn when using the fMRI-based NF to train its brain activity up-regulation and down-regulation with visual motion imagery strategies. The comparison between successful and non-successful NF training on hMT+/V5 modulation allowed for the identification of a specific neural circuit involved in visual motion imagery and perceptual stabilization, recruited only during the successful runs. We suggest this circuit as a potential target for NF training applied to attentional disorders where a boost of activity of the already hyperactive DMN is undesirable.

The proof-of-concept of volitional control of hMT+/V5 using visual motion imagery strategies was the basis for a more detailed study that aimed to explore the potential of these kind of mental tasks to achieve volitional multilevel neuromodulation. Three levels of volitional control of hMT+/V5 visual area by using real-time fMRI training were achieved. As in visual motion stimulation, in imagery, different number of motion alternations led to distinct levels of hMT+/V5 activity. We demonstrated that using the same imagery strategy across participants is possible to achieve up to three levels of volitional control of hMT+/V5, which is of potential interest to implement in multilevel BCI and/or NF approaches.

The attempt to transfer the proposed new methodology of brain activity self-regulation from the fMRI basis to EEG showed that using the same visual motion imagery strategies than in the fMRI study is possible to achieve up to three classes of volitional EEG activity, but not in a multilevel way. The pattern of power changes of frontal alpha activity varied depending on the number of imagined visual motion alternations. However, these differences were only distinguishable by means of a classifier. Although we were not able to achieve different levels EEG activity neuromodulation, we show that the proposed visual motion imagery strategies evoke different patterns of brain activity with potential of discrimination. A 3-class classifier was learned using only a few channels and achieved high classification accuracy, showing the potential of the proposed strategies of brain activity control in BCI research. Furthermore, we suggest that the proposed imagery strategies have the potential to evoke different levels of EEG brain activity when trained via EEG-based NF.

Finally, taking advantage of high-resolution 7T fMRI, we demonstrated that the hMT+/V5 is composed by perceptual sub-domains, whose neural responses reflect perceptual interpretation of motion matching local tuning and not strict physical stimulus properties. These findings support our future goal of use NF to train visual motion perception, based on participant driven, by self-controlled perceptual decision, modulation of activity.

References

- Benedek, M. et al., 2011. EEG alpha synchronization is related to top-down processing in convergent and divergent thinking. *Neuropsychologia*, 49(12), pp.3505–3511.
- Caria, A. et al., 2007. Regulation of anterior insular cortex activity using real-time fMRI. *NeuroImage*, 35(3), pp.1238–1246.
- Castelo-Branco, M. et al., 2002. Activity patterns in human motion-sensitive areas depend on the interpretation of global motion. *Proceedings of the National Academy of Sciences of the United States of America*, 99(21), pp.13914–13919.
- Coben, R. & Evans, J.R., 2010. *Neurofeedback and Neuromodulation Techniques and Applications*, Academic Press.
- Cooper, N.R. et al., 2003. Paradox lost? Exploring the role of alpha oscillations during externally vs. internally directed attention and the implications for idling and inhibition hypotheses. *International Journal of Psychophysiology*, 47, pp.65–74.
- DeBettencourt, M.T. et al., 2015. Closed-loop training of attention with real-time brain imaging. *Nature Neuroscience*, 18(3), pp.1–9.
- DeCharms, R.C. et al., 2005. Control over brain activation and pain learned by using real-time functional MRI. *Proceedings of the National Academy of Sciences of the United States of America*, 102(51), pp.18626–31.
- DeCharms, R.C. et al., 2004. Learned regulation of spatially localized brain activation using real-time fMRI. *NeuroImage*, 21(1), pp.436–443.
- deCharms, R.C., 2007. Reading and controlling human brain activation using real-time functional magnetic resonance imaging. *Trends in cognitive sciences*, 11(11), pp.473–481.
- Emmerling, T. et al., 2015. Decoding the direction of imagined visual motion using 7T ultra-high field fMRI. *NeuroImage*, 125, pp.61–73.
- Enriquez-Geppert, S. et al., 2013. The morphology of midcingulate cortex predicts frontal-midline theta neurofeedback success. *Frontiers in Human Neuroscience*, 7, p.453.
- Foxe, J.J. & Snyder, A.C., 2011. The role of alpha-band brain oscillations as a sensory suppression mechanism during selective attention. *Frontiers in Psychology*, 2(JUL).
- Goebel, R. et al., 2004. BOLD brain pong: self-regulation of local brain activity during synchronously scanned, interacting subjects. In *Society for Neuroscience, Washington, DC*.
- Goebel, R. et al., 2014. Revealing columnar level neural correlates of perceptual switches in area hMT using fMRI at 7 Tesla. In *Society For Neuroscience (SfN) Annual meeting*.
- Goebel, R. et al., 1998. The constructive nature of vision: Direct evidence from functional magnetic resonance imaging studies of apparent motion and motion imagery. *European Journal of Neuroscience*, 10(5), pp.1563–1573.
- Harel, N., 2012. Ultra high resolution fMRI at ultra-high field. *NeuroImage*, 62(2), pp.1024–1028.
- Harmelech, T., Friedman, D. & Malach, R., 2015. Differential Magnetic Resonance Neurofeedback Modulations across Extrinsic (Visual) and Intrinsic (Default-Mode) Nodes of the Human Cortex. *Journal of Neuroscience*, 35(6), pp.2588–2595.
- Harmony, T. et al., 1999. Do specific EEG frequencies indicate different processes during mental calculation? *Neuroscience Letters*, 266(1), pp.25–28.
- Harmony, T. et al., 2004. Specific EEG frequencies signal general common cognitive processes as well as specific task processes in man. *International Journal of Psychophysiology*, 53(3), pp.207–216.
- Huk, A.C. & Heeger, D.J., 2002. Pattern-motion responses in human visual cortex. *Nature Neuroscience*, 5(1), pp.72–75.
- Huster, R. et al., 2014. Brain-computer interfaces for EEG neurofeedback: Peculiarities and solutions. *International Journal of Psychophysiology*, 91(1), pp.36–45.
- Kim, D.-Y. et al., 2015. The Inclusion of Functional Connectivity Information into fMRI-based Neurofeedback Improves Its Efficacy in the Reduction of Cigarette Cravings. *Journal of Cognitive Neuroscience*, 27(8), pp.1552–1572.
- Klimesch, W., 2012. Alpha-band oscillations, attention, and controlled access to stored information. *Trends in Cognitive Sciences*, 16(12), pp.606–617.
- Klimesch, W., Fellinger, R. & Freunberger, R., 2011. Alpha oscillations and early stages of visual encoding. *Frontiers in Psychology*, 2(MAY).
- Klimesch, W., Sauseng, P. & Hanslmayr, S., 2007. EEG alpha oscillations: The inhibition-timing hypothesis. *Brain Research Reviews*, 53(1), pp.63–88.
- Larsson, J., Landy, M.S. & Heeger, D.J., 2006. Orientation-selective adaptation to first-and second-order patterns in human visual cortex. *Journal of Neurophysiology*, 95, pp.862–881.

- Lee, J.H. et al., 2009. Brain-machine interface via real-time fMRI: Preliminary study on thought-controlled robotic arm. *Neuroscience Letters*, 450(1), pp.1–6.
- Lemm, S. et al., 2011. Introduction to machine learning for brain imaging. *NeuroImage*, 56(2), pp.387–399.
- McFarland, D.J. & Wolpaw, J.R., 2011. Brain-Computer Interfaces for Communication and Control. *Communications of the ACM*, 54(5), pp.60–66.
- Movshon, J. et al., 1985. The analysis of moving visual patterns. *Pattern Recognition Mechanisms*, pp.117–151.
- Neumann, N. & Birbaumer, N., 2003. Predictors of successful self control during brain-computer communication. *J Neurol Neurosurg Psychiatry*, 74, pp.1117–1121.
- Niedermeyer, E. & Lopes Da Silva, F., 2005. *Electroencephalography: Basic Principles, Clinical Applications, and Related Fields* 5th Ed., Lippincott Williams and Wilkins.
- Rebola, J. et al., 2012. Functional parcellation of the operculo-insular cortex in perceptual decision making: An fMRI study. *Neuropsychologia*, 50(14), pp.3693–3701.
- Ruiz, S. et al., 2014. Real-time fMRI brain computer interfaces: Self-regulation of single brain regions to networks. *Biological Psychology*, 95(1), pp.4–20.
- Sauseng, P. et al., 2005. EEG alpha synchronization and functional coupling during top-down processing in a working memory task. *Human Brain Mapping*, 26(2), pp.148–155.
- Scharnowski, F. et al., 2012. Improving Visual Perception through Neurofeedback. *Journal of Neuroscience*, 32(49), pp.17830–17841.
- Schomer, D. & Lopes Da Silva, F., 2011. *Niedermeyer's Electroencephalography: Basic Principles, Clinical Applications, and Related Fields* 6th Ed., Lippincott Williams & Wilkins.
- Shibata, K. et al., 2011. Perceptual learning incepted by decoded fMRI neurofeedback without stimulus presentation. *Science*, 334(6061), pp.1413–5.
- Shih, J.J., Krusienski, D.J. & Wolpaw, J.R., 2012. Brain-computer interfaces in medicine. *Mayo Clinic Proceedings*, 87(3), pp.268–279.
- Sorger, B. et al., 2012. A real-time fMRI-based spelling device immediately enabling robust motor-independent communication. *Current Biology*, 22(14), pp.1333–1338.
- Sorger, B. et al., 2004. Voluntary modulation of regional brain activity to different target levels based on real-time fMRI neurofeedback. In *Society for Neuroscience Society for Neuroscience, 34th edition San Diego, USA*.
- Sorger, B., 2010. *When the brain speaks for itself: Exploiting hemodynamic brain signals for motor-independent communication*. Universitaire Pers Maastricht: Maastricht.
- Thibault, R.T., Lifshitz, M. & Raz, A., 2016. The self-regulating brain and neurofeedback: Experimental science and clinical promise. *Cortex*, 74, pp.247–261.
- Tootell, R.B. et al., 1995. Functional analysis of human MT and related visual cortical areas using magnetic resonance imaging. *Journal of Neuroscience*, 15(4), pp.3215–3230.
- Tootell, R.B. et al., 1998. Functional analysis of primary visual cortex (V1) in humans. *Proceedings of the National Academy of Sciences of the United States of America*, 95(3), pp.811–817.
- Violante, I.R. et al., 2012. Abnormal brain activation in neurofibromatosis type 1: a link between visual processing and the default mode network. *PLoS One*, 7(6), p.e38785.
- Wan, F. et al., 2014. Resting alpha activity predicts learning ability in alpha neurofeedback. *Frontiers in human neuroscience*, 8(July), p.500.
- Weiskopf, N., 2012. Real-time fMRI and its application to neurofeedback. *NeuroImage*, 62(2), pp.682–692.
- Weiskopf, N. et al., 2007. Real-time functional magnetic resonance imaging: methods and applications. *Magnetic Resonance Imaging*, 25(6), pp.989–1003.
- Weiskopf, N. et al., 2004. Self-regulation of local brain activity using real-time functional magnetic resonance imaging (fMRI). *Journal of Physiology Paris*, 98(4–6 SPEC. ISS.), pp.357–373.
- Wolpaw, J.R. et al., 2002. Brain-computer interfaces for communication and control. *Clinical neurophysiology: official journal of the International Federation of Clinical Neurophysiology*, 113(6), pp.767–91.
- Yoo, S.-S. et al., 2004. Brain-computer interface using fMRI: spatial navigation by thoughts. *Neuroreport*, 15(10), pp.1591–1595.
- Zimmermann, J. et al., 2011. Mapping the organization of axis of motion selective features in human area mt using high-field fmri. *PLoS ONE*, 6(12), pp.1–10.
- Zotев, V. et al., 2011. Self-regulation of amygdala activation using real-time FMRI neurofeedback. *PLoS ONE*, 6(9).

CURRICULUM VITAE

Teresa Sousa was born on May 22th, 1987 in Barcelos, Portugal, where she completed her high school education at Escola Secundária de Barcelinhos in 2005. Following she attended Biomedical Engineering at the School of Engineering of the University of Minho, Braga. During her specialization studies in Medical Electronics field she did a research internship at the Neurophysiology Service of the S. João Hospital in Oporto, to develop a Master thesis entitled “The impact of rhythms analysis technique on electrographic seizure detection”. In 2010 she received her M.Sc. degree on Biomedical Engineering from University of Minho and started a research work focused in automatic sleep scoring at the Institute of Systems and Robotics of the University of Coimbra. At the end of 2011 she started her PhD in Biomedical Engineering at University of Coimbra, in both the Institute for Biomedical Imaging and Life Sciences and the Institute of Systems and Robotics. In the context of this joined project she investigated the feasibility of a multilevel control system based on voluntary neuromodulation to apply in BCI and neurofeedback approaches. During her PhD she also spent nine months between 2014 and 2015 at the Maastricht Brain Imaging Center of the University of Maastricht in a research collaboration.

Publications

Sousa, T., Direito, B., Lima, J., Ferreira, C., Nunes, U., Castelo-Branco, M., 2016. Control of brain activity in hMT+/V5 at three response levels using fMRI-based neurofeedback/BCI. *PLoS ONE*, 11(5): e0155961.

Khalighi, S., **Sousa, T.**, Santos, J.M., Nunes, U., 2016. ISRUC-Sleep: A comprehensive public dataset for sleep researchers. *Computer Methods and Programs in Biomedicine*, 124: 180-192.

Banca, P.*, **Sousa, T.***, Duarte, I.C., Castelo-Branco, M., 2015. Visual motion imagery neurofeedback based on the hMT+/V5 complex: evidence for a feedback-specific neural circuit involving neocortical and cerebellar regions. *Journal of Neural Engineering*, 12 (6): 066003.

**both authors contributed equally*

Sousa, T., Cruz, A., Khalighi, S., Pires, G., Nunes, U., 2015. A two-step automatic sleep stage classification method with dubious range detection. *Computers in Biology and Medicine*, 59: 42-53.

Khalighi, S., **Sousa, T.**, Pires, G., Nunes, U., 2013. Automatic sleep staging: A computer assisted approach for optimal combination of features and polysomnographic channels. *Expert Systems with Applications*, 40(17): 7046-7059.

Publications Submitted And In Preparation

Sousa, T., Kemper, V., Duarte, J. V., Costa, G., Martins, R., Goebel, R., Castelo-Branco, M., 2016. Perceptual interpretation of visual motion revealed at high-resolution 7T fMRI in functional domains within visual area hMT+/V5. (*In preparation*)

Sousa, T., Amaral, C., Andrade, J., Pires, G., Nunes, U., Castelo-Branco, M., 2016. Visual motion imagery as a tool for multiclass EEG-based BCI. (*submitted*)

Conferences

Sousa, T., Kemper, V., Costa, G., Duarte, J. V., Martins, R., Goebel, R., Castelo-Branco, M., 2016. Long-range perceptual integration of visual motion revealed at high-resolution 7T fMRI. In *Annual Meeting of the Organization for Human Brain Mapping*.

Sousa, T., Amaral, C., Andrade, J., Castelo-Branco, M., 2015. Visual motion imagery as tool for parametric BCI, In *Annual Conference on Clinical Neurophysiology and Neuroimaging*, 41-42.

- Khalighi, S., **Sousa, T.**, Nunes, U., 2012. Adaptive automatic sleep stage classification under covariate shift. In *Annual International Conference of the IEEE Engineering in Medicine and Biology Society*, 2259-2262.
- Sousa, T.**, Oliveira, D., Khalighi, S., Pires, G., Nunes, U., 2012. Neurophysiologic and statistical analysis of failures in automatic sleep stage classification. In *International Joint Conference on Biomedical Engineering Systems and Technologies*, 423-428.
- Sousa, T.**, Mendes, P., Ribeiro, J., 2012. The impact of rhythms analysis technique on electrographic seizure detection (EEG). In *IEEE Portuguese Meeting in Bioengineering*, 1-5.
- Khalighi, S., **Sousa, T.**, Oliveira, D., Pires, G., Nunes, U., 2011. Efficient feature selection for sleep staging based on maximal overlap discrete wavelet transform and SVM. In *Annual International Conference of the IEEE Engineering in Medicine and Biology Society*, 3306-3309.

